creative commons
COMMONS DEED

저작자표시-비영리-변경금지 2.0 대한민국

이용자는 아래의 조건을 따르는 경우에 한하여 자유롭게

- 이 저작물을 복제, 배포, 전송, 전시, 공연 및 방송할 수 있습니다.

다음과 같은 조건을 따라야 합니다:

저작자표시. 귀하는 원저작자를 표시하여야 합니다.

비영리. 귀하는 이 저작물을 영리 목적으로 이용할 수 없습니다.

변경금지. 귀하는 이 저작물을 개작, 변형 또는 가공할 수 없습니다.

- 귀하는, 이 저작물의 재이용이나 배포의 경우, 이 저작물에 적용된 이용허락조건을 명확하게 나타내어야 합니다.
- 저작권자로부터 별도의 허가를 받으면 이러한 조건들은 적용되지 않습니다.

저작권법에 따른 이용자의 권리는 위의 내용에 의하여 영향을 받지 않습니다.

이것은 이용허락규약(Legal Code)을 이해하기 쉽게 요약한 것입니다.

Disclaimer

dCollection

약학박사학위논문

Heat shock protein 70의 결합에 의한 AIMP2-DX2 안정화 기전과 결합 억제제를 이용한 항암 효능 연구

Tumor-promoting interaction between Heat shock protein 70 and AIMP2-DX2

2019년 8월

서울대학교 대학원

약학과 의약생명과학전공

임 세 미

Abstract

Heat shock protein 70 (HSP70) takes charge of regulating the level of several oncoproteins via folding, disaggregation, and degradation. Since the level and activity of HSP70 are upregulated and hyperactivated in cancer cells compared to normal's, HSP70 belongs to potential anti-cancer target. High level of aminoacyl-tRNA synthetase-interacting multi-functional protein 2-deleted exon 2 (AIMP2-DX2), an oncoprotein as well as anti-cancer target, accelerates the cancer progression. Since inhibition of AIMP2-DX2 showed tumor regression, studies targeting AIMP2-DX2 have been conducted by using siRNA, shRNA, and chemicals.

AIMP2-DX2 is increased in cancer cells compared to normal cells through the stabilization by HSP70. HSP70 binds to AIMP2-DX2 with two modes of interactions. N-terminal flexible region of AIMP2-DX2 is recognized by substrate binding pocket in HSP70 as a substrate and N-terminal GST domain of AIMP2-DX2 interacts with substrate binding domain of HSP70 with hydrophobic and electrostatic interactions. Binding of HSP70 on AIMP2-DX2 kicks off the access of Siah1, E3 ligase of AIMP2-DX2, and elevates the AIMP2-DX2 stability. Increased AIMP2-DX2 by HSP70 promotes AIMP2-DX2-mediated cancer progression *in vitro* and *in vivo*. Inhibition of the AIMP2-DX2:HSP70 interaction by BC-DXI-495, AIMP2-DX2 inhibitor, suppresses the AIMP2-DX2-mediated cancer progression.

Post-translational modification such as phosphorylation on HSP70 modulates its function and affects the cancer cell proliferation. Epidermal growth factor (EGF) phosphorylates serine residues on the linker and substrate binding domain of HSP70 via

activated ERK. Phosphorylation of the two sites on HSP70 by ERK changes the conformation of HSP70 from un-extended form to extended form which has strong binding affinity to client proteins and high folding activity. Enhanced client folding augments the level of HSP70 substrates such as Akt and Cdk4, proteins required for cancer cell survival and proliferation. Consequentially, phosphorylated HSP70 promotes the cancer cell proliferation and progression *in vivo*.

Through the two studies, the regulation of HSP70 function in cancer is revealed. Interrupting the interaction of HSP70 with AIMP2-DX2 suppressed stabilization of AIMP2-DX2 by HSP70, that only influences on the specific substrate, but not others. Phosphorylation of HSP70 modulates its folding function and the level of cellular proteins, so inhibition of the phosphorylation would affect HSP70-dependent cancer. In conclusion, the studies suggest AIMP2-DX2:HSP70 interaction and HSP70 phosphorylation as potential targets against cancer.

Keywords: AIMP2-DX2, HSP70, interaction, phosphorylation, cell proliferation, cancer progression

Student number: 2014-30557

Introduction

Proliferation of cancer cell is accelerated by various high level of oncoproteins compared to normal cell. In order to support the cancer cell growth, factors related to protein synthesis and quality control are increased especially in cancer cells. Heat shock proteins (HSPs) are critical factors to facilitate the production of oncoproteins such as Raf, Akt and Cdk4. HSPs implement the role by folding the newly synthesized proteins, refolding the misfolded proteins, disaggregating the damaged proteins, and degradation via ubiquitin-mediated process. There are several families of HSPs and they are largely categorized according to the size of HSPs. HSP90 and HSP70 are well-known HSPs, because those proteins are abundant and in charge of central chaperone. HSP90 has been reported as the most important HSP, however, the recent studies about HSP70 shed light on the critical role of HSP70 in chaperone network. HSP70 has its specific substrates different from HSP90's and is a hub of chaperone network, transferring the folded substrates by HSP70 to HSP90 or other HSPs. In addition to this, HSP70 solely do the chaperone function by itself. Therefore, HSP70 has been focused as a potential target against cancer addicted to oncoproteins. Several types of the HSP70 inhibitors are developed, retaining the possibility for implication in clinical studies. Nevertheless, side effects of HSP70 inhibitor are predicted in reference to the results of HSP90 inhibitors from clinical studies.

Aminoacyl-tRNA synthetase-interacting multi-functional protein 2-deleted exon 2 (AIMP2-DX2) is a splicing variant of AIMP2 and their roles are very opposite in cancer cells. While AIMP2 primarily exists in multi-tRNA synthetase complex (MSC) serving as a

scaffolding protein of the macromolecular protein complex, AIMP2-DX2 exists as a free form in cytoplasm. Since MSC is a central hub of protein translation, AIMP2 influences on translation, but also other cellular signaling. Upon the signaling such as UV irradiation, TNF-α, and TGF-β, AIMP2 is released from the MSC and affects on p53, FBP, and TRAF2 by conducting tumor suppressor. In cancer cell lines, AIMP2-DX2 competes with AIMP2 that interacts with its partners like p53, FBP, and TRAF2 and consequently results in cancer cell proliferation and inhibition of apoptosis. While rarely expressed in normal tissues, AIMP2-DX2 highly expressed in lung, colon, pancreatic cancer cells and higher level of AIMP2-DX2 releases drug resistance *in vitro* and *in vivo*. Since carcinogen induces the expression of AIMP2-DX2 causing carcinogenesis *in vivo* and higher AIMP2-DX2 in cancer patient tissues shows poor prognosis, pathological implication of AIMP2-DX2 is proved. Several studies focused on the repressive effect by targeting AIMP2-DX2 using siRNA or inhibitive chemicals in cancer progression. Nevertheless, the effective strategy to suppress AIMP2-DX2 has been veiled and the mechanism of AIMP2-DX2 stabilization has to be disclosed in order to inhibit AIMP2-DX2. Here, this study suggests the mechanism of AIMP2-DX2 stabilization and anti-cancer strategy by targeting the interaction of AIMP2-DX2.

HSP70 promotes the cancer progression through augmentation of oncoprotein, essential for cell proliferation and anti-apoptosis, caused by increase of its folding. HSP70 folds its client proteins depending on ATP/ADP binding via chaperone cycle. HSP70 has 3 domains: nucleotide-binding domain, substrate-binding domain (SBD), and lid which covers substrate-binding domain when the client binds. In ATP-binding state, lid binds to nucleotide-binding domain, that opens the substrate binding pocket in SBD to make easy access of substrate. HSP40 delivers the client to SBD of HSP70. When the clients bind, ATPase

function of HSP70 is activated and induces ADP-bound HSP70. ADP-bound HSP70 goes through conformation change from lid-docked form to -undocked form, also called as extended form. HSP70 in extended form has strong affinity, enough to fold, for the clients. Shortly, the folding activity of HSP70 in cellular condition is regulated by the level or ATP-dependent cycle of HSP70. However, interestingly, it is newly reported that the level of HSP70 is not correlated with the amount of folded proteins by HSP70. Moreover, recent studies show the importance of modification on HSP70 for its activity. Among the various post-translational modification, phosphorylation of HSP70 significantly affects the function and disposition of its phosphorylation is distinctive in cancer from normal. Since difference of the phosphorylation of HSP70 in cancer from normal would be helpful to use HSP70 as an anti-cancer target without side effect in normal tissue, the detailed mechanism of HSP70 phosphorylation should be unveiled. This report unravels the molecular and cellular effect of phosphorylated HSP70 by ERK implying possibility for its pathological implication.

Contents

Chapter I

Tumor-promoting interaction between heat shock protein 70 and AIMP2-DX2

Title ---------- 1

Abstract ---------- 4

Introduction ---------- 5

Results ---------- 7

Discussion ---------- 59

Methods ---------- 62

References ---------- 73

Chapter II

ERK-dependent phosphorylation on linker and substrate-binding domain of HSP70 increases folding activity and cell proliferation

Title ---------- 78

Abstract ---------- 81

Introduction ---------- 82

Results ---------- 84

Discussion ---------- 102

Methods ---------- 105

References -- 111

국문초록 -- 115

Chapter 1

Tumor-promoting interaction between heat shock protein 70 and AIMP2-DX2

Running title: HSP70 stabilizes tumorigenic DX2

Keywords: AIMP2-DX2, HSP70, Stabilization, Ubiquitination, Protein-protein interaction, Cancer progression

Abbreviations list

AIMP2-DX2: Aminoacyl-tRNA synthetase interacting multifunctional protein 2-deleted exon 2

HSP70: Heat Shock Protein 70

IP: Immunoprecipitation

EV: Empty vector

si-con : si-control

WCL: Whole cell lysate

The list of figures and tables

Figure 1. HSP70s as interactors of DX2.

Figure 2. Specific binding of DX2 and HSP70 through its 1-151 amino acids and substrate binding domain.

Figure 3. Significance of HSP70 for stabilization of DX2.

Figure 4. Analysis of DX2 and HSP70 expression in lung cancer patient tissue.

Figure 5. Effect of HSP70 on DX2-mediated proliferation.

Figure 6. Evaluation of DX2 region significant for its binding to the substrate-binding pocket of HSP70.

Figure 7. Determination of the binding structure of DX2 peptide on HSP70-substrate binding pocket.

Figure 8. Determination of DX2 residues on GST domain involved in the interaction with HSP70.

Figure 9. Determination of HSP70 residues involved in the interaction with DX2.

Figure 10. Validation of the significance of HSP70 binding for stabilization of DX2, and a complex model of DX2 and HSP70 binding.

Figure 11. HSP70-mediated protection of DX2 from Siah1-mediated degradation.

Figure 12. Screening for identification of the DX2 inhibitor, BC-DXI-495.

Figure 13. PPI inhibitor, BC-DXI-495, interrupts DX2-HSP70 interaction.

Figure 14. Effect of the PPI inhibitor, BC-DXI-495, on DX2-mediated proliferation.

Figure 15. Significance of BC-DXI-495 on DX2 binding.

Figure 16. Mode of action of BC-DXI-495 on DX2.

Figure 17. Significance of BC-DXI-495 binding on DX2 in *in vivo* model.

Table 1. List of the DX2 top50 interactome

Table 2. Data collection and Refinement statistics of X-ray crystallography

Abstract

A tumorigenic factor, AIMP2-DX2, is often up-regulated in many cancers. However, how its cellular level is determined is not understood. Here it is reported that HSP70 as a critical determinant for AIMP2-DX2 level. The interaction of the two factors was identified by interactome analysis and structurally determined by x-ray crystallography and NMR analyses. HSP70 recognizes the N-terminal flexible region as well as the GST domain of AIMP2-DX2 *via* its substrate-binding domain, blocking the Siah1-dependent ubiquitination of AIMP2-DX2. AIMP2-DX2-induced cell transformation and cancer progression *in vivo* was further augmented by HSP70. Positive correlation between HSP70 and AIMP2-DX2 levels was shown in various lung cancer cell lines and patient tissues. Chemical intervention of the AIMP2-DX2:HSP70 interaction suppressed cancer cell growth *in vitro* and *in vivo*. Thus, this work demonstrates the specific tumor-promoting interaction between AIMP2-DX2 and HSP70 and its therapeutic potential against cancer.

Keywords: AIMP2-DX2, HSP70, Stabilization, Ubiquitination, Protein-protein interaction, Cancer progression

Student number: 2014-30557

Introduction

The 70 kDa heat shock proteins (HSP70s) belongs to a family of HSPs[1], that play roles in the control of protein folding, aggregation, and degradation as well as stress responses[2]. HSP70 levels are elevated in response to heat shock or toxins[1,3] and are often upregulated in cancer[4,5].According to the oncogene addiction model, the high demand for protein synthesis and folding control in progressed cancers makes them more dependent on HSP70[6,7], prompting investigations into HSP70 as an anti-cancer target[4,8].

HSP70 is composed of the N-terminal ATPase, substrate-binding, and C-terminal lid domains[9]. The ATP or ADP-binding status of the N-terminal domain influences the open and close movement of the lid, thereby modulating the affinity of the substrate-binding domain to the client protein[10].The ATP-bound HSP70 forms an open structure that binds to the substrate, which in turn activates hydrolysis of ATP. The ADP-bound HSP70 possesses a high affinity for and helps proper folding of the bound protein substrate[11]. Substrates not successfully folded by HSP70 are then transferred to HSP90 and undergo an additional folding process[12,13]. It was recently reported that HSP70 can prevent the bound substrates from ubiquitin-dependent degradation by disaggregation although the detailed working mechanism remains unclear[14].

Aminoacyl-tRNA synthetase-interacting multi-functional protein 2 (AIMP2) serves as a scaffold in the assembly of the multi-tRNA synthetase complex (MSC), macromolecular protein complex[15,16]. AIMP2 dissociation from the MSC influences the activity of the p53, TGF-β, TNF-α and WNT signaling pathways, which inhibits tumorigenesis[17-21]. Interestingly,

a splicing variant of AIMP2 lacking exon 2, AIMP2-DX2 (DX2 hereafter), that is generated by alternative splicing positively correlates with the aggressiveness of cancer. DX2compromises the tumor suppressive function of the native AIMP2 (AIMP2-F hereafter) through competitive interactions with p53, FBP, and TRAF2[22,23]. While rarely expressed in normal tissues, DX2 is highly expressed in lung, pancreatic and colon cancer tissues[22,24] and can be induced by a chemical carcinogen to promote cancer progression[22]. Increased levels of DX2 have been observed in chemo-resistant ovarian cancer cells[23] and its levels positively correlate with cancer stage and patient lethality[22,24]. Specific suppression ofDX2 expression with its specific siRNA or chemicals was shown to reduce tumor growth, suggesting its potential efficacy as therapeutic target[22,23,25,26]. Despite its significance as a potential marker and therapeutic target against cancer, the factor and mechanism to determine the cellular level of DX2 are not known yet. Here, this study shows that HSP70 specifically recognizes and stabilizes DX2 and demonstrate a mechanism for this activity. It is also validated the therapeutic potential of modulating the HSP70-DX2 interaction through chemical inhibitor.

Results

The interaction of DX2 with HSP70

To understand the mechanisms by which cells augment the levels of DX2 protein, DX2-interacting cellular factors are identified by affinity purification using immobilized streptavidin (strep)-tagged DX2, followed by liquid chromatography-mass spectrometry (LC-MS) (Fig. 1a). 107 proteins were identified as potential DX2 interactors (Fig. 1b-c, and Table 1), and ontological classification revealed that HSP70 family proteins were predominant among the top 50 interactors. These included HSPA8, HSPA5, HSPA9, HSPA2, HSPA1L, HSPA4, and HSPA1A (Fig. 1d).

To determine whether the interaction of DX2 with HSP70 is direct and specific, I performed an *in vitro* pull-down assay using purified GST-DX2 in cell lysates expressing GFP-HSP70 or -HSP90. As shown in Fig. 2a, DX2 bound to HSP70, but not to HSP90. I also showed the endogenous interaction of HSP70 and DX2 by co-immunoprecipitation using specific antibodies against DX2 and HSP70 (Fig. 2b). The domains responsible for the interaction were determined by repeating the co-immunoprecipitation experiments using truncated versions of DX2 and HSP70 containing different domains. HSP70 consists of a nucleotide-binding domain (NBD, 1-384 aa), substrate-binding domain (SBD, 385-536 aa) and Lid (537-641 aa)[9], while DX2 contains an N-terminal flexible region (NFR, 1-50 aa), GST-N-terminal domain (51-151 aa), and GST-C-terminal domain (152-251 aa) (Fig. 2e)[22]. Using different combinations of these domains in *in vitro* pull-down assay and immunoprecipitation showed that DX2's NFR and N-terminal GST sub-domain (1-151 aa)

interacted withHSP70's SBD (Fig. 2c-e).

Roles of HSP70 in stabilization and oncogenicity of DX2

To gain insight into the functional importance of the HSP70-DX2 interaction, I monitored the level of DX2 in cells which HSP70 was either overexpressed or downregulated by siRNA. It was observed that a positive dependence of the DX2 protein, but not its mRNA, on HSP70 expression, suggesting that HSP70 plays a role in modulating DX2 abundance at the post-transcriptional level (Fig. 3a). To determine the effect of HSP70 on cellular turnover of DX2, nanoluciferase-tagged DX2 was expressed in HSP70 up- and down-regulated 293T cells that were treated with cycloheximide to block *de novo* protein synthesis. The cellular stability of DX2 was significantly extended by the overexpression of HSP70 while reduced by the suppression of HSP70 (Fig. 3b). Then, it was examined whether levels of HSP70 affected the ubiquitination of DX2 by monitoring the ubiquitinated-DX2 using an HA-tagged ubiquitin (ub) and immunoblotting with HA antibody. As shown in Fig. 3c, high levels of HSP70 reduced the ubiquitination of DX2. To see whether the effect of HSP70 on DX2 stability I observed in cell culture extends more broadly, I determined the cellular levels of HSP70 and DX2 in various human lung normal and cancer cell lines by Western blot analysis. Out of the 29 tested cell lines, 21 showed that expression levels of the two proteins positively correlated (Fig. 3d-e). Using four cell lines in which endogenous DX2 levels are intrinsically low, I tested whether ectopic expression of HSP70 increases the endogenous DX2 expression. As shown in Fig. 3f, HSP70 enhanced DX2 levels in dose-dependent manner.

The relationship between HSP70 and DX2 was tested by measuring their levels in tissues from human lung cancer patients using immunohistochemistry staining (Fig. 4a).

Among the 112 tissues tested, 73% showed a positive correlation between HSP70 and DX2 expression (Fig. 4b and 4d left). To further confirm this observation, levels of the two proteins were compared in tumor and matched normal (MN) tissues from same patients. Of the tissues from the 75 patients tested, 27 showed a simultaneous, tumor-specific increase in the levels of both proteins (Fig. 4c and 4d right). Together, these results suggest that HSP70 plays a significant role in controlling DX2 stability with pathological implications when the two factors are present in tumors.

To assess the tumorigenicity of the two factors, I monitored the combined effects of HSP70 and DX2 levels on cell viability. Strep-DX2 was introduced into 293T cells which is expressed with siRNA against HSP70, and cell viability was determined by colorimetric assay. Ectopic expression of DX2 resulted in enhanced cell viability whereas suppression of HSP70 expression resulted in decreased cell viability (Fig. 5a-b). To validate these results, I conducted an analogous experiment using the constructs in a DX2-inducible A549 stable cell line. A549 cells were transfected with construct expressing DX2 under control of an inducible promoter (Strep-DX2) and empty vector control (Strep-EV) and si-RNA against HSP70, treated with doxycycline to induce DX2, and cell viability was determined. When DX2 was induced by the treatment of doxycycline, cell viability was increased significantly (Fig. 4c, red). However, this effect was reduced in cells which HSP70 expression was suppressed (Fig. 4c, blue). Then, it was evaluated that the relationship between HSP70 and DX2 in cell transformation using an anchorage-independent colony formation assay, using the same strategy but with a sh-HSP70 construct to suppress HSP70 expression. Cells expressing both Strep-DX2 and HSP70 yielded the highest number of colonies while cells expressing Strep-EV and sh-HSP70 yielded the lowest (Fig. 4d). Together, these results confirmed that HSP70

augments the tumorigenicty of DX2.

Structural analysis of the DX2 and HSP70 interaction

The data above in Figure 1 showed the significance of DX2's NFR (DX2-NFR) for its interaction with HSP70. The substrate-binding pocket of HSP70's substrate-binding domain (HSP70-SBD) is known to preferentially accept flexible peptides containing hydrophobic amino acids[27]. Since DX2-NFR harbors several hydrophobic residues (Fig. 6a), It was determined whether DX2-NFR could bind to HSP70-SBD by performing a competition assay between DX2 and NRLLLTG, a well-known substrate sequence corresponding to the substrate binding pocket of HSP70-SBD, and monitoring the binding of DX2-NFR to HSP70 by NMR analysis[*]. The NMR signals detected theDX2-NFR shifted upon HSP70 binding (Fig. 6b, red) and shifted back upon the addition of NRLLLTG peptide (Fig. 6b, green), implying that DX2-NFRbound to the substrate-binding pocket of HSP70-SBD.

The binding region of DX2-NFR was next determined by measuring heteronuclear nuclear Over hauser effects (NOE), which indicated that the amide signals of DX2-NFR with the restricted motions were presented in an HSP70-bound state. When in the HSP70-bound state, the DX2-NFR residues ranging from Y25 to R33 showed positive values for the heteronuclear NOEs, whereas in the free state, the same residues showed negative values, indicating that the HSP70 binding enhanced the rigidity of those residues (Fig. 6c, upper). The amide signals of those residues also showed large chemical shift perturbation (CSP)

[*] NMR analysis, crystallization, and modeling of protein structure were supported from professor Young ho Jeon in Korea university.

values when in the bound state (Fig. 6c bottom, and 6d). To further validate these results, I determined the region of DX2-NFR responsible for its interaction with HSP70 using a co-immunoprecipitation assay and observed that $DX2_{24-34}$ (the peptide from M24 to S34 of DX2) showed the strongest binding to HSP70 (Fig. 6e), consistent to the results of the heteronuclear NOE measurement. Taken together, these data indicated that the region of DX2-NFR spanning residues M24 to R33 is critical for its access to the substrate-binding pocket of HSP70.

Next the X-ray crystal structure of the DX2-NFR-derived peptide, ^{24}MYRLPNVHG^{32}, complexed with HSP70-SBD was determined. Crystals from a fusion protein denoting $HSP70_{395-537-MYRLPNVHG,}$ comprised of HSP70-SBD and the DX2 peptide were obtained (Fig. 7a). The protein was crystallized in a space group $P2_12_12_1$ with two molecules in the asymmetric unit. The structure was refined at 1.79Å resolution to R_{work} and R_{free} values of 0.18 and 0.22, respectively (Fig. 7b).The structure revealed that the T429, A406 and L439 residues of HSP70 form hydrogen bonds with Y25 and L27, R26, and P28 of DX2, respectively. In addition, the L27 residue of DX2 binds to a hydrophobic pocket formed by the L403, F428, V438, and I440 residues of HSP70. The L27 position of DX2 is designated S0 in the sequence of substrate bound to HSP70[28] (Fig. 7c). The bound structure of MYRLPNVHG in HSP70 was strikingly similar to the pyrrhocoricin-derived peptide, LY Cha LPRPT, of DnaK (PDB 3DPP)[29] (Fig. 7d), showing that the mode of binding may be similar in the two cases.

Based on the information from crystal structure, I substituted hydrophobic residues in DX2 with alanine and conducted further binding assays. Among the four mutants of $DX2_{24-34}$that I tested, alanine substitutions of the Y25 and L27 residues most significantly reduced

HSP70 binding (Fig. 7e), suggesting the importance of these residues for the interaction of DX2 with HSP70. In HSP70, substituting alanine for F428, a residue known to be critical for substrate binding[30], also reduced the interaction between HSP70 and $DX2_{24\text{-}34}$ (Fig. 7f). The binding of $DX2_{24\text{-}34}$to HSP70 was reduced by the addition of the "NRLLLTG" peptide in a dose-dependent manner, suggesting that DX2-NFR accesses the substrate-binding pocket of HSP70-SBD (Fig. 7g). Taken together, these results indicate that HSP70 recognizes DX2 through its typical substrate-binding mode.

Deletion mapping suggested that DX2 makes an additional interaction with HSP70 *via* its GST domain (Fig. 2e). To uncover the exact mode of binding between DX2-GST and HSP70-SBD, the residues of each protein responsible for this interaction were determined using NMR-based chemical-shift-perturbation (CSP) analysis. The CSP analysis using ^{15}N-labelled $DX2_{51\text{-}251}$ suggested that upon binding the HSP70, several residues on the surface of the β-sheet in DX2-GST were perturbed (Fig. 8b and c), and that four hydrophobic and four positively charged residues are proposed to be critical for the interaction with HSP70. These eight DX2 residues were then mutated and co-immunoprecipitation experiments were performed to confirm their importance for binding to HSP70 (Fig. 8d). This analysis indicated that the L97 and T117residues in the hydrophobic pocket and the K125 and K129 residues on the positively-charged electrostatic surface of DX2-GST were required for HSP70 binding (Fig. 8a and 8e-g). A further CSP analysis using ^{15}N-labelled $HSP70_{386\text{-}543}$ uncovered the perturbation of the residues located near the hinge region between the α-helical Lid and β-stranded SBD domains (Fig. 9b and c). Since several residues in hydrophobic and negatively-charged electrostatic surface were suggested to be critical for the interaction with DX2,these residues were also mutated and tested for the interaction with DX2 using the co-

immunoprecipitation assay (Fig. 9d). These results suggested that the L486 and I503 in the hydrophobic pocket and the D395 and D481 residues on the negative-charged electrostatic surface are critical for HSP70 binding to DX2 (Fig. 9a and 9e-g). Interestingly, the binding surfaces of the DX2-GST and HSP70-SBD domains show charge-complementarities in which the surfaces of DX2 and HSP70 are highly positive and negative (Fig. 8a and 9a), respectively, which is reminiscent of the typical substrate-binding mode of HSPs[31].

Next I investigated the significance of HSP70 for stabilization and tumor-promoting function of DX2 using the binding-defective mutants of both proteins. In contrast to DX2 wild type (WT), whose levels increased upon introduction of HSP70, the levels of the HSP70-binding defective DX2 mutants such as T117A, K125A and L27A remained unchanged (Fig. 10a, left). Conversely, all of the HSP70 mutants defective in binding to DX2, such as L486A, D395A and F428A, also failed to increase the levels of DX2 (Fig. 10a, right). Moreover, a cell viability assay showed that unlike wild type (WT), the HSP70-binding defective DX2 mutants, T117A, K125A and L27A, failed to enhance 293T cell viability (Fig. 10b).

Based on information from the binding studies using NMR, x-ray crystallography and site-directed mutagenesis, a model for the complex of DX2 and HSP70 $SBD_{395-537}$ was generated (Fig. 10c). This model shows the hydrophobic interaction of DX2-NFR in the substrate-binding pocket of HSP70-SBD, and the hydrophobic and electrostatic interactions of DX2-GST with the hinge region between alpha-helical Lid and beta-stranded SBD. The interactions occurring at the two separated regions of HSP70 may cooperatively facilitate the binding and stabilization of DX2.

Inhibitory effect of HSP70 on Siah1-mediated degradation of DX2

I then investigated the detailed mechanism by which HSP70 inhibits the ubiquitination of DX2. Siah1 was previously reported to be an E3 ligase that delivers ubiquitin to DX2[32]. I confirmed this previous observation by checking the interaction of endogenous Siah1 and DX2 by mutual co-immunoprecipitation in 293T cells (Fig. 11a). Then, it was tested whether HSP70 affects the binding of Siah1 to DX2 using co-immunoprecipitation and *in vitro* pull-down assays in 293T cells expressing Strep-DX2, FLAG-Siah1 and GFP-HSP70, and co-precipitated Siah1 and HSP70 with DX2 were analyzed. As shown in Fig. 10b, the binding of Siah1 to DX2 was suppressed by ectopic expression of HSP70 (Fig. 10b). Direct binding of the two proteins was also reduced by an increase in HSP70, as shown by a pull-down assay in which purified GST-DX2 was mixed with the cell lysates expressing FLAG-Siah1 and different levels of GFP-HSP70 (Fig. 10c). These results suggest that HSP70 could competitively block the binding of Siah1 to DX2.The DX2 level was decreased by ectopic expression of Siah1and restored by HSP70 (Fig. 10d), confirming that HSP70 and Siah1 have a functional relationship in the control of DX2 level.

To determine the interaction regions of Siah1 and DX2, I performed co-immunoprecipitation using the separate domains of the two proteins. The substrate-binding domain (SBD) of Siah1 showed to bind to the same NFR and GST-N domain of DX2 (Fig. 10e and f) responsible for binding to HSP70 (Fig. 10g). To confirm whether HSP70 binding is critical for blocking Siah1-mediated ubiquitination of DX2, I induced DX2 ubiquitination by ectopic expression of Siah1 and compared the effect of HSP70 WT and DX2-binding-defective F428A mutant on DX2 ubiquitination. As shown in Fig. 10h, Siah1-dependent ubiquitination of DX2 was inhibited by HSP70 WT but not by F428A mutant. Together, these

data suggest that HSP70 competitively inhibits Siah1 binding to and ubiquitination of DX2, resulting in an increase in DX2 levels.

Chemical inhibition of HSP70-DX2 interaction

The data above shows that HSP70 augments the oncogenic activity of DX2 and expression of the two proteins are positively correlated in many cancer cells. To determine the therapeutic potential of blocking the interaction between DX2 and HSP70, a chemical screen was conducted to identify inhibitors that can reduce the cellular stability of DX2 as a consequence of disrupting its interaction with HSP70. A549 cells expressing nanoluciferase-tagged DX2 were treated with 100 chemicals[†] that were derived from the BC-DXI-04, which has previously revealed to decrease the level of DX2[25]. The effect of the chemicals on the nanoluciferase-DX2 stability was determined by monitoring its luminescence (Fig. 12a). 34 chemicals were selected that reduced the luminescence signal by more than 40 % compared to the untreated control. These chemicals were subjected to a secondary screening to determine their effect on the AIMP2-F level and cell viability in lung cancer and normal cells (Fig. 12b). One of the chemicals, BC-DXI-495, was finally selected as a hit compound (Fig. 12c). BC-DXI-495 specifically reduced the levels of DX2 (IC_{50}: 4.2 μM), but not AIMP2-F, and reduced the viability of lung cancer cells (EC_{50}: 14 μM), but not normal cells (Fig. 12d). Moreover, in H460 cells, BC-DXI-495 specifically reduced the levels of endogenous DX2 protein, not mRNA (Fig. 12e).

[†] 100 chemicals are derivatives of BC-DXI-04 and all the chemicals were synthesized from professor Kyeong Lee's laboratory in Dongguk university.

To confirm BC-DXI-495's specific inhibition of the DX2-HSP70 interaction in cells, Strep-DX2-expressing cell lysates in the presence and absence of the chemical were reacted with Strep-tactin column. Co-precipitated proteins were separated by SDS-PAGE (Fig. 13a, left). In the cell lysate without BC-DXI-495, a major protein band was detected that co-precipitated with Strep-DX2. This band was eliminated in the chemical-treated lysate (Fig. 13a, right). Isolation of the protein band and LC-MS analysis revealed that the protein was HSP70. These results suggest that the interaction of DX2 with HSP70 was specifically inhibited by BC-DXI-495. I then performed an enzyme-linked immunosorbent assay (ELISA) by adding different amounts of BC-DXI-495 to the DX2 and HSP70 pair to test for its ability to directly inhibit the binding of two proteins. The addition of BC-DXI-495 reduced the interaction of the two proteins in a dose-dependent manner (Fig. 13b). I also performed Siah1-mediated ubiquitination of DX2 to determine whether BC-DXI-495 affects this process. As shown in Fig. 13c, increasing amounts of the chemical gradually enhanced the Siah1-mediatedubiquitination of DX2, which was blocked by HSP70. Together, the data suggests that BC-DXI-495 inhibits the interaction between DX2 and HSP70 and increase the ubiquitination-dependent turnover of DX2.

The effect of BC-DXI-495 on DX2-dependent cancer progression

Since BC-DXI-495 stimulates DX2 degradation by inhibiting HSP70 binding to DX2, I tested whether it also affects DX2-dependent cell growth in a DX2-inducible cell line. The data indicated that induction of DX2 significantly enhanced cell viability and BC-DXI-495 efficiently diminished DX2 activity (Fig. 14a, pink lines). However, the effect of the chemical on cell viability was not as apparent as in the control cells (Fig. 14a, blue lines). I also

measured the changes in DX2 levels after treating the same cells with BC-DXI-495 and observed that the levels of DX2 induced by the doxycycline treatment was decreased by the treatment of BC-DXI-495 (Fig. 14b). I then estimated the EC_{50} of BC-DXI-495 in lung cell lines expressing different levels of DX2 and observed that the cell lines with higher amounts of DX2 were more sensitive to the cytotoxicity of BC-DXI-495 (Fig. 14c). The effect of BC-DXI-495 on cancer progression *in vivo* was then further evaluated using a xenograft model of H460 cells. Tumor growth was significantly diminished by the administration of BC-DXI-495 with little effect on body weight (Fig. 14d-g). I also determined the endogenous levels of DX2 and HSP70 in isolated tumors and observed a specific decline in DX2 which indicated that BC-DXI-495 exerted a specific suppressive effect on DX2 levels (Fig. 14h).

Determination of the chemical binding surface in DX2

To understand the mode of action of BC-DXI-495, BC-DXI-495 was biotinylated at several positions (Biotin-495) and compared the effects on DX2 levels in H460 cells. Among the four biotinylated derivatives, biotin-495-#1 was selected for further experiments since it showed most potent suppression of DX2 levels (Fig. 15a). To identify the target of BC-DXI-495, I reacted biotin-495 either with GFP-DX2 or GFP-HSP70, co-precipitated the complex, and analyzed them by Western blot analysis. As shown in Fig. 15b, the precipitate contained GFP-DX2 but not GFP-HSP70. To further confirm the specific binding of BC-DXI-495 to DX2, I performed competitive binding assay of BC-DXI-495 and biotin-495 to DX2. The amount of DX2 that co-precipitated with Biotin-495 was significantly decreased in the group pre-treated with BC-DXI-495 (Fig. 15c).

The binding affinity of BC-DXI-495 to DX2 was measured using a surface plasmon

resonance (SPR) assay and the results indicate that BC-DXI-495 binds to DX2 with a K_D of approximately 14 μM (Fig. 15d), which is similar to the IC_{50} value for its suppression of DX2 levels (Fig. 12d). Then, the BC-DXI-495 binding region of DX2 was determined using a NMR-based chemical shift perturbation (CSP) assay. Several residues of DX2 were perturbed by adding BC-DXI-495 (Fig. 16a-b) that suggested a hydrophobic pocket on surface of DX2 as a candidate chemical binding region. To identify the residues responsible for binding, I introduced alanine substitutions at potentially important residues and determined the effect on the HSP70-DX2 interaction. The alanine substitution at the L80, T82, F116, T117 and K129 residues ablated the effect of BC-DXI-495 (Fig. 16c), suggesting they engage in binding to the chemical. Based on these results, a structural modeling study was performed in which BC-DXI-495 was docked into the hydrophobic pocket of DX2 surrounding L80, T82, F116 and T117 residues (Fig. 16d). This hydrophobic pocket is proximal to the binding surface for HSP70, suggesting that binding of BC-DXI-495 to DX2 could interfere with the binding of HSP70 (Fig. 16e). Prompted by our data showing that BC-DXI-495 specifically inhibited the interaction of HSP70 with DX2, I tested its effect on DX2-induced tumor growth *in vivo* by intraperitoneally administering the chemical into mice embedded with H460 cells stably expressing either DX2 wild type (WT) or the DX2 L80A mutant that does not bind the chemical. BC-DXI-495 significantly suppressed the growth and weight of tumors expressing DX2 WT and not those expressing the L80A mutant (Fig. 17a-c), while not affecting body weights of the tested mice (Fig. 17d). In addition, the level of DX2 WT was significantly reduced whereas the level of the L80A mutant was unaffected in the chemical-treated tumors (Fig. 17e). Taken together, the results indicate that BC-DXI-495 exerts its tumor suppressive activity by specifically binding to DX2 and blocking its tumor-promoting interaction with HSP70.

Figure 1. HSP70s as interactors of DX2.

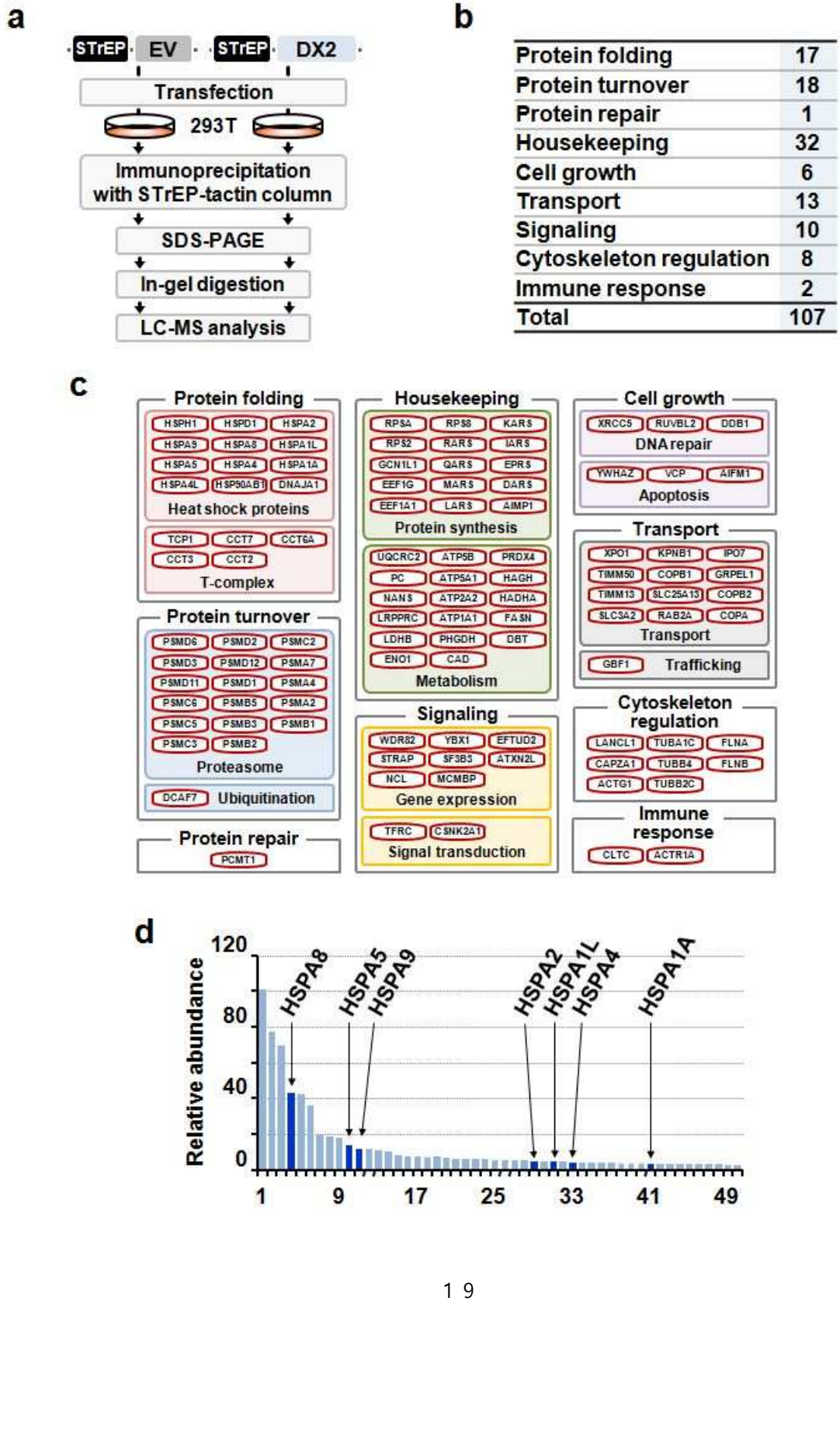

Figure 1. a, Strategy for interactome analysis of DX2. Proteins co-precipitated with Strep-tagged DX2 were identified by LC-MS analysis. Empty vector (EV) was used as a negative control for DX2. **b**, Ontology classification of proteins that interacted with DX2. **c**, Ontology classification of proteins interacted with DX2. The symbols of the interacting proteins are indicated in the ovals. Most of DX2-interacting proteins involved in protein folding are isoforms of the HSP70 family. **d**, Relative abundance of top 50 proteins specifically identified as binding proteins of DX2 from interactome analysis. Identified isoforms of HSP70 were presented as a deep blue color in bar graph. X-axis denotes the order of the identified proteins.

Figure 2. Specific binding of DX2 and HSP70 through its 1-151 amino acids and substrate binding domain.

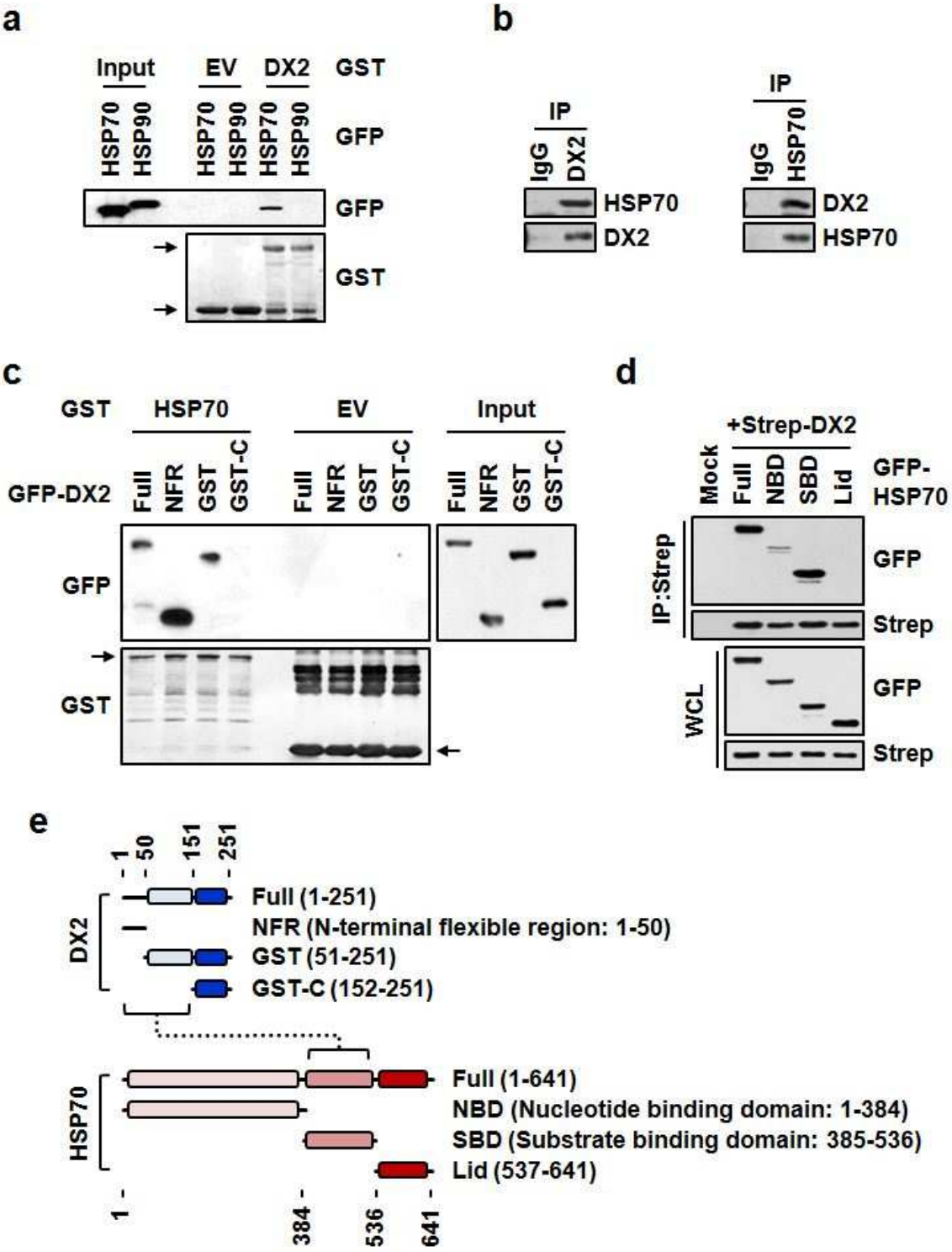

Figure 2. **a**, *In vitro* pull-down showing specific interaction of DX2 with HSP70. GST-DX2 protein was incubated with cell lysates expressing GFP-HSP70 or -HSP90 and precipitated with glutathione-Sepharose beads. Co-precipitates were subjected to SDS-PAGE and immunoblotting using specific antibody against GFP. The amounts of GST proteins were determined by Coomassie staining. Arrows denotes the GST proteins. **b**, Endogenous immunoprecipitation showing the binding between DX2 and HSP70. Endogenous DX2 and HSP70 were precipitated with their specific antibodies in left and right panel experiment, respectively. **c**-**e**, Determination of peptide regions responsible for binding of DX2 and HSP70. (**c**) GST-HSP70 was incubated with the cell lysates containing the full length GFP-tagged DX2 (Full) and three GFP-tagged DX2 fragments: NFR, GST and GST-C. HSP70 co-precipitated were subjected to SDS-PAGE and immunoblotting with the antibody against GFP was used to detect GFP fusion or full length DX2 and its fragments, and coomassie staining to detect GST. (**d**) Each of version of GFP-, either fused to full-length HSP70 (Full)or its NBD, SBD, and Lid domains, was introduced into 293T cells expressing Strep-DX2. DX2 was precipitated using a Strep-tactin column and the co-precipitated HSP70 domain was detected by Western blotting using a specific antibody against GFP. **e**, Schematic diagram showing the interaction between DX2 and HSP70. Peptide regions involved in the interaction of two proteins are depicted as a dashed line. NFR, N-terminal flexible region; SBD, substrate-binding domain.

Figure 3. Significance of HSP70 for stabilization of DX2.

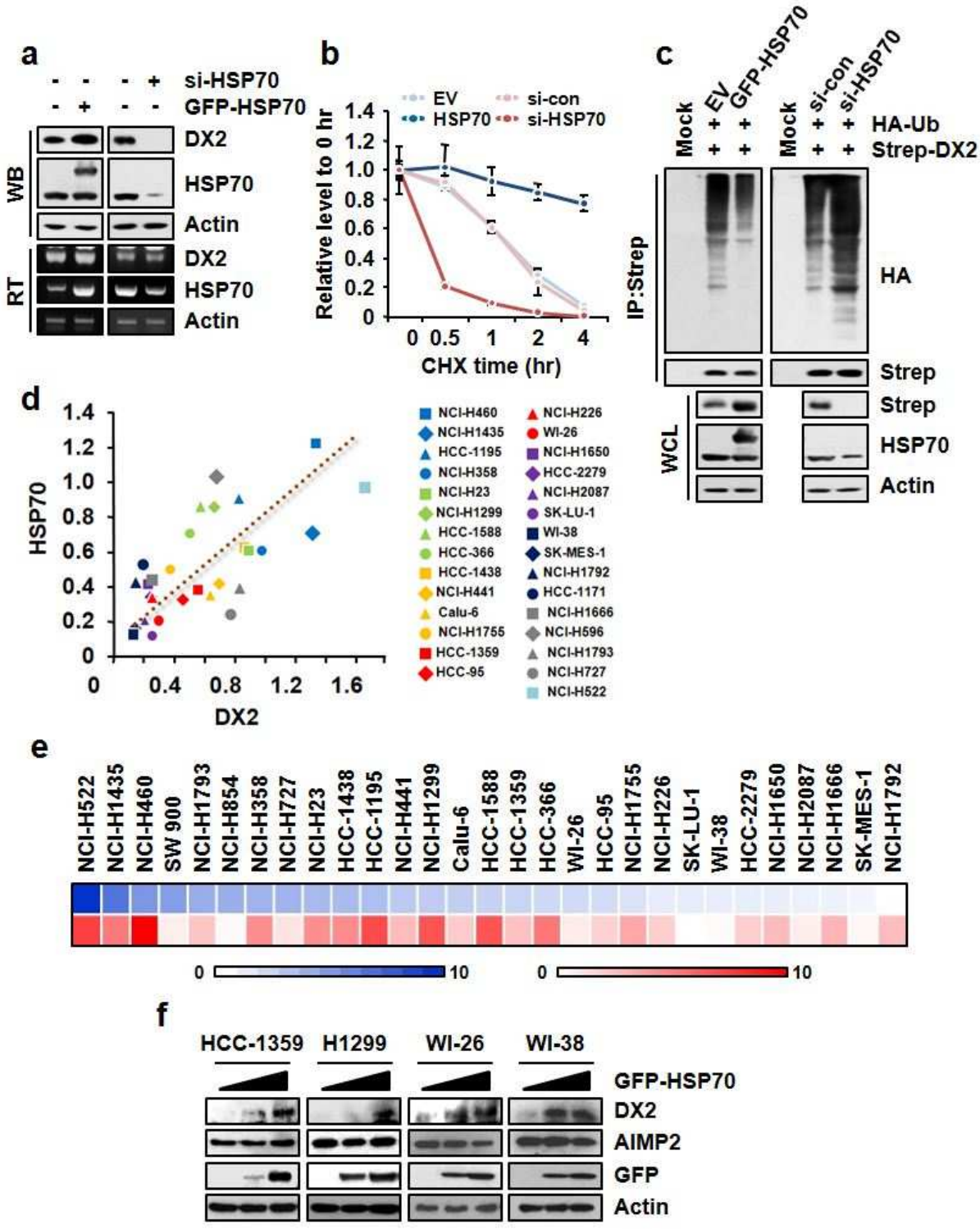

Figure 3. a, HSP70 was overexpressed and suppressed in 293Tcells by the introduction of

GFP-HSP70 or a specific si-RNA against HSP70, respectively. Protein and mRNA levels of DX2 in these cells were detected by Western blotting (WB) and RT-PCR (RT), respectively. Actin was used as a loading control. **b**, Protein stability of nanoluciferase-tagged-DX2 was evaluated at time intervals after cycloheximide (CHX) treatment using a luciferase assay. HSP70 expression was modulated as described above in Fig. 2a. **c**, HSP70-dependent control of DX2 ubiquitination. HSP70 was overexpressed or suppressed by the introduction of GFP-HSP70 or si-HSP70, respectively, in 293T cells expressing Strep-DX2 and HA-ub. Amounts of ubiquitinated DX2 were determined by immunoblotting with an anti-HA antibody. **d**, Levels of DX2 and HSP70 in various lung cell lines including cancer and normal were analyzed by Western blotting. Relative levels of both proteins in different cell lines were measured and presented in the graph. A dotted line shows the relationship between the expression of DX2 and HSP70. X and Y axis denotes the relative level of DX2 and HSP70. **e**, Levels of DX2 and HSP70 in 29 cancer and normal lung cell lines were determined by immunoblotting using their specific antibodies. Protein levels were normalized using actin as a loading control. The normalized levels were graded from 0 to 10 and visualized as blue and red for DX2 and HSP70, respectively. Cell lines were arranged according to their grade of DX2 level. **e**, Increasing amounts of GFP-HSP70 were introduced into four different cells expressing low levels of endogenous DX2 and HSP70, and the level of DX2, GFP, and actin was assessed by Western blotting using their specific antibodies.

Figure 4. Analysis of DX2 and HSP70 expression in lung cancer patient tissue.

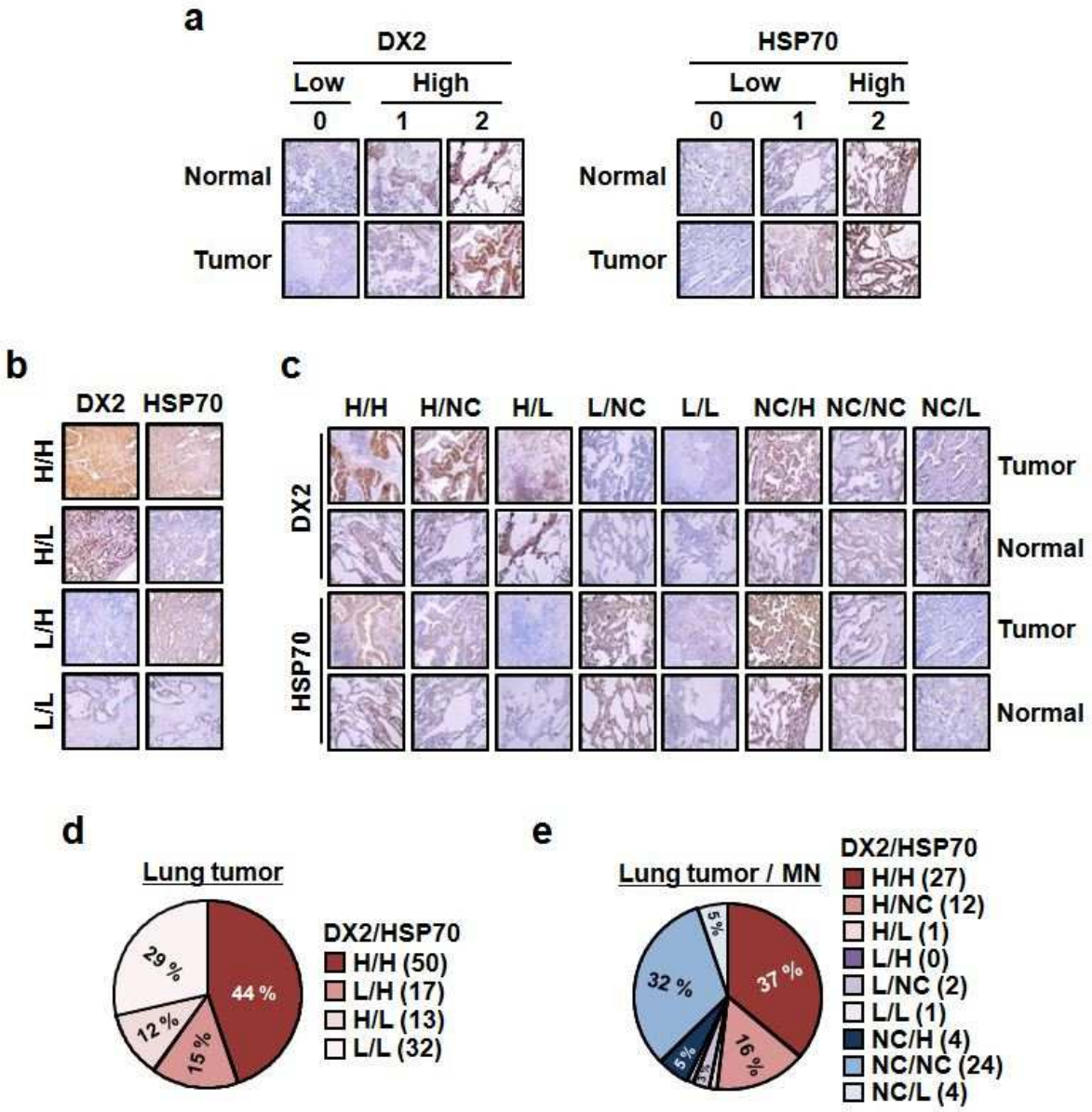

Figure 4. a-c, (**a**) Tissue micro array including lung cancer and matched normal tissues was subjected to immunohistochemistry (IHC) staining with anti-DX2 and -HSP70 antibodies. The staining levels were graded from 0 to 2 (for DX2, 0 is low and 1 and 2 are high; for HSP70, 0 and 1 are low, and 2 is high). (**b-c**) Representative stained images for *pi* chart. L, H

and NC denote low, high and not changed, respectively. **d-e**, Analyzed results in the tissues from cancer patients (lung tumor; d) and cancer compared to matched normal (MN) from same patients (lung tumor/MN; e) are presented as *pi* charts with the number of analyzed tissues shown in parentheses. L, H and NC denote low, high and not changed, respectively

Figure 5. Effect of HSP70 on DX2-mediated proliferation.

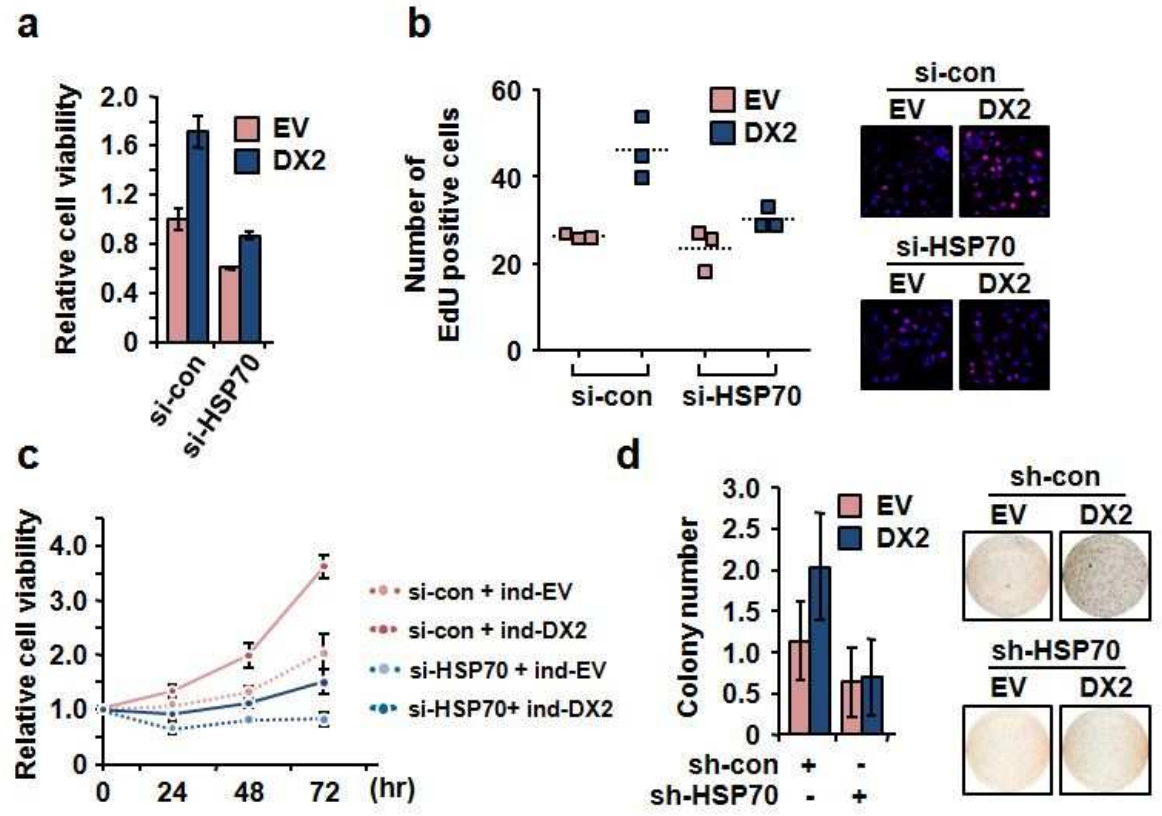

Figure 5..a-b, (**a**) Cell viability of 293T cells expressing the indicated combination of si-HSP70 and Strep-DX2 was measured by MTT assay. Empty vector (EV) and si-control (si-con) were used as a negative control. The values of the cell viability relative to that of the cells expressing EV and si-control are shown as a bar graph. (**b**) The same cells as described above were subjected to EdU staining to determine levels of DNA synthesis. DAPI was used for staining of nuclei and normalization. **c**, Strep-EV- or Strep-DX2-inducible A549 cells (ind-EV and ind-DX2, respectively) were transfected with si-RNA against HSP70 or control siRNA (si-con and si-HSP70, respectively) and treated with doxycycline to induce DX2 expression. Cell viability was determined at time intervals by MTT assay. **d**, H460 cells stably expressing Strep-EV or -DX2 and sh-con or -HSP70 were subjected to an anchorage-

independent colony formation assay. The colony number from each cell line was presented as a bar graph (left) with representative images of processed cells shown (right). All the experiments were independently repeated three times with error bars denoting S.D.

Figure 6. Evaluation of DX2 region significant for its binding to the substrate-binding pocket of HSP70.

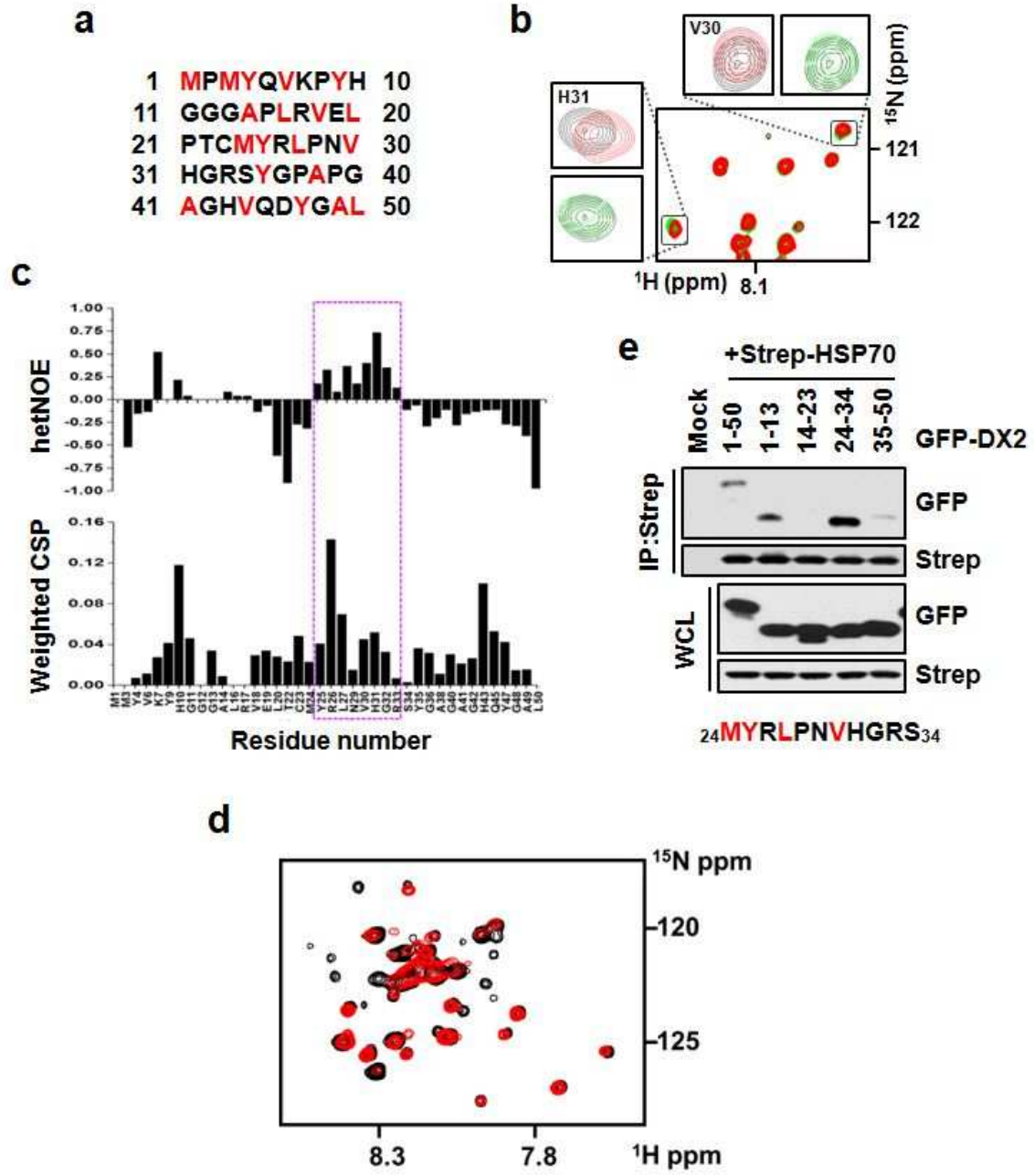

Figure 6. a, Sequence of N-terminal flexible region (NFR). Hydrophobic amino acids are indicated by red. **b**, Close-up view of the superposition of the 2-dimensional (2D) ^{1}H-^{15}N

TROSY spectra of ^{15}N-labeled DX2$_{1\text{-}251}$ (black contours) in the presence of HSP70$_{1\text{-}641}$ (red), or in the presence of both HSP70$_{1\text{-}641}$ and NRLLLTG peptide (green). Boxes represent the shifted NMR signals for H31 (left) and V30 (top). **c**,^{15}N-^{1}H heteronuclear NOEs for the amide groups of DX2-NFR in the presence of HSP70$_{395\text{-}613}$ along the residue numbers. Heteronuclear NOE values are plotted in the scale of -1.0 to 1.0 (upper). Weighted ^{1}H-^{15}N chemical shift perturbations (CSP) ($\Delta\delta$ (ppm) = $[0.5 \times ((\delta H)^2 + 0.2 \times (\delta N)^2)]^{1/2}$) between the bound and free DX2-NFRare plotted along the residue number (lower). 0.4 mM 15N-labeled DX2-NFRand 4mM HSP70$_{395\text{-}613}$was used in the assay. Residues from Y25 to R33 showing positive heteronuclear NOEs and large CSP values are highlighted by the dotted box. **d**, A close-up view of the superimposed 2D ^{1}H-^{15}N TROSY spectra of 0.4 mM ^{15}N-labeled DX2-NFR (black) with 4mM HSP70$_{395\text{-}613}$ (red). **e**, Each fragment of DX2-NFR was introduced into 293T cells expressing Strep-HSP70. The cell lysates were subjected to precipitation with a Strep-tactin column and co-precipitated DX2 was separated by SDS-PAGE and immunoblotted with an anti-GFP antibody.

Figure 7. Determination of the binding structure of DX2 peptide on HSP70-substrate binding pocket.

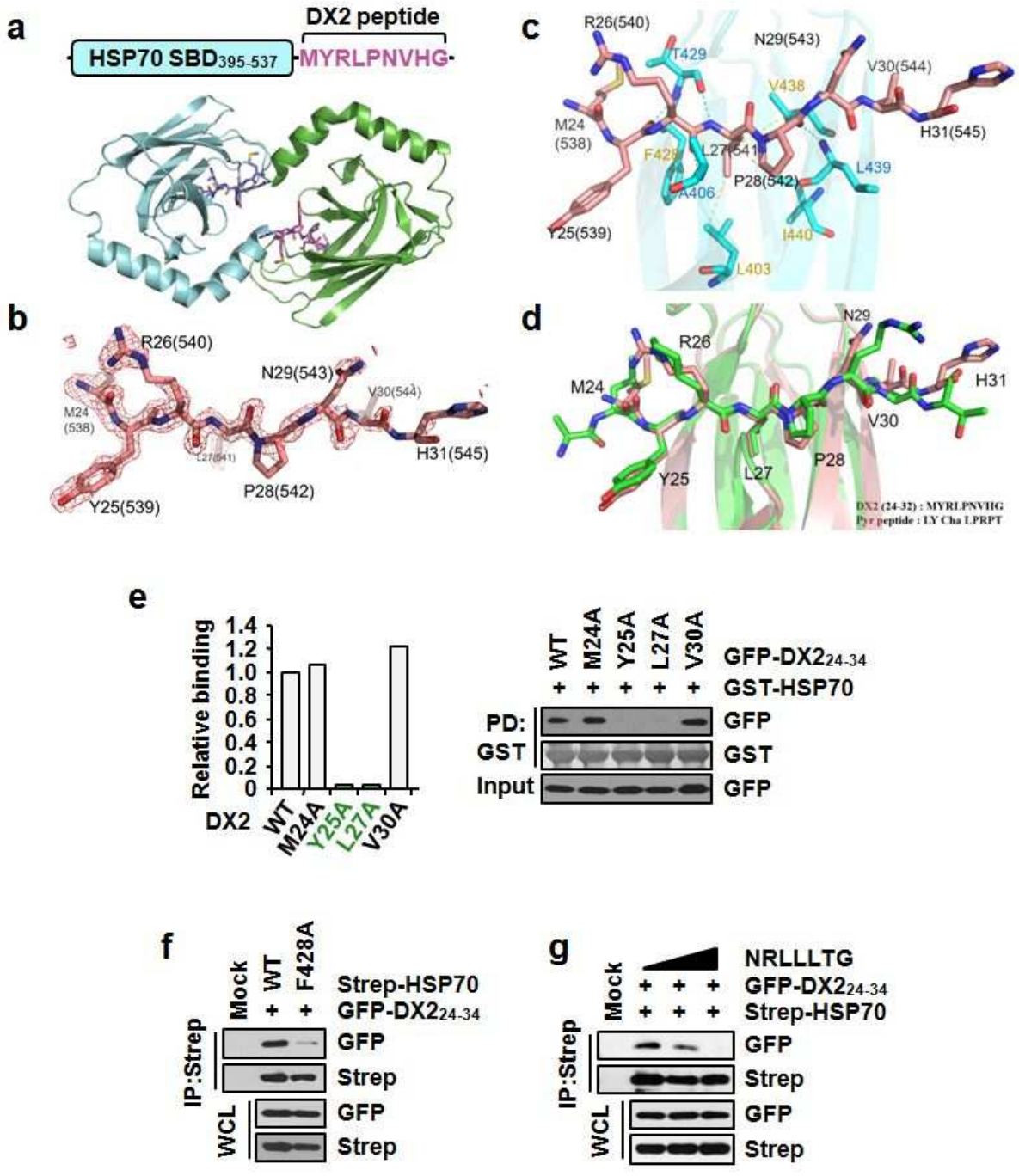

Figure 7. a, Overall dimeric structure of a chimeric protein where the[24]MYRLPNVHG[32] of DX2 is fused into the C-terminus of $HSP70_{395-537}$. Cartoon showing the chimera protein is

shown (top). The cartoon model shows a dimeric structure in an asymmetric unit. The peptide sequences, MYRLPNVHG, is shown as the stick models colored by magenta and purpleblue. $HSP70_{395\text{-}537}$ is colored by sky-blue and green. **b**, Difference Fourier map (Fo-Fc) at 3σ contour level showing the MYRLPNVHG peptide depicted as a stick model as it is situated in the substrate-binding pocket of HSP70. This map was calculated by the deletion model in MYRLPNVHG. Residue numbers corresponding to the DX2 sequence are labeled for the stick model. The numbers in the parenthesis correspond to the amino acid sequence numbers in the chimeric protein. **c**, MYRLPNVHG bound to HSP70 amino acid residues. The main chains of HSP70 containing A406, T429 and L439 residues (blue lettering) are shown interacting with the peptide by hydrogen bonding, as indicated by blue dashed lines. The L27(541) residue of the peptide sequence is bound to the hydrophobic core comprising the L403, F428, V438 and I440 residues (yellow lettering) of HSP70. The bonds for involved in the hydrophobic interaction are depicted by the yellow dashed lines. **d**, Structural similarity of the human HSP70-DX2 chimeric protein ($HSP70_{395\text{-}537\text{-}MYRLPNVHG}$) and *E. coli* DnaK-SBD containing the pyrrhocoricin-derived peptide (PDB ID: 3DPP). The carbon backbones of the chimeric protein and *E. coli* DnaK are shown in salmon and green colors, respectively. The MYRLPNVH sequence from DX2 binds to the substrate-binding site of HSP70 in a similar binding mode to that of pyrrhocoricin-derived peptide into the substrate-binding site. The sequences of pyrrhocoricin-derived peptide include LY-Cha-LPRPT (Cha denotes D-cyclohexyalanine) residues[29]. **e**, Graph showing the effect of mutations in the N-terminus of DX2 on its binding to HSP70. Significant amino acids revealed from crystallization were mutated to alanine residues and the mutant proteins tested for their ability to bind to HSP70 by an *in vitro* pull-down assay. Significant amino acids were colored in green. **f**, Strep-HSP70 wild type (WT) and F428A mutant were introduced into 293T cells expressing GFP-$DX2_{24\text{-}34}$.

Binding of the two proteins was determined by immunoprecipitation, followed by SDS-PAGE and Western blotting. **g**, 293T cells expressing GFP-DX2$_{24\text{-}34}$ and Strep-HSP70 were lysed and mixed with the different amounts of NRLLLTG peptide. After immunoprecipitation with streptavidin-Sepharose beads, the indicated proteins were determined by immunoblotting with the specific antibodies.

Figure 8. Determination of DX2 residues on GST domain involved in the interaction with HSP70.

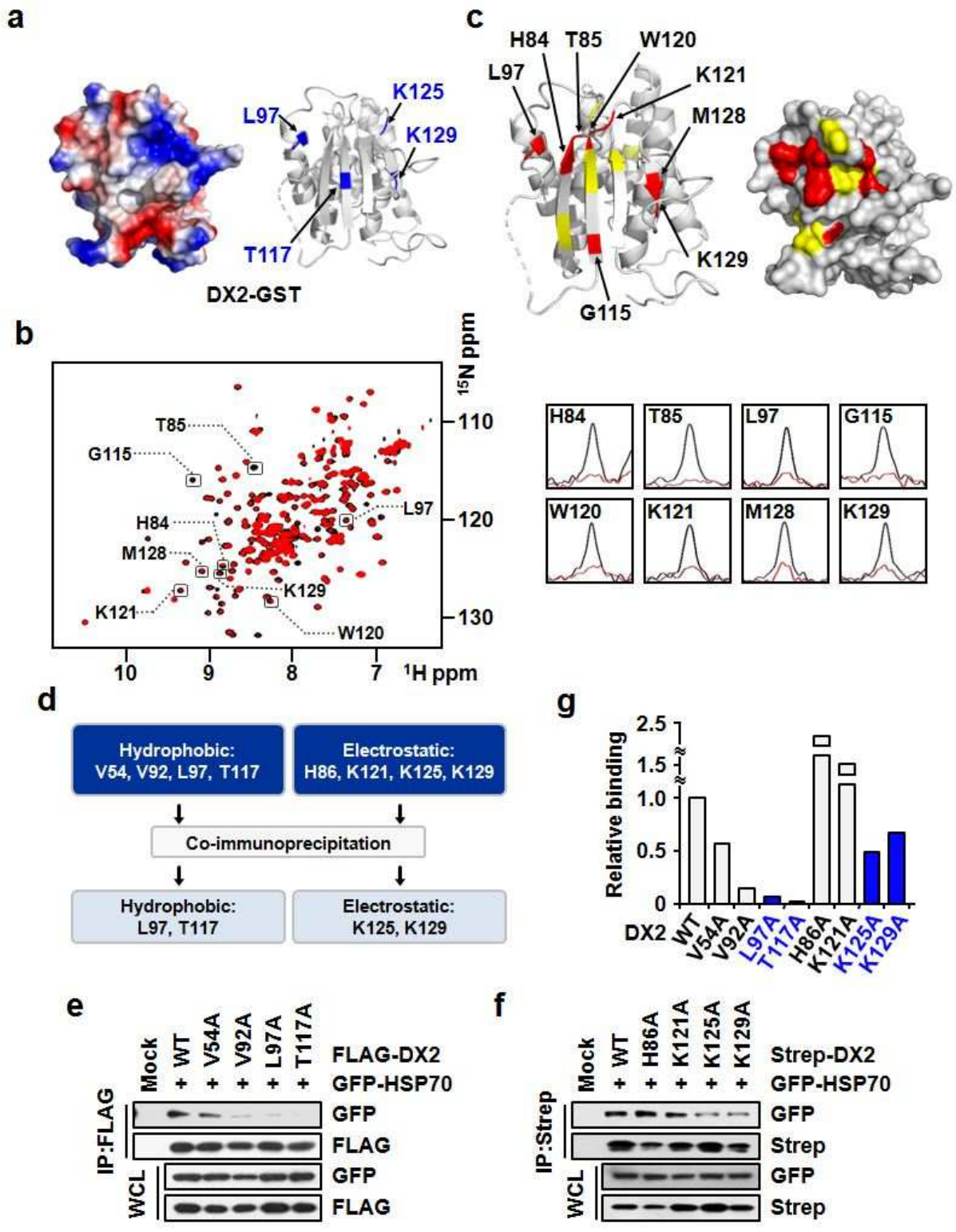

Figure 8. a, 3D structural models indicating the amino acid residues of the DX2-GST domain that are critical for binding, as predicted by NMR CSP analysis and mutation assays. The blue and red colors in the surface model indicate positive and negative charges, respectively. **b**, Superposition of the 2D ^{1}H-^{15}N TROSY spectra of ^{15}N-labeled $DX2_{51\text{-}251\text{-}C136S/C222S}$ in the presence (red) and absence (black) of $HSP70_{386\text{-}543}$. 1D cross sections of the perturbed residues with or without $HSP70_{386\text{-}543}$are shown in the boxes on the right. **c**, Mapping of the residues of DX2 GST that are perturbed in the presence of $HSP70_{386\text{-}543}$,based on the decreased NMR signal intensity. The DX2 structure is represented as a backbone ribbon (left) and surface model (right). Strongly and weakly perturbed residues are shown in red and yellow, respectively. **d**, Schematic flow diagram for identification of DX2 residues that are significant for its interaction with HSP70. From NMR analysis, 4 amino acids (V54, V92, L97 and T117) were selected as feasible for a hydrophobic interaction and another 4 amino acids (H86, K121, K125 and K129) for an electrostatic interaction. L97 and T117, and K125 and K129, which are involved in the hydrophobic and electrostatic interactions, respectively, were selected as the critical residues by co-immunoprecipitation. **e**, Validation of hydrophobic interaction residues of DX2 with HSP70. FLAG-DX2 mutants were immunoprecipitated with an anti-FLAG antibody and co-precipitation of GFP-HSP70 was determined by Western blotting with an anti-GFP antibody. **f**, Validation of electrostatic interaction residues of DX2 with HSP70. Indicated mutants were subjected to co-immunoprecipitation using a Strep-tactin column. **g**, Quantified binding intensity was normalized by expression in whole cell lysates (WCL), as shown in graph.

Figure 9. Determination of HSP70 residues involved in the interaction with DX2.

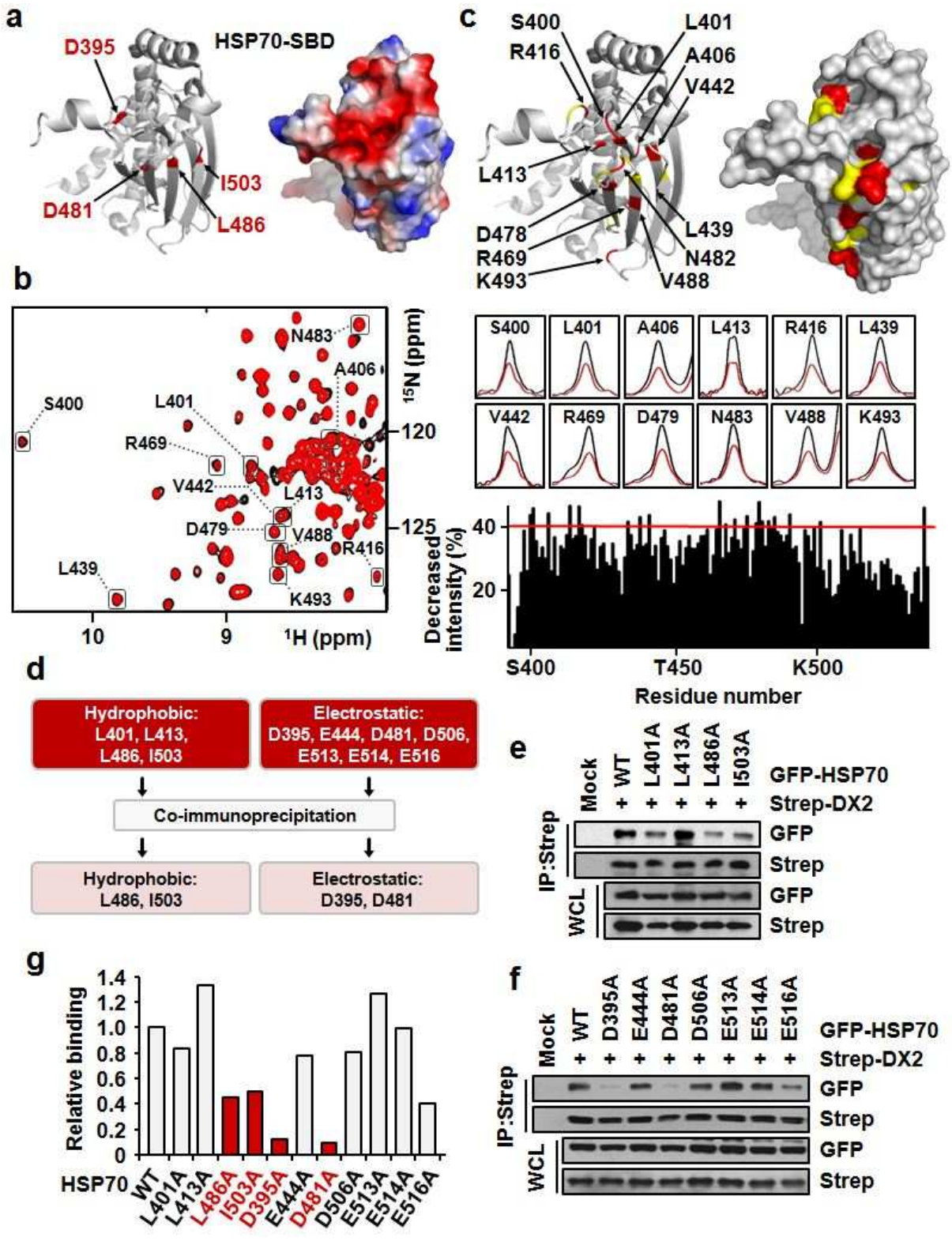

Figure 9. a, 3D structural models indicating the amino acid residues of the HSP70-SBD that are critical for binding, as predicted by NMR CSP analysis and mutation assays. The blue and red colors in the surface model indicate positive and negative charges, respectively. **b**, Close-up view of the superposition of the 2D ^{1}H-^{15}N TROSY spectra of ^{15}N-labeled $HSP70_{386-543}$ in the presence (red) and absence (black) of full length DX2. 1D cross sections of the perturbed residues with or without DX2 are shown in boxes (upper right). The decreased percentages of the signal intensities along the residue numbers of $HSP70_{386-543}$ through the DX2 binding are shown as a bar graph (bottom right). The residues showing more than 40% of signal broadening were selected for binding site mapping. **c**, Mapping of the residues in $HSP70_{386-543}$ perturbed by DX2 binding based on the decreased NMR signal intensity. The HSP70 structure is represented as a backbone ribbon (left) and surface model (right). Strongly and weakly perturbed residues are shown in red and yellow, respectively. **d**, Schematic flow for determination of the HSP70 residues critical for DX2 binding. From NMR analysis, 4 amino acids (L401, L413, L486 and I503) were selected as feasible for hydrophobic interactions with DX2 and another 7 amino acids (D395, E444, D481, D506, E513, E514 and E516) of HSP70 for electrostatic interactions. Among them, L486 and I503, and D395 and D481 were identified as significant residues for hydrophobic and electrostatic interactions with DX2, respectively, by co-immunoprecipitation assays. **e**, Validation of HSP70 residues involved in the hydrophobic interaction with DX2.Cells expressing GFP-HSP70 mutants and Strep-DX2 were subjected to co-immunoprecipitation with an anti-Strep antibody and co-precipitated GFP-HSP70 was determined by Western blotting with anti-GFP antibody. **f**, Validation of HSP70 residues involved in the electrostatic interaction with DX2. Co-immunoprecipitation using the indicated mutants was performed with streptavidin-Sepharose beads. **g**, Quantified binding intensity was normalized by expression of WCL and shown.

Figure 10. Validation of the significance of HSP70 binding for stabilization of DX2, and a complex model of DX2 and HSP70 binding.

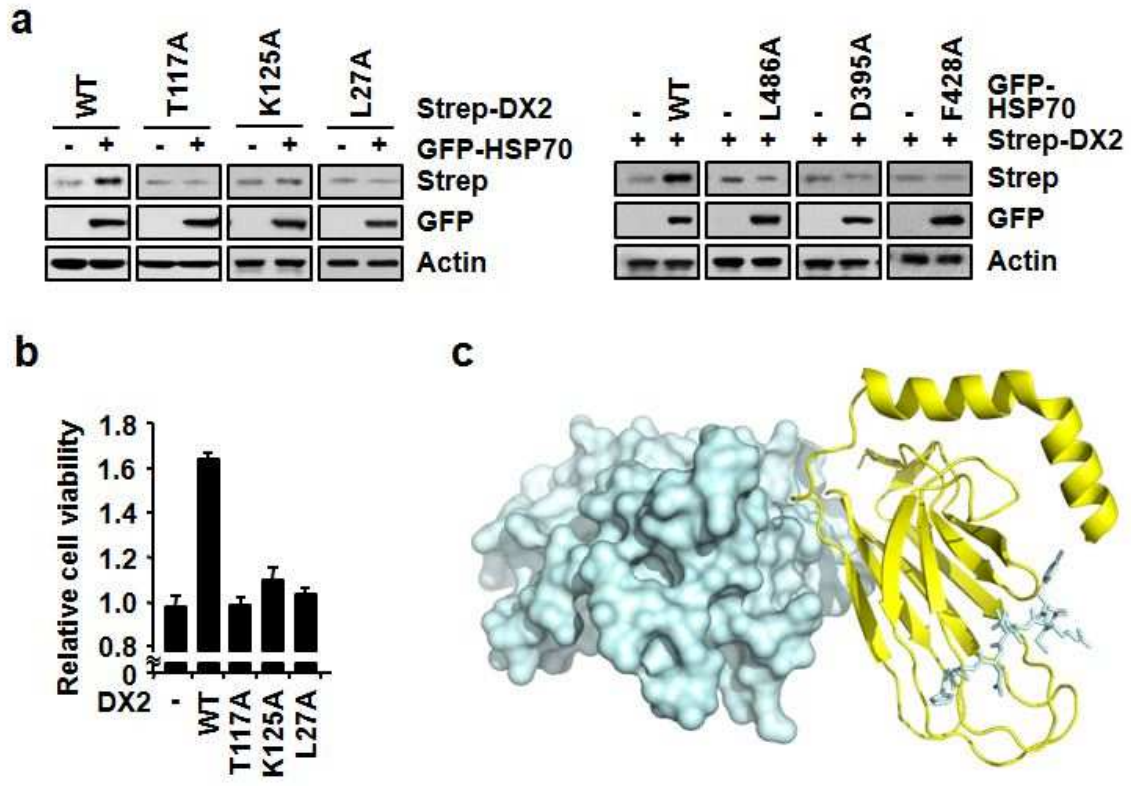

Figure 10. a, The effect of binding-defective mutations on HSP70-dependent stabilization of DX2. GFP-HSP70 was introduced into the cells expressing Strep-DX2 mutants (left) and GFP-HSP70 mutants were introduced into the Strep-DX2-expressing cells (right). Expressed proteins were determined by immunoblotting using a specific antibody against the protein tag. Actin was used as a loading control. **b**, Relative cell viability of 293T cells expressing Strep-DX2 wild type (WT) or mutants as determined by MTT assay. Each of the tested mutations was represented for hydrophobic (T117A) and electrostatic (K125A) binding of GST domain and N-terminal region (L27A) of DX2. The experiment was independently repeated three times and error bar means S.D. **c**, The complex model between DX2 and $HSP70_{395-537}$ based

on the $HSP70_{395\text{-}537\text{-}MYRLPNVHG}$ crystal structure and NMR binding studies. DX2 and $HSP70_{395\text{-}537}$ are represented as pale-cyan surface and pale-yellow ribbon model, respectively.

Figure 11. HSP70-mediated protection of DX2 from Siah1-mediated degradation.

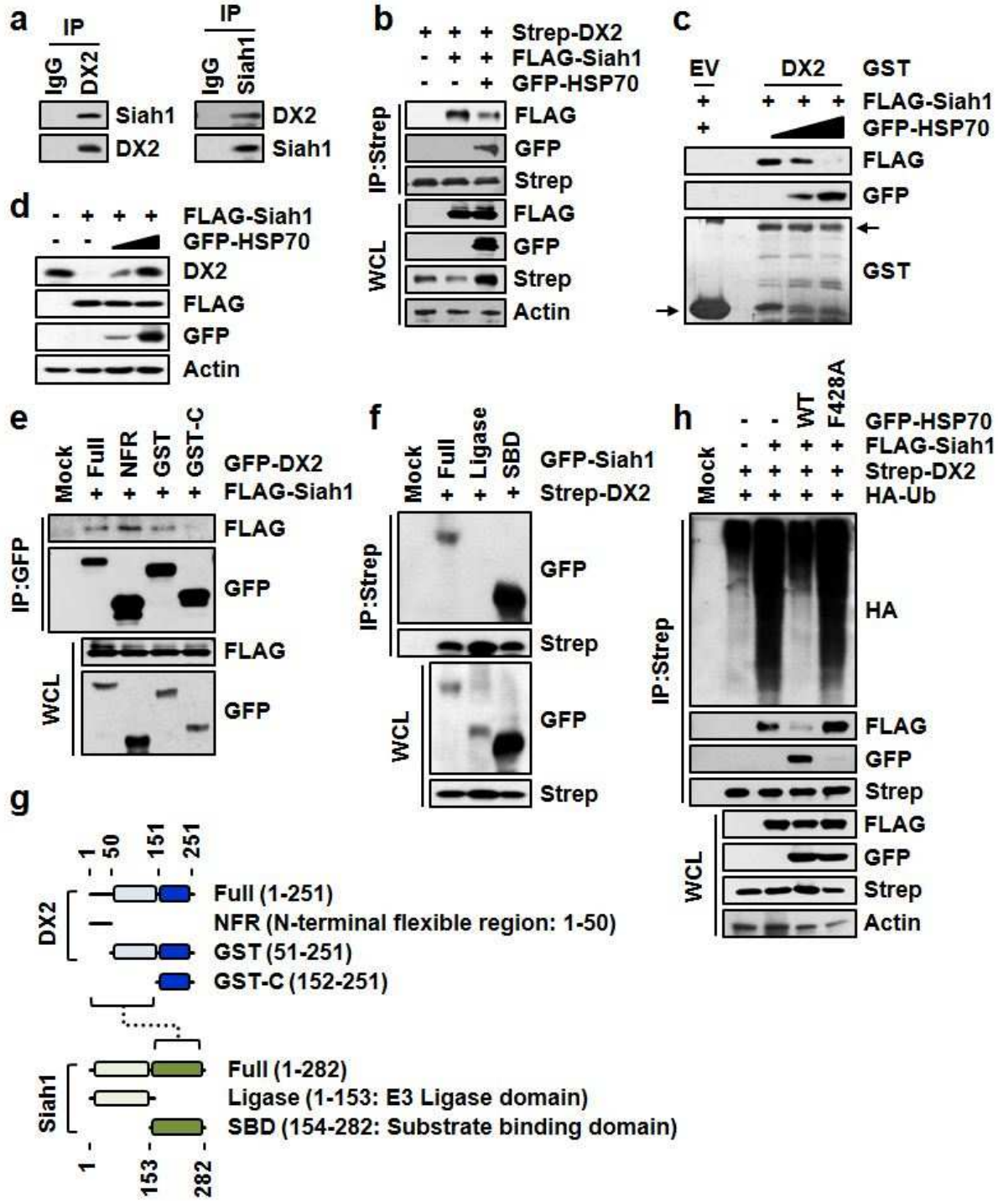

Figure 11. a, Endogenous binding between DX2 and Siah1 as revealed by immunoprecipitation. Both proteins were precipitated with their specific antibodies.

Endogenous DX2 and Siah1 were precipitated with their specific antibodies in left and right panel experiment, respectively. **b**, Binding of Siah1 to DX2 in the presence of ectopically-expressed HSP70. Strep-DX2, FLAG-Siah1, and GFP-HSP70 were expressed in 293T cells as indicated by labels on the top, and DX2-co-precipitated Siah1 and HSP70 were analyzed by SDS-PAGE and Western blotting using specific antibodies. Actin was used as a loading control. **c,** The effect of HSP70 on direct binding of DX2 and Siah1. Purified GST-DX2 was mixed with cell lysates expressing FLAG-Siah1 and different levels of GFP-HSP70 and precipitated with glutathione-Sepharose. Co-precipitated HSP70 and Siah1 were analyzed by SDS-PAGE and immunoblotting as described in Fig. 4b. GST-DX2 was detected and quantified by Coomassie staining. Arrows denotes the GST proteins. **d**, Levels of endogenous DX2 was detected in 293T cells expressing FLAG-Siah1 and GFP-HSP70 as indicated by labels. **e**-**f**, Determination of DX2 region mediating its binding to Siah1. (**e**) GFP-fusions of the full-length DX2 (Full) and the indicated deletion mutants (NFR, GST, and GST-C) were introduced into 293T cells expressing FLAG-Siah1 and precipitated with an anti-GFP antibody. Siah1 co-precipitated with DX2 was determined by Western blotting with an anti-FLAG antibody. (**f**) Interaction regions of Siah1 and DX2. GFP-fusions of the full-length Siah1 (Full) and the indicated mutants (Ligase and SBD) were co-expressed in 293T cells and complexes containing DX2 were precipitated with streptavidin-Sepharose beads. DX2 co-precipitating proteins were detected by Western blotting with an anti-GFP antibody. **g**, Schematic diagram of the interaction between Siah1, HSP70 and DX2. The binding regions of each protein are indicated by a dashed line. **h**, Siah1-dependent ubiquitination of DX2 in the presence of HSP70. HSP70 wild type (WT) or F428A mutant were introduced into 293T cells expressing FLAG-Siah1, Strep-DX2 and HA-tagged ubiquitin (HA-ub). Strep-DX2 in

the cell lysates was precipitated with streptavidin-Sepharose beads and its ubiquitination levels were analyzed by immunoblotting with the anti-HA antibody.

Figure 12. Screening for identification of the DX2 inhibitor, BC-DXI-495.

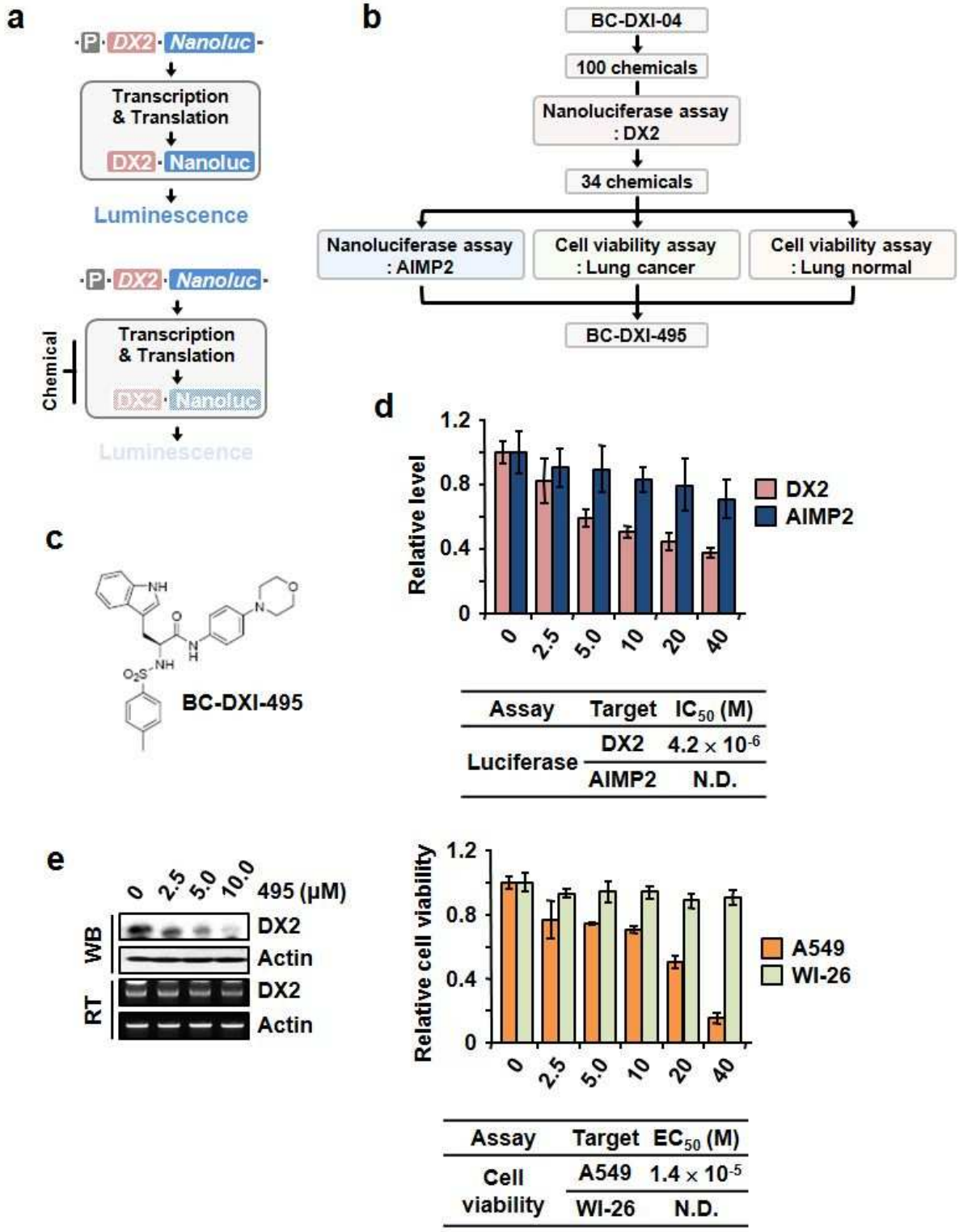

Figure 12. a, Schematic diagram of screening system using nanoluciferase assay. Nanoluciferase-tagged DX2 (Nanoluc-DX2) was expressed in A549 cells. The DX2 levels were estimated by luciferase assay after treatment with chemicals for 4 hours. **b**, Workflow of screening for selection of DX2 inhibitor, BC-DXI-495, from BC-DXI-04[25]. In primary screening for detecting the nanoluc-DX2, 34 out of 100 chemicals (library containing derivatives of BC-DXI-04)were selected with 60% as a cut-off value. 34 chemicals were subjected to secondary screenings, nanoluciferase assay for estimating level of AIMP2 and cell viability assay in lung cancer or normal cells. Chemicals that diminished the levels of AIMP2 and viability of normal lung cells were excluded. BC-DXI-495 was chosen as a hit chemical. **c**, Chemical structure of BC-DXI-495. **d**, A549 cells expressing each of nanoluc-DX2 or -AIMP2 were treated with BC-DXI-495 and subjected to luciferase assay (upper). A549 (cancer lung) and WI-26 (normal lung) cells were treated with BC-DXI-495 as above, and cell viability was determined by MTT assay (bottom). The relative level of each protein or cell viability compared to DMSO treatment is shown as a bar graph. IC_{50} and EC_{50} values were calculated (under the graph). All the experiments were repeated three times and error bar indicates S.D. **e**, Effect of BC-DXI-495 (495) on DX2 protein and mRNA levels. H460 cells were treated with the indicated amounts of BC-DXI-495 for 12 hrs. Levels of DX2 protein and mRNA were determined by immunoblotting and RT-PCR, respectively. Actin was used as a loading control.

Figure 13. PPI inhibitor, BC-DXI-495, interrupts DX2-HSP70 interaction.

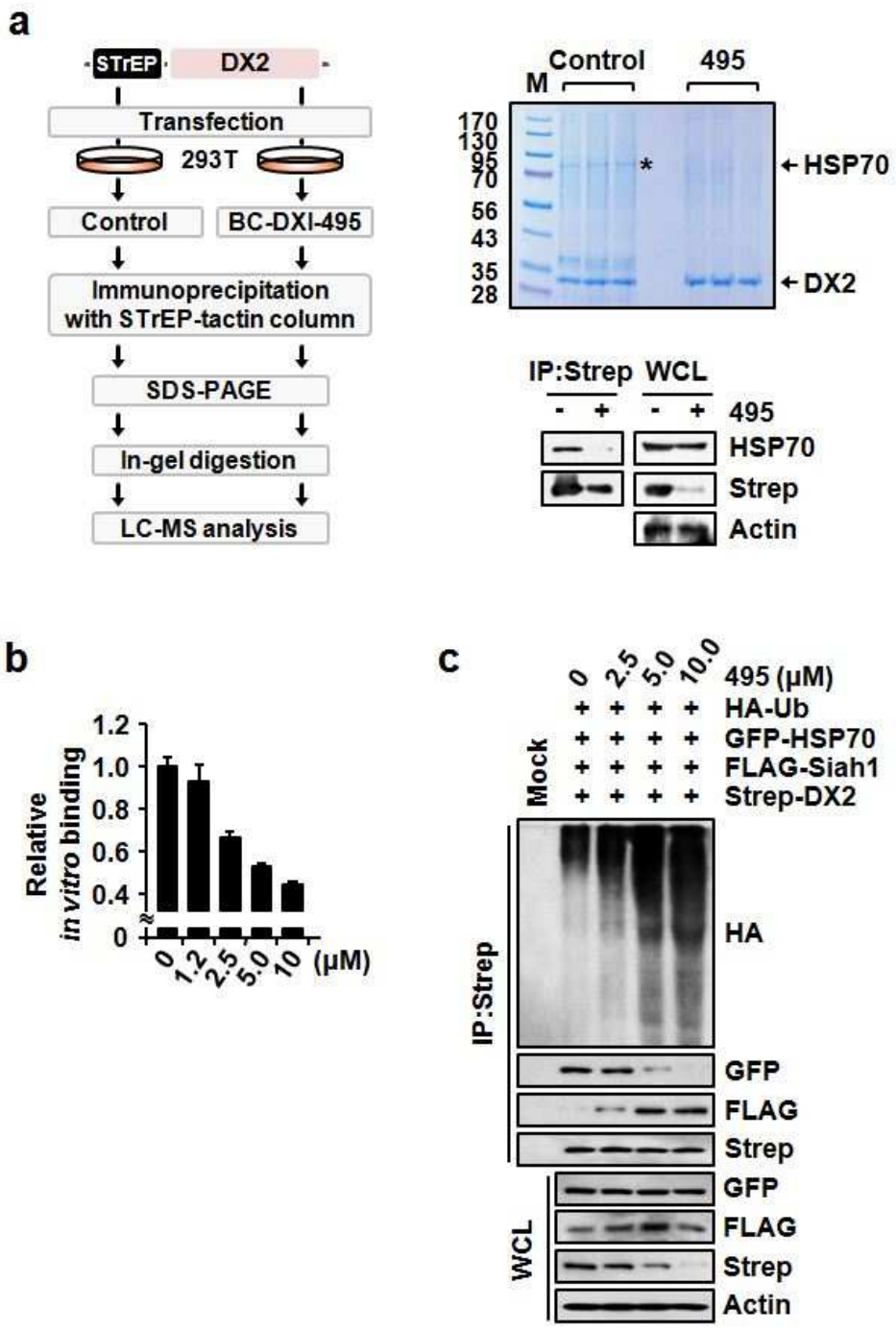

Figure 13. a, Effect of BC-DXI-495 on the DX2-HSP70 interaction in 293T cells. Experimental strategy (left). Strep-DX2-expressing 293T cells were treated with BC-DXI-

495 (40 μM) and precipitated with a Strep-tactin column. Co-precipitates with DX2 were subjected to SDS-PAGE and LC-MS analysis. A coomassie-stained gel and immunoblot containing immunoprecipitates (right top and bottom, respectively). Asterisk indicates HSP70 co-precipitated with DX2 that was further validated by mass analysis (right top). The result was confirmed by Western blotting (right bottom). DMSO was used as a control. M denotes the size marker. The numbers on the left of the gel image denotes molecular weight (kDa). **b**, The ability of BC-DXI-495 to inhibit binding of DX2 and HSP70. The indicated concentration of BC-DXI-495 were pre-incubated with DX2 and the binding of DX2 to HSP70 was monitored by ELISA. **c**, The effect of BC-DXI-495 on Siah1-mediated DX2 ubiquitination. 293T cells expressing Strep-DX2, FLAG-Siah1, GFP-HSP70 and HA-ub were treated with the indicated concentrations of BC-DXI-495. After immunoprecipitation of Strep-DX2, the amounts of ubiquitination and binding of DX2 were determined by SDS-PAGE and immunoblotting using the indicated antibodies.

Figure 14. Effect of the PPI inhibitor, BC-DXI-495, on DX2-mediated proliferation.

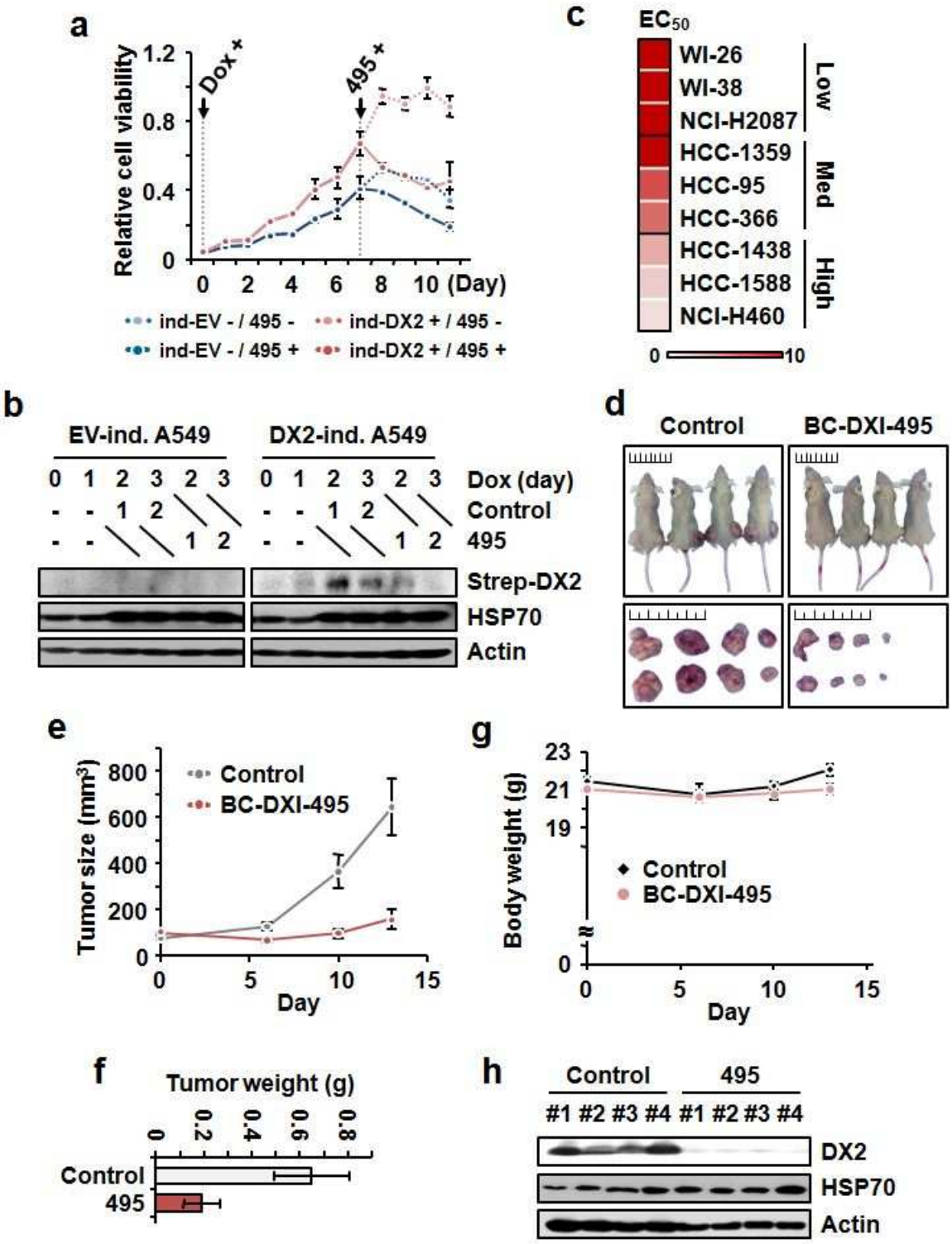

Figure 14. a, The effect of BC-DXI-495 on cell viability in DX2-expressing A549 cells. The MTT assay was used to determine cell viability in DX2-inducible A549 cells (ind-DX2) after doxycycline (Dox+) and BC-DXI-495 (495+; 40 μM) were added at the indicated time. DMSO was used as a negative control for BC-DXI-495. Ind-EV denotes the empty vector-, negative control for DX2, inducible A549 cells. **b**, In DX2-inducible cells treated with doxycycline and 495 as indicated, DX2 and HSP70 levels were determined by Western blotting with their specific antibodies. Actin was used as a loading control. **c**, The EC_{50} of BC-DXI-495 in lung cell lines expressing different levels of DX2, The EC_{50} of BC-DXI-495 in lung cancer and normal cell lines (WI-26 and WI-38) expressing various level of DX2 (low to high, as indicated on the right) was determined by the MTT assay. The relative EC_{50}values were graded from 0 to 10, as represented in the heat map. **d**-**j**, The effect of BC-DXI-495 on cancer progression in an *in vivo* mouse xenograft model. H460 cells were subcutaneously xenografted in nude mice, and BC-DXI-495 (50 mg/kg) was intraperitoneally administered for 2 weeks. Tumor size (**e**) and body weight (**g**) were monitored for the period of injection. Photos of the tumor-bearing mice and excised tumors (**d**) and bar graph showing tumor weight (**f**). The cellular levels of the indicated proteins in excised tumors were analyzed by Western blotting using their specific antibodies. The number of mouse was indicated on top (**j**). All the experiments were independently repeated three times and the error bars indicate S.D.

Figure 15. Significance of BC-DXI-495 on DX2 binding.

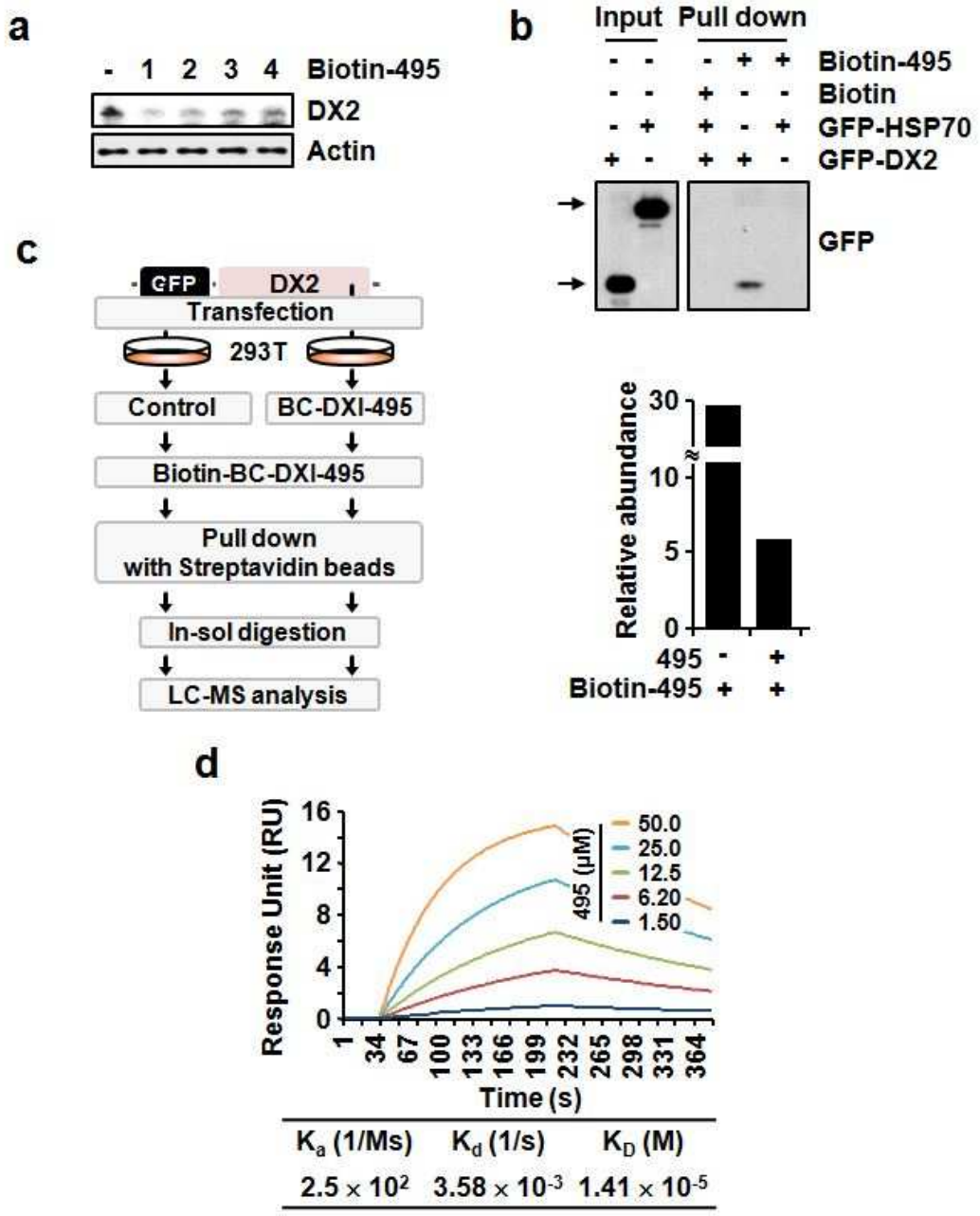

Figure 15. a, H460 cells were treated with 4 other biotinylated BC-DXI-495 (Biotin-495) and endogenous level of DX2 was determined by immunoblotting. Actin was used as a loading control. **b**, Specificity of BC-DXI-495 (495) binding to DX2. Biotin-495 was mixed with cell lysates from cells expressing GFP-HSP70 or GFP-DX2. Proteins that co-

precipitated with biotin-495 in an *in vitro* pull-down using streptavidin-Sepharose beads were subjected to SDS-PAGE and Western blotting using anti-GFP antibody. Biotin was used as a negative control for biotin-495. Arrows denotes GFP-tagged proteins. **c**, Strategy of LC-MS analysis for confirmation of interaction between BC-DXI-495 and DX2. Biotin-495 was used to compete with BC-DXI-495. After pull-down with biotin-495, the abundance of DX2 in the precipitates was analyzed by mass spectrometry and represented as a bar graph. **d**, Purified DX2 proteins were immobilized and multiple concentration of BC-DXI-495 were flowed for SPR analysis. BC-DXI-495 directly bound to DX2 with a value of 14 μM $K_{D.}$

Figure 16. Mode of action of BC-DXI-495 on DX2.

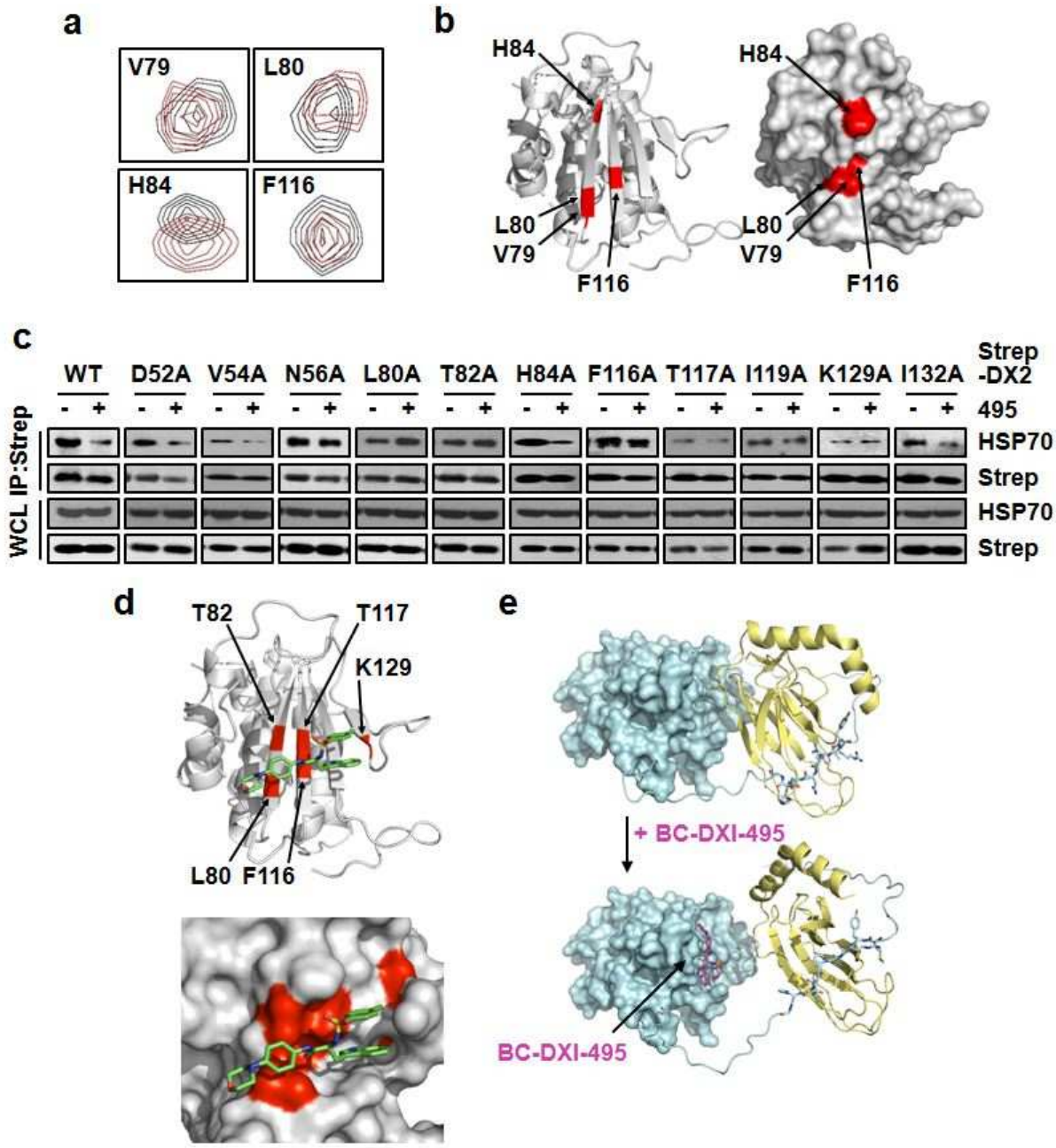

Figure 16. a, Detection of BC-DXI-495 binding region of DX2 using an NMR-based chemical shift perturbation (CSP) assay. Superposition of the 2D ^{1}H-^{15}N TROSY spectra of ^{15}N-labeled $DX2_{51\text{-}251\text{-}C136S/C222S}$ in the presence (red) and absence (black) of BC-DXI-495. The residues perturbed byBC-DXI-495 are shown in boxes. **b**, Mapping of the residues of

DX2 GST domain that are perturbed in the presence of BC-DXI-495,based on the decreased NMR signal intensity and CSP, represented as a backbone ribbon model (left) and surface model (right). Strongly perturbed residues are shown in red. **c**, Identification of DX2 residues critical for binding to BC-DXI-495. 293T cells expressing each of the Strep-DX2 alanine-substitution mutants were treated with BC-DXI-495. Strep-DX2 proteins in the cell lysates were isolated by immunoprecipitation with streptavidin-Sepharose beads. **d**, Docking of BC-DXI-495 in the DX2 GST domain based on the NMR CSP analysis and mutation assay. Residues led to loss of binding via mutation are represented on the backbone model (upper) and surface model (bottom) in red. **e**, Proposed model of the DX2 and $HSP70_{395\text{-}537}$ complex based on the $HSP70_{395\text{-}537\text{-}MYRLPNVHG}$ structure and NMR binding studies. DX2 and $HSP70_{395\text{-}537}$ are represented as sky-blue surface and pale-yellow ribbon models, respectively. The line model represents the DX2 N-terminal (residues 1-23) and linker region (residues 33-50). The N-terminal M24-G32 residues of DX2 were represented as stick model. The BC-DXI-495 compound is represented as a magenta stick model on the surface of the DX2 GST domain.

Figure 17. Significance of BC-DXI-495 binding on DX2 in *in vivo* model.

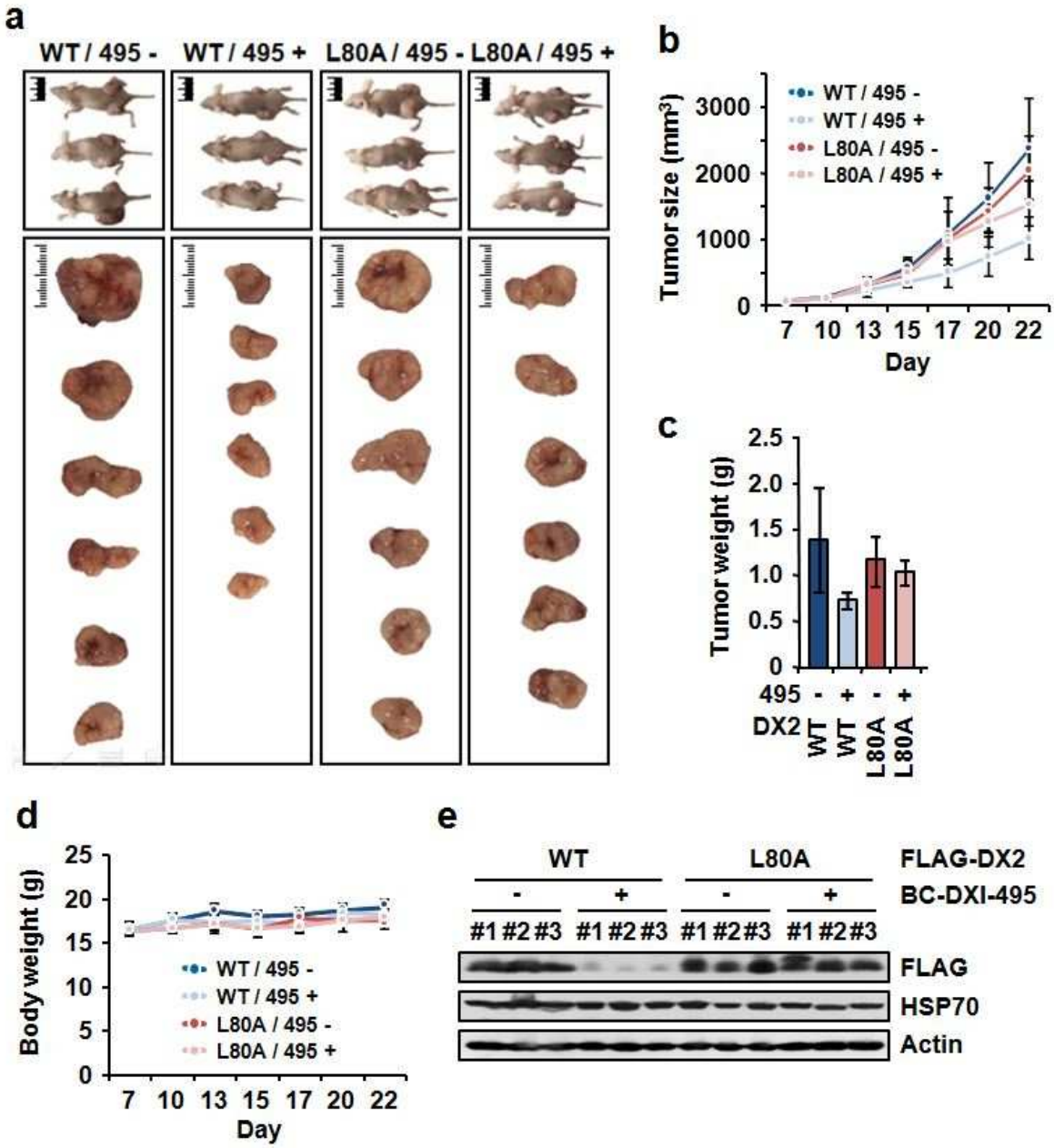

Figure 17. a-e, H460 cells stably expressing FLAG-DX2 wild type (WT) or the DX2 L80A mutant were subcutaneously injected into the backs of nude mice and BC-DXI-495 (50 mg/kg) was injected intraperitoneally for 15 days. The tumor volume (**b**) and body weight (**d**) were monitored during the experimental period. The embedded tumors were excised and

weighed after sacrifice of the mice (**c**), and the protein levels of FLAG-DX2, HSP70 and actin in the excised tumor were analyzed by Western blotting using their specific antibodies (**e**).

Table 1. List of the DX2 top50 interactome

* The protein list is sorted according to the fold change.

Description	Gene symbol	Fold Change (DX2/EV)
Bifunctional aminoacyl-tRNA synthetase	EPRS	4640.0
Aspartyl-tRNA synthetase, cytoplasmic	DARS	3563.3
Isoleucyl-tRNA synthetase, cytoplasmic	IARS	3193.3
aminoacyl tRNA synthetase complex-interacting multifunctional protein 2	AIMP2	2370.0
heat shock 70kDa protein 8	HSPA8	1960.0
heat shock 60kDa protein 1 (chaperonin)	HSPD1	1944.5
leucyl-tRNA synthetase	LARS	1656.7
actin, gamma 1	ACTG1	886.7
methionyl-tRNA synthetase	MARS	840.0
Isoform Cytoplasmic of Lysyl-tRNA synthetase	KARS	806.7
78 kDa glucose-regulated protein	HSPA5	603.3
Stress-70 protein, mitochondrial (mortalin)	HSPA9	510.0
arginyl-tRNA synthetase	RARS	506.7
ATP synthase, H+ transporting, mitochondrial F1 complex, beta polypeptide	ATP5B	496.7
Isoform 1 of Clathrin heavy chain 1	CLTC	443.3
T-complex protein 1 subunit alpha	TCP1	350.0
chaperonin containing TCP1, subunit 7 (eta)	CCT7	333.3
heat shock 105kDa/110kDa protein 1	HSPH1	330.0
Mitochondrial import inner membrane translocase subunit Tim13	TIMM13	320.0
splicing factor 3b, subunit 3, 130kDa	SF3B3	316.7
glutaminyl-tRNA synthetase	QARS	303.3
chaperonin containing TCP1, subunit 6A (zeta 1)	CCT6A	276.7
Aminoacyl tRNA synthase complex-interacting multifunctional protein 1	AIMP1	266.7
Isoform 1 of Protein-L-isoaspartate(D-aspartate) O-methyltransferase	PCMT1	260.0
dihydrolipoamide branched chain transacylase E2	DBT	240.0
chaperonin containing TCP1, subunit 2 (beta)	CCT2	236.7

GrpE protein homolog 1, mitochondrial	GRPEL1	230.0
ATPase, Na+/K+ transporting, alpha 1 polypeptide	ATP1A1	230.0
carbamoyl-phosphate synthetase 2, aspartate transcarbamylase, and dihydroorotase	CAD	220.0
cDNA FLJ56386, highly similar to Heat shock 70 kDa protein 1L	HSPA1L	200.0
ataxin 2-like	ATXN2L	186.7
heat shock 70kDa protein 2	HSPA2	176.7
filamin A, alpha	FLNA	173.3
heat shock 70kDa protein 4	HSPA4	170.0
damage-specific DNA binding protein 1, 127kDa	DDB1	170.0
ATP synthase, H+ transporting, mitochondrial F1 complex, alpha subunit 1, cardiac muscle	ATP5A1	166.7
Proteasome subunit beta type-1	PSMB1	160.0
Isoform 1 of Filamin-B	FLNB	153.3
proteasome (prosome, macropain) 26S subunit, non-ATPase, 1	PSMD1	150.0
Proteasome subunit beta type-3	PSMB3	146.7
apoptosis-inducing factor, mitochondrion-associated, 1	AIFM1	146.7
Heat shock 70 kDa protein 1A	HSPA1B	143.4
ATPase, Ca++ transporting, cardiac muscle, slow twitch 2	ATP2A2	143.3
cDNA FLJ56389, highly similar to Elongation factor 1-gamma	EEF1G	140.0
Proteasome 26S non-ATPase subunit 11 variant (Fragment)	PSMD11	136.7
proteasome (prosome, macropain) subunit, alpha type, 4	PSMA4	133.3
WD repeat domain 82	WDR82	130.0
33 kDa protein	RPSA	126.7
26S proteasome non-ATPase regulatory subunit 2	PSMD2	126.7
leucine-rich pentatricopeptide repeat containing	LRPPRC	113.3
cDNA FLJ55002, highly similar to Alpha-centractin	ACTR1A	110.0

Table 2. Data collection and Refinement statistics

	HSP70 $_{394\text{-}537\text{-}MYRLPNVHG}$
Wavelength (Å)	0.9795
Resolution (Å)	28.08 - 1.79 (1.854 - 1.79)
Space group	$P\ 2_1\ 2_1\ 2_1$
Unit cell	41.111 77.054 88.711 90 90 90
Total reflections	211834 (19718)
Unique reflections	27052 (1776)
Multiplicity	7.8 (8.0)
Completeness (%)	94.56 (66.54)
Mean *I/sigma* (I)	10.42 (2.52)
Wilson B-factor	17.31
R-merge	0.1388 (0.8994)
Refinement	
Reflections used in refinement	25781 (1776)
Reflections used for *R*-free	2000 (138)
R-work	0.1835 (0.2819)
R-free	0.2194 (0.3337)
Protein residues	305
RMS (bonds, Å)	0.006
RMS (angle, °)	0.95
Ramachandran favoured, allowed (%)	100.00
Ramachandran outliers (%)	0.00
Rotamer outliers (%)	0.76
Statistics for the highest-resolution shell are shown in parentheses.	

R-work is the conventional crystallographic *R* factor, ∑|FO-FC|/∑|FO|;FO and FC mean the observed and calculated structure factors, respectively. R-free is a free *R*factor evaluated for

the 5% reflections excluded from the refinement in the PHENIX program

Discussion

The chaperone activities of HSPs have attracted much attention as potential cancer therapy targets[7]. However the ability to specifically control the pathologic activities of HSPs without affecting their physiological roles in protein folding remains challenge. Here, I show one example of how a tumor-promoting interaction of HSPs can be specifically controlled. While HSP70 traditionally has been known as a helper that delivers protein clients to HSP90[12], recent reports have shown that HSP70 also can function as a chaperone independently of HSP90[14,33]. In addition to its inherent chaperone activity, studies have also suggested that HSP70 protects the client from physical attack, access of E3 ligase, through an interaction with HSP70's SBD[14]. The underlying mechanism for this interaction, is not yet well understood. However, to this end, the structural analysis presented herein shows that the binding of the substrate-binding domain of HSP70 to the N-terminal flexible region and GST domain of DX2 protects DX2 from Siah1-mediated ubiquitination. Moreover, preventing HSP70 binding to DX2 by mutational and chemical inhibition destabilized DX2, suggesting HSP70 is functionally significant in maintaining cellular levels of DX2.

The binding between DX2 and HSP70 takes place in two phases. In the first phase, the NFR of DX2 accesses the substrate-binding pocket of the HSP70's SBD through hydrophobic interactions, as visualized by x-ray crystallography (Fig. 7). I determined that the Y25 and L27 residues of DX2 and L403, F428, V438 and I440 residues of HSP70 are potentially important for hydrophobic interactions. The substrate-binding pocket in HSP70's SBD recognizes the substrates *via* specifically aligned hydrophobic amino acids[30]. Although

the N-terminal sequence of DX2 differs from the canonical sequence of HSP70 substrates, a few hydrophobic amino acids in DX2-NFR such as Y25 and L27 appear to play crucial roles in HSP70 binding. Determined binding mode of DX2-NFR's hydrophobic peptide region is highly similar to the pyrrhocoricin-derived peptide that tightly binds to DnaK (PDB 3DPP)[29]. In addition, the F428 residue of HSP70, which is a well-known hydrophobic residue involved in client recognition, was also determined crucial for the interaction with DX2-NFR, suggesting that HSP70 uses the consensus-binding mode[11,34]in its recognition of DX2.

The second phase of binding involves the β-sheet surface in the DX2 GST domain and the hinge region between the α-helical Lid and β-stranded SBD of HSP70 (Fig. 8-9). The DX2's L97 and T117 residues and HSP70's L486 and I503 residues participate in a hydrophobic interaction while DX2's positively charged K125 and K129 residues and HSP70's negatively charged D395 and D481 residues participate in an electrostatic interaction. The DX2-GST domain and HSP70-SBD are likely precisely positioned through electrostatic interaction and bind with strong affinity through the hydrophobic interaction. Our structural model based on the x-ray and NMR data herein provides critical information on how HSP70 could recognize its clients and protect them from ubiquitin-mediated degradation (Fig. 10c).

Here I clearly demonstrated that Siah1 functions as the E3 ligase for DX2 ubiquitination, extending earlier observation that the levels of DX2 and Siah1 are negatively correlated[32]. Our data also shows that Siah1 binding to DX2 was competitively blocked by HSP70. While the competitive regulation between HSP70 and Siah1 appears to maintain the appropriate cellular levels of DX2, the high levels of HSP70 in cancer cells may lead to elevated levels of DX2 by preventing its ubiquitin-mediated degradation[4,7]. Since DX2-NFR

is structurally disordered, it is vulnerable to protease attack and ubiquitination-mediated degradation. Binding of this peptide region to the substrate-binding pocket of HSP70-SBDmay protect DX2 from ubiquitination by Siah1, leading to high levels of DX2. Whether HSP70 binding to DX2 also mediates proper folding will be the focus of future studies.

Given its high levels of expression in cancer cells and tumorigenic activities, DX2 can be considered a promising target for cancer therapies. However, finding ways to suppress its expression or activity has been challenging for its structural disorder and lack of stabilizing mechanism. Thus, our identification of a specific, tumor-promoting interaction between HSP70 with DX2has provided a novel and attractive target point. This concept was validated by our demonstration that chemical inhibition of the DX2-HSP70 interaction suppressed DX2-induced tumor growth. This result also provides insight into potential mechanisms for specifically controlling the activities of HSPs. While HSPs could also serve as attractive cancer targets, inhibiting chaperone activities might cause adverse effects since their clients include numerous cellular factors. However, here I demonstrated the fine control of HSP70 activity by specifically blocking one particular client, DX2. Clinical application of such an approach would be most effective for patients expressing high levels of HSP70 and DX2.

Methods

Cell culture and materials. H522, H1435, H460, SW900, H1793, H854, H358, H727, H23, HCC-1438, HCC-1195, H441, H1299, Calu-6, HCC-1588, HCC-1359, HCC-366, WI-26, HCC-95, H1755, H226, SK-LU-1, WI-38, HCC-2279, H1650, H2087, H1666, SK-MES-1, NCI-H1792 and 293T cell lines were purchased from ATCC and the Korea Cell Line Bank. 293T cells and other cell lines were cultured in DMEM and RPMI supplemented with 10% FBS and 1% penicillin/streptomycin, respectively, and grown in 5% CO_2 at 37°C. GFP-tagged HSP70 (#15215) and HSP90 (#108221) were purchased from Addgene. The gene encoding DX2 was cloned into the *Eco*RI/*Xho*I sites of pEXPR-IBA5, pEGFP-C2 and pcDNA3.0 vectors. FLAG-tagged Siah1 was purchased from the Korea Human Gene Bank, Medical Genomics Research Center, KRIBB. Mutagenesis of DX2 and HSP70 was performed with Quik-ChangeII (Promega), following the manufacturer's instruction. Cycloheximide, MG-132, and okadaic acid were purchased from and Sigma. The procedure for preparing the anti-DX2 antibody and its characterization will be provided upon request. Specific antibodies against Strep and FLAG were purchased from IBA and Sigma, respectively, and other antibodies used in this study were purchased from Santa Cruz Biotechnology.

Protein preparation. DX2 (residues 1-251), $DX2_{1\text{-}50}$, and $DX2_{51\text{-}251\text{-}C136S\text{-}C222S}$ were cloned into yeast Small Ubiquitin-like modifier (SUMO)-modified pET28a vector (yeast SUMO-pET28a). The SUMO sequence was inserted between *Nhe*I and *Bam*HI of pET28a vector to

prepare the epitope-tagged version of SUMO, His-SUMO. The DX2 sequence was inserted between the *Bam*HI and XhoI sites of the vector. The plasmid was transformed into *E.coli* BL21-Codon Plus(DE3)-RIPL (Stratagene, USA), cells were grown in Luria-Bertani (LB) media (Merck Millipore) at 18°C, and expression was induced by 0.5 mM isopropyl β-D-1-thiogalactopyranoside (IPTG). The cells were harvested and disrupted in lysis buffer (50 mM Tris-HCl pH 7.4, 500 mM NaCl, 7 mM β-mercaptoethanol, 1 mM PMSF and 10% glycerol). After centrifugation at 32,500×g for 60 min, the His-SUMO fused DX2 was purified using Ni-NTA column chromatography using 50 mM Tris-HCl pH 7.4, 500 mM NaCl, 40mM imidazole as the equilibrium buffer. After elution with 500 mM imidazole, the His-SUMO tag was cleaved by the SUMO protease Ulp1. The tag-free version of DX2 was concentrated by ultrafiltration and further purified by size exclusion chromatography using a Superdex 75 16/60 column (GE Healthcare, UK) equilibrated with a buffer containing 25 mM Tris-HCl pH 7.4, 150 mM NaCl, 7 mM β-mercaptoethanol, 0.1 mM EDTA and 1 mM PMSF. Human HSP70, $HSP70_{1\text{-}613}$, $HSP70_{386\text{-}543}$, $HSP70_{395\text{-}543}$, $HSP70_{395\text{-}613}$, $HSP70_{395\text{-}537\text{-}MYRLPNVHG}$ were cloned and purified using the same protocol as for DX2. NRLLLTG peptide was synthesized and provided by the Korea Basic Science Institute (KBSI)

Protein crystallization and data collection. Crystallization of the chimeric $HSP70_{395\text{-}537\text{-}MYRLPNVHG}$ protein was initially performed with the JBScreen wizard (Jena Bioscience) using the sitting-drop vapor diffusion method, and was optimized by the hanging-drop vapor diffusion method at 20°C. After optimization, the best crystal was obtained under reservoir conditions of 25% PEG1500, 15 mM SPG (pH 5.5) in drops where 1.2 μl of protein solution (8 mg/ml) was mixed with 1.2 μl of reservoir solution. The crystal was transferred to a cryo-

protectant solution containing an additional 10% glucose in the crystallization solution, prior to x-ray diffraction data collection. The diffraction screening and data collection were performed by using the CCD detector, ADSC Q315r and Q270, at beamline 5C and 7A at Pohang Accelerator Laboratory (PAL), respectively (Pohang, Korea). The HKL2000 was used for data processing, involved index, and integration and merging[35]. This crystal belongs to the space group *P*212121. The unit cell dimensions are *a*=41.111, *b*=77.054, *c*=88.711 and α=β=γ=90°. This structure contains two protein monomers in an asymmetric unit.

Structure determination and refinement. The structure of the human HSP70-DX2 chimera protein ($HSP70_{395\text{-}537\text{-}MYRLPNVHG}$) was determined by molecular replacement and refinement using the PHENIX program[36]. The Coot[37] and PHENIX program were also used for modeling and structural refinement, respectively. A model published by another group (PDB ID: 4WV5) was used as an initial model for molecular replacement[38]. PHENIX and CCP4i were used to generate of each of maps, including the composite-omit map for refinements[39]. The final structure of the human HSP70-DX2 chimera protein was determined at 1.79Å resolution. Statistics of the intensity data and the refinement are summarized in Table 2.

NMR spectroscopy. The ^{15}N-labelled proteins were prepared by growing the bacterial cells in M9-minimal media enriched with $^{15}NH_4Cl$ as the sole nitrogen source (99% ^{15}N; Cambridge Isotope Laboratories). Protein expression and purification were carried out as described above. Protein samples were dialyzed overnight at 4°C against a buffer containing 20 mM Bis-Tris pH 6.0, 150 mM NaCl, 7 mM β-mercaptoethanol, 0.1 mM EDTA and 1 mM PMSF. All NMR measurements were performed at 298°K with an Avance 600 MHz NMR

spectrometer (Bruker, Germany). For the binding and competition experiment using the DX2, HSP70 and NRLLLTG peptide, the ^{1}H-^{15}N TROSY (transverse relaxation optimized spectroscopy) experiments were performed after a 1day at 4°C incubation of 0.2 mM ^{15}N-labeled full length DX2 ($DX2_{1-251}$) in the absence and presence of 0.1 mM full length HSP70 ($HSP70_{1-641}$). Then, we added the mixture of 1 mM NRLLLTG peptide and 0.1 mM $HSP70_{1-641}$ after incubation at 4°C for 1 day to 0.2 mM ^{15}N-labeled $DX2_{1-251}$ and performed ^{1}H-^{15}N TROSY. As a control experiment, ^{1}H-^{15}N TROSY was performed on a mixture of 0.2 mM ^{15}N-labeled $DX2_{1-251}$ and 1 mM NRLLLTG peptide. To determine the region of DX2 that bind to $HSP70_{386-543}$, ^{1}H-^{15}N TROSY experiments were performed on 0.4 mM ^{15}N-labeled DX2-NFDin the presence and absence of 4 mM $HSP70_{395-613}$ after incubating the mixture at 4°C for 1 day. Steady-state ^{15}N-^{1}H-heteronuclear NOE spectra were measured with either 10-s delays between each free-induction decay or 6-s delays followed by a 4-s series of nonselective ^{1}H pulses. ^{15}N-^{1}H NOE experiments were performed with time-domain sizes of 152 × 2048 complex points. A 25% non-uniform sampling (NUS) schedule was applied and sweep widths of 6009.615 Hz and 1338.330 Hz were set along the ^{1}H and ^{15}N dimensions, respectively, with 64 scans for the experiment. Data were processed with MddNMR (version 2.5) in the NmrPipe environment. ^{15}N-^{1}H-heteronuclear NOE values were calculated from the ratio of peak intensities, I_{sat}/I_{unsat}, where I_{sat} and I_{unsat} represent the intensities of peaks in saturated and unsaturated spectra, respectively. To determine the binding region of DX2 with BC-DXI-495, the ^{1}H-^{15}N TROSY experiments were performed with 0.2 mM ^{15}N-labeled $DX2_{1-251}$ with 0.5% DMSO in the presence and absence of 0.2 mM BC-DXI-495.

Modeling for the complex of DX2 and HSP70 substrate-binding domain. Docking

simulations were performed with the HADDOCK program[40] using the energy minimized atomic coordinates of the DX2 GST domain (PDB ID 5A34) and HSP70 substrate binding domain from the structure of $HSP70_{395\text{-}537\text{-}MYRLPNVHG}$. For HADDOCK calculations, the N56, L80, S81, H84, T85, S87, L97, G115, L118, I119, W120, K121, M128 and K129 residues of the AIMP2 GST domain were treated as active residues, and the S400, L401, L413, R416, N417, D479, A482, N483, G484 and L486 residues of the human HSP70 substrate-binding domain were treated as active residues based on the CSP data. The active residues were treated as flexible in the docking simulation. The remaining residues in the interfaces were treated as passive. The most stable structure of the major populated first cluster was used for analysis.

Docking of BC-DXI-495 on the structure of DX2. Structure of DX2-GST obtained from PDB 5A34 was energy minimized and prepared for docking using Gasteiger charge, protein structure was kept rigid in docking and BC-DXI-495 binding site was defined from CSP mapped residues obtained from NMR binding experiments. Dimensions of a grid with 72 × 54 × 64 points and 0.375 Å grid spacing were used for the sampling of ligand conformations. BC-DXI-495 was modeled with SYBYL-X 2.0 molecular modeling package(http://tripos.com), and energy minimized with Gasteiger-Hückel charge setin vacuum dielectric environment, using Powell algorithm and Tripos force field for 5000 iterations subject to a termination gradient of 0.05 kcal/(mol·Å). Energy minimized BC-DXI-495 was prepared for Autodock, Gasteiger charges were assigned. Autodock4.2[41] (http://autodock.scripps.edu/) was used to sample 200 docking poses of ligand. Ligand conformations were sampled by Lamarckian genetic algorithm, parameters were set as 200

independent runs, an initial population of 150 randomly placed individuals, with 2.5×10^6 energy evaluations, a maximum number of 27000 iterations, a mutation rate of 0.02, a crossover rate of 0.80, and an elitism value of 1. A representative docking pose was selected from the highest populated cluster. PyMOL[42] (http://www.pymol.org) was used for manual inspection of distances.

Chemical library generation and chemical probe synthesis. Previous study reported that four chemicals were identified as a DX2-inhibitory chemicals from the screening the ChemDiv's library. Four chemicals were named BC-DXI-01~04, and BC-DXI-04, a sulfonamide type chemical, was selected for further study in this research. Of note, sulfonamides are significant class of synthetic compounds that are present in various drugs or drug candidates targeting diuretics, antibiotics, caner, or inflammation[43]. Accordingly, in-house chemical library was constructed, including derivatives of BC-DXI-04, and BC-DXI-495 was chosen as a novel lead. In addition the chemical probes of BC-DXI-495 were designed and prepared for further mechanism study.

Mass spectrometry. 293T cell lysates (5 mg) expressing Strep-empty vector (EV) or -DX2 were subjected to Strep-tactin column chromatography. Elutes were digested by in-gel digestion using trypsin/Lys-C (Promega). After purification of tryptic peptides using a C_{18} spin column, the peptide mixture was subjected to analysis using LTQ-Orbitrap Velos (Thermo Fisher Scientific) connected to an Easy-nano LC II system (Thermo Fisher Scientific) that incorporated an autosampler. One-tenth of the peptides re-suspended in 0.1% formic acid was injected into a reversed-phase peptide trap EASY-Column (L 2 cm, ID 100

μm, 5 μm, 120 Å, ReproSil-Pur C_{18}-AQ, Thermo Fisher Scientific) and a reversed-phase analytical EASY-Column (L 10 cm, ID 75 μm, 3 μm, 120 Å, ReproSil-Pur C_{18}-AQ, Thermo Fisher Scientific). Electrospray ionization was subsequently performed using a 30 μm nano-bore stainless steel online emitter (Thermo Fisher Scientific). The total duration of LC gradient procedure was 120 min. The LTQ-Orbitrap Velos mass analyzer was operated in positive ESI mode using collision induced dissociation (CID) to fragment the HPLC separated peptides. The data were analyzed with Sequest (XCorr Only) (Thermo Fisher Scientific, San Jose, CA, USA; version v.27, rev.11) and X! Tandem (The GPM, thegpm.org; version CYCLONE (2010.12.01.1)) using a human database (Uniprot human, release 2014). Scaffold program (version 4.6.1, Proteome Software Inc., Portland, OR) was used to validate the MS/MS-based peptide and protein identifications and to process the quantitative analysis. For identifying the BC-DXI-495-binding protein, GFP-DX2-expressing 293T cells treated with BC-DXI-495 were lysed and the lysates subjected to pull-down using a Strep-tactin column. Proteins in the elutes were analyzed as above. To validate the binding of BC-DXI-495 to DX2, 293T cells expressing GFP-tagged DX2 were serially treated with BC-DXI-495 and biotinylated BC-DXI-495. The biotinylated chemicals were pulled down and co-precipitates analyzed by the same protocol as described above.

Surface plasmon resonance (SPR) analysis. The binding affinity of BC-DIX-495 to DX2 was measured using a Reichert SR7500DC instrument (Reichert Technologies, Depew, NY). To determine the binding affinity between DX2 and BC-DXI-495, TRX-DX2 and TRX was immobilized at levels of 5580 and 2000RU, respectively, with 10 mM sodium acetate buffer (pH 5.5) on a PEG chip (Reichert, Depew, NY). BC-DXI-495 (1.5 - 50 μM) in 2% DMSO-

containing PBS binding buffer (pH 7.4) was flowed at a rate of 30 μl/min. Sensorgrams were fitted to a simple 1:1 Langmuir interaction model (A + B AB) using the Scrubber 2.0 analysis program (BioLogic Software, Australia, and Kaleida Graph Software, Australia).

Xenograft. DX2 wild type (WT) and L80A mutant were cloned into pcDNA3.0 and expressed in H460 cells cultured for two weeks in the presence of 800 μg/mlG418 (Duchefa). After selection, the settled colonies were picked and the level of overexpressed proteins was evaluated by immunoblotting using an anti-FLAG antibody. The cells (2×10^7) stably expressing DX2 WT and the L80A mutant were subcutaneously inoculated into the left and right sites of the back of 7-weeks-old female BALB/cAnCr mice (n=3 / group), and BC-DXI-495 (50 mg/kg) was intraperitoneally administrated every other day for 15 days. The embedded tumor sizes and body weights were measured two times a week for the experimental period. All the mice were sacrificed and the size and weight of the embedded tumor were measured after photos of mice were taken. Animal experiments were in compliance with the University Animal Care and Use Committee guidelines at Seoul National University.

Immunohistochemistry staining. Tissue micro array (TMA) slides (US Biomax, Inc.) containing lung tumor and matched normal tissues from same patients were deparaffinized and rehydrated in different percentages (100, 95, 80 and 70%) of ethanol. To remove the endogenous peroxidases and retrieve the antigen samples were incubated with PBS containing 0.3% H_2O_2 (Sigma) for 10 minutes and 10 mM citric buffer (pH 6.0) at 95°C for 5 minutes, respectively. After blocking with PBS containing 4% BSA for 30 minutes, the slides

were incubated with the primary antibodies, DX2 or HSP70 (Novusbio), at 4°C for 12 hours and anti-rabbit- or -mouse-HRP (Dako) for 1 hour, respectively. A 3,3′-Diaminobenzidine (DAB) and Chromogen mixture (Dako) was used to develop the slides and nuclear counter staining was performed with Mayer's hematoxylin (Sigma). The slides were dehydrated with different concentrations of ethanol (70, 80, 90 and 100%) and then mounted. The staining intensity of the proteins was graded to 0 (<5% positive), 1 (5-40% positive), and 2 (>40% positive). The numerical grade was confirmed by a second independent examination.

***In vitro* pull-down assay**. Cell lysates expressing the GFP-tagged proteins were mixed with purified GST-tagged proteins in 50 mM Tris-HCl (pH 7.4) binding buffer containing 100 mM NaCl, 0.5% Triton X-100, 10% glycerol, 1 mM EDTA, and protease inhibitor (Calbiochem) and incubated for 12 hours at 4°C. After incubation, the GST proteins were precipitated using glutathione Sepharose beads and washed with binding buffer three times. Proteins that co-precipitated with GST proteins were then subjected to SDS-PAGE. The amounts of GFP-tagged proteins were determined by immunoblotting with a GFP-specific antibody and amounts of GST-tagged proteins were determined by Coomassie staining..

Enzyme-linked immunosorbent assay (ELISA). Purified DX2 protein (150 ng/well) was coated on a flat-bottom 96-well plate (Thermo) in 0.05M sodium carbonate buffer (pH 9.6). After washing with PBST (0.05% Tween20), PBST including 1% BSA solution was used for blocking for 1 hour at room temperature. The plates were pre-incubated with diluted BC-DXI-495and purified HSP70 (150 ng/well) was added to the wells for the binding reaction. After washing with PBST, the primary antibody against HSP70and secondary antibody were

sequentially bound for overnight and 1 hour, respectively. After washing, 3,3',5,5'-tetramethylbenzidine (TMB) solution (Thermo) was added for the detection of bound HSP70 and incubated for 10 minutes. The reaction was then stopped by the addition of 1N H_2SO_4 and absorbance was evaluated at 450 nm (Ref: 620 nm).

Co-immunoprecipitation. H460 cells were lysed with 50 mM Tris-HCl (pH 7.4) lysis buffer containing 100 mM NaCl, 0.5% Triton X-100, 0.1% SDS, 10% glycerol, 1 mM EDTA, and protease inhibitor (Calbiochem). The cell lysates were mixed with HSP70 antibody that was pre-incubated with agarose G for 12 hours and washed three times with cold lysis buffer excluding 0.1% SDS. 293T cells expressing Strep- and GFP-tagged proteins were lysed as described above and Strep-tagged proteins were precipitated with a Strep-tactin column (IBA), following the manufacturer's instruction. Co-precipitates with bait proteins were separated by SDS-PAGE and subjected to Western blotting with specific antibodies to the proteins of interest.

Anchorage-independent colony formation assay. The Strep-empty vector (EV) or Strep-DX2 was introduced into H460 cells stably expressing sh-con or sh-HSP70 (Santa Cruz Biotechnology). The cells were subjected to anchorage-independent colony formation assay using a cell transformation assay kit (CELL BIOLABS, INC.), following the manufacturer's instruction. After culturing the cells for 1 week, the number of colonies stained by MTT solution (Sigma) was counted as described below. The experiments were repeated three times.

MTT assay. H460 cells (1 x 10^4) were cultured in 96 well plate for 24 hours. 10 μl of MTT solution (5 mg/ml, Sigma) was added to each well and incubated for 1.5 hour at 37 °C. The precipitated formazan crystals were dissolved with 100 μl DMSO (Duchefa) after discarding the cell culture media. Absorbance was measured at 560 nm using a micro plate reader (Sunrise, TECAN). The experiments were repeated three times independently.

EdU assay. The Strep-empty vector (EV) or -DX2 was introduced into 293T cells grown on coverslips in 24 well plates that expressed si-HSP70 (Santa Cruz Biotechnology).After determining the levels of DX2 and HSP70 by Western blotting using specific antibodies to the proteins, the cells were subjected to an ethynyldeoxyuridine (EdU) assay using the EdU Cell Proliferation Assay kit (Merck), following the manufacturer's instruction. DAPI was used for staining the nuclei. The fluorescence signal was detected by confocal microscopy and quantified for equal numbers of cells. The experiments were repeated three times independently.

RT-PCR. Total RNA from H460 cells was extracted using an RNeasy Mini Kit (Qiagen) and subjected to RT-PCR with dNTP, random hexamer and Moloney murine leukemia virus (MMLV). The same volume of RNA was used in a PCR assay to detect the mRNA expression of DX2, HSP70, and Actin using the following specific primers:

DX2: CTGGCCACGTGCAGGATTACGGGG and AAGTGAATCCCAGCTGATAG;

HSP70: GTCGTCCAGCACCCAGGCCAGC and GCTCTTGTTCAGGTCGCGCCCG;

Actin: CCTTCCTGGGCATGGAGTCCT and GGAGCAATGATCTTGATCTT.

References

1. Hartl, F.U., Bracher, A. & Hayer-Hartl, M. Molecular chaperones in protein folding and proteostasis. *Nature***475**, 324-32 (2011).
2. Mayer, M.P. Hsp70 chaperone dynamics and molecular mechanism. *Trends Biochem Sci***38**, 507-14 (2013).
3. Feder, M.E. & Hofmann, G.E. Heat-shock proteins, molecular chaperones, and the stress response: evolutionary and ecological physiology. *Annu Rev Physiol***61**, 243-82 (1999).
4. Kumar, S. et al. Targeting Hsp70: A possible therapy for cancer. *Cancer Lett***374**, 156-166 (2016).
5. Goloudina, A.R., Demidov, O.N. & Garrido, C. Inhibition of HSP70: a challenging anti-cancer strategy. *Cancer Lett***325**, 117-24 (2012).
6. Calderwood, S.K. & Gong, J. Heat Shock Proteins Promote Cancer: It's a Protection Racket. *Trends Biochem Sci***41**, 311-323 (2016).
7. Wu, J. et al. Heat Shock Proteins and Cancer. *Trends Pharmacol Sci***38**, 226-256 (2017).
8. Sherman, M.Y. & Gabai, V.L. Hsp70 in cancer: back to the future. *Oncogene***34**, 4153-61 (2015).
9. Alderson, T.R., Kim, J.H. & Markley, J.L. Dynamical Structures of Hsp70 and Hsp70-Hsp40 Complexes. *Structure***24**, 1014-30 (2016).
10. Sekhar, A., Rosenzweig, R., Bouvignies, G. & Kay, L.E. Hsp70 biases the folding

pathways of client proteins. *Proc Natl Acad Sci U S A***113**, E2794-801 (2016).

11. Sekhar, A., Rosenzweig, R., Bouvignies, G. & Kay, L.E. Mapping the conformation of a client protein through the Hsp70 functional cycle. *Proc Natl Acad Sci U S A***112**, 10395-400 (2015).
12. Alvira, S. et al. Structural characterization of the substrate transfer mechanism in Hsp70/Hsp90 folding machinery mediated by Hop. *Nat Commun***5**, 5484 (2014).
13. Nillegoda, N.B., Wentink, A.S. & Bukau, B. Protein Disaggregation in Multicellular Organisms. *Trends Biochem Sci***43**, 285-300 (2018).
14. Mashaghi, A. et al. Alternative modes of client binding enable functional plasticity of Hsp70. *Nature***539**, 448-451 (2016).
15. Kim, S., You, S. & Hwang, D. Aminoacyl-tRNA synthetases and tumorigenesis: more than housekeeping. *Nat Rev Cancer***11**, 708-18 (2011).
16. Park, S.G., Ewalt, K.L. & Kim, S. Functional expansion of aminoacyl-tRNA synthetases and their interacting factors: new perspectives on housekeepers. *Trends Biochem Sci***30**, 569-74 (2005).
17. Han, J.M. et al. AIMP2/p38, the scaffold for the multi-tRNA synthetase complex, responds to genotoxic stresses via p53. *Proc Natl Acad Sci U S A***105**, 11206-11 (2008).
18. Kim, M.J. et al. Downregulation of FUSE-binding protein and c-myc by tRNA synthetase cofactor p38 is required for lung cell differentiation. *Nat Genet***34**, 330-6 (2003).
19. Kim, D.G. et al. Oncogenic Mutation of AIMP2/p38 Inhibits Its Tumor-Suppressive Interaction with Smurf2. *Cancer Res***76**, 3422-36 (2016).
20. Choi, J.W. et al. AIMP2 promotes TNFalpha-dependent apoptosis via ubiquitin-

mediated degradation of TRAF2. *J Cell Sci***122**, 2710-5 (2009).

21. Yum, M.K. et al. AIMP2 Controls Intestinal Stem Cell Compartments and Tumorigenesis by Modulating Wnt/beta-Catenin Signaling. *Cancer Res***76**, 4559-68 (2016).
22. Choi, J.W. et al. Cancer-associated splicing variant of tumor suppressor AIMP2/p38: pathological implication in tumorigenesis. *PLoS Genet***7**, e1001351 (2011).
23. Choi, J.W. et al. Splicing variant of AIMP2 as an effective target against chemoresistant ovarian cancer. *J Mol Cell Biol***4**, 164-73 (2012).
24. Jung, J.Y. et al. Ratio of Autoantibodies of Tumor Suppressor AIMP2 and Its Oncogenic Variant Is Associated with Clinical Outcome in Lung Cancer. *J Cancer***8**, 1347-1354 (2017).
25. Lee, H.S. et al. Chemical suppression of an oncogenic splicing variant of AIMP2 induces tumour regression. *Biochem J***454**, 411-6 (2013).
26. Won, Y.S. & Lee, S.W. Selective regression of cancer cells expressing a splicing variant of AIMP2 through targeted RNA replacement by trans-splicing ribozyme. *J Biotechnol***158**, 44-9 (2012).
27. Clerico, E.M., Tilitsky, J.M., Meng, W. & Gierasch, L.M. How hsp70 molecular machines interact with their substrates to mediate diverse physiological functions. *J Mol Biol***427**, 1575-88 (2015).
28. Zahn, M. et al. Structural studies on the forward and reverse binding modes of peptides to the chaperone DnaK. *J Mol Biol***425**, 2463-79 (2013).
29. Taniguchi, M. et al. Pyrrhocoricin, a proline-rich antimicrobial peptide derived from insect, inhibits the translation process in the cell-free Escherichia coli protein synthesis system. *J Biosci Bioeng***121**, 591-8 (2016).

30. Zhang, P., Leu, J.I., Murphy, M.E., George, D.L. & Marmorstein, R. Crystal structure of the stress-inducible human heat shock protein 70 substrate-binding domain in complex with peptide substrate. *PLoS One***9**, e103518 (2014).

31. Xu, W. et al. Surface charge and hydrophobicity determine ErbB2 binding to the Hsp90 chaperone complex. *Nat Struct Mol Biol***12**, 120-6 (2005).

32. Oh, A.Y. et al. Inhibiting DX2-p14/ARF Interaction Exerts Antitumor Effects in Lung Cancer and Delays Tumor Progression. *Cancer Res***76**, 4791-804 (2016).

33. Verchot, J. Cellular chaperones and folding enzymes are vital contributors to membrane bound replication and movement complexes during plant RNA virus infection. *Front Plant Sci***3**, 275 (2012).

34. Meng, W., Clerico, E.M., McArthur, N. & Gierasch, L.M. Allosteric landscapes of eukaryotic cytoplasmic Hsp70s are shaped by evolutionary tuning of key interfaces. *Proc Natl Acad Sci U S A***115**, 11970-11975 (2018).

35. Otwinowski, Z. & Minor, W. Processing of X-ray diffraction data collected in oscillation mode. *Methods Enzymol***276**, 307-26 (1997).

36. Adams, P.D. et al. PHENIX: a comprehensive Python-based system for macromolecular structure solution. *Acta Crystallogr D Biol Crystallogr***66**, 213-21 (2010).

37. Emsley, P. & Cowtan, K. Coot: model-building tools for molecular graphics. *Acta Crystallogr D Biol Crystallogr***60**, 2126-32 (2004).

38. Hassan, A.Q. et al. The novolactone natural product disrupts the allosteric regulation of Hsp70. *Chem Biol***22**, 87-97 (2015).

39. Winn, M.D. et al. Overview of the CCP4 suite and current developments. *Acta Crystallogr D Biol Crystallogr***67**, 235-42 (2011).

40. Dominguez, C., Boelens, R. & Bonvin, A.M. HADDOCK: a protein-protein docking approach based on biochemical or biophysical information. *J Am Chem Soc***125**, 1731-7 (2003).

41. Morris, G.M. et al. AutoDock4 and AutoDockTools4: Automated docking with selective receptor flexibility. *J Comput Chem***30**, 2785-91 (2009).

42. Alexander, N., Woetzel, N. & Meiler, J. bcl::Cluster : A method for clustering biological molecules coupled with visualization in the Pymol Molecular Graphics System. *IEEE Int Conf Comput Adv Bio Med Sci***2011**, 13-18 (2011).

43. Gulcin, I. & Taslimi, P. Sulfonamide inhibitors: a patent review 2013-present. *Expert Opin Ther Pat***28**, 541-549 (2018).

Chapter 2

ERK-dependent phosphorylation on linker and substrate-binding domain of HSP70 increases folding activity and cell proliferation

Running title: Phosphorylation of HSP70 by ERK enhances activity

Keywords: HSP70, ERK, phosphorylation, conformational change, folding, proliferation

Abbreviations list

EGF: Epidermal growth factor

ERK: Extracellular signal-regulated kinase

HSP70: Heat Shock Protein 70

ATP: Adenosine triphosphate

IP: Immunoprecipitation

WCL: Whole cell lysate

The list of figures

Figure 1. EGF-dependent phosphorylation of HSP70 *via* ERK.

Figure 2. Identification of HSP70 phosphorylation residues.

Figure 3. Significance of HSP70 phosphorylation on protein folding.

Figure 4. Phosphorylation-mediated conformational change of HSP70.

Figure 5. Significance of HSP70 phosphorylation in cell proliferation.

Figure 6. Schematic representation for phosphorylation of HSP70 *via* ERK and its cellular function.

Abstract

Enhanced productive folding of a translated polypeptide *via* heat shock protein 70 (HSP70) is often required for survival of cancer cells. Although the folding activity of HSP70 is considered a significant determinant for progression of cancer cells, it is still unknown how this activity could be regulated. Here, I report the phosphorylation of HSP70 that facilitates its folding activity, enhancing cell proliferation. Mass spectrometry confirmed serine residues at positions 385 and 400 on the linker and substrate-binding domain of HSP70, respectively, as the phosphorylation sites upon EGF signal, and this result was further confirmed by site-directed mutagenesis. ERK is discovered to be a specific kinase. Phosphorylation of the two sites induces the extended conformation of HSP70 *via* control the binding of linker to nucleotide- and substrate-binding domain, augmenting the binding affinity of substrate to HSP70 and folding activity, resulting in pro-proliferative function. Cell lines harboring activated ERK basically showed the phosphorylation of HSP70,and a positive correlation between phosphorylation of HSP70 and activity of ERK was observed. Thus, this study demonstrates that ERK-dependent phosphorylation of HSP70 facilitates its folding activity and cellular proliferative function.

Keywords: HSP70, ERK, phosphorylation, conformational change, folding, proliferation

Student number: 2014-30557

Introduction

The 70-kDa heat shock protein (HSP70) is a family of ubiquitous molecular chaperone proteins that play an important role in protein folding and protecting the cell from the heat shock and toxic stresses[1,2]. In addition to its canonical function, HSP70 is critical for cell proliferation, apoptosis and protein degradation in various diseases, especially cancer, and thus, it has been considered as a potential target for anticancer therapeutics[3-5]. HSP70 is composed of two other highly conserved domains, nucleotide-binding domain (NBD) and substrate-binding domain (SBD), which are connected *via* a flexible linker[6]. SBD is further divided into the two parts; one is SBDβ, which is existing substrate-binding pocket for binding with the client, and the other is SBDα, called lid, which is involved in tightening the binding of client[7]. For proper folding of client protein, HSP70 undergoes two conformational changes, adenosine triphosphate (ATP)- and adenosine diphosphate (ADP)-bound form[6]. When client binds with the SBD of ATP-bound form, HSP70 conducts hydrolysis of ATP, inducing the conformational change to ADP-bound form, closing and exposing the lid and linker, respectively[7,8]. After the release of properly folded protein, HSP70 again transforms to ATP-bound form followed by reduced linker dynamics[7,8]. Although only fine-tuning of the nucleotide-dependent cycling of HSP70 conformation has been studied as a determinant of protein folding, recently, a new aspect, post-translational modification, has also attracted attention for regulation of the function of HSP70.

Phosphorylation among the various post-translational modifications is transient, however it is considered as a strong determinant of various cellular signaling pathways[9].

Phosphorylation of HSP70 has been slightly unraveled in various cellular contexts by a few studies. During protein translation, phosphorylation of HSP70 regulates its dimerization or protein degradation *via* HSP70-binding protein, CHIP[10,11]. Regulation of cell cycle and apoptosis *via* phosphorylation of HSP70 has been already reported, and phosphorylation of HSP70 was explored in terms of chemoresistance of cancer cells[12,13].Studies on phosphorylation of HSP70 are focused on phosphorylation in NBD and SBD because of unawareness of the significance about linker, which is critical for regulating the activity of HSP70. However, several reports have recently focused on the fine-tuned dynamics of HSP70 *via* linker[8,14]. Here I report the phosphorylation sites, serine 385 and 400, on the linker. Both the phosphorylation sites are phosphorylated by ERK upon EGF signal and induce the extended conformation of HSP70. Phosphorylation-dependent extended conformation leads to the enhanced activity of HSP70, resulting in the increased cell proliferation.

Results

ERK phosphorylates HSP70

Augmented productive folding of the translated peptides is very important for the enhanced proliferation capacity of cancer cells[4]. Although the level of heat shock proteins in cancer cells is not associated with successful folding, the translated peptides are folded well[17,18]. Since the activity of HSP70 in cancer cells has been reported to be increased by phosphorylation, I investigated whether HSP70 is phosphorylated *via* EGF signaling pathway, critical for cancer progression[19,20]. Using immunoprecipitation on the cells expressing Strep-HSP70, it was monitored that the serine residues of HSP70 are phosphorylated *via* EGF signaling (Fig. 1a). To determine the kinase responsible for phosphorylation of HSP70, I treated the cells with several inhibitors, U0126, SB203580, SP600125 and LY294002, for targeting the downstream kinases of EGF signal pathway[21]. EGF-dependent phosphorylation on serine residues of HSP70 was diminished by treatment with only U0126, inhibitor of mitogen-activated protein kinase kinases, MEK-1 and MEK-2, and no other inhibitors, implying that ERK is specific kinase for phosphorylation of HSP70 *via* EGF signaling (Fig. 1b). To investigate whether ERK directly phosphorylates HSP70, I performed *in vitro* kinase assay using purified ERK proteins and confirmed ERK-mediated increase of HSP70's phosphorylation in dose-dependent manner (Fig. 1c), suggesting that ERK is direct kinase for phosphorylation of HSP70. The phosphorylation on serine residues of HSP70 was also observed by overexpression of ERK (Fig. 1d).

Next, I investigated whether the binding between HSP70 and ERK is induced via

EGF signaling, because binding between substrate and kinase is essential for phosphorylation. When the cells were treated with EGF, endogenous and exogenous binding of ERK to HSP70 was induced (Fig. 1e and f, respectively), suggesting that EGF-dependent phosphorylation of HSP70 is mediated by ERK. Direct interaction of the two proteins was further confirmed by *in vitro* pull-down assay (Fig. 1g). I also checked whether EGF signal-mediated activation of ERK is required for binding of the two proteins. Upon treatment with U0126, binding of ERK to HSP70 declined, suggesting the significance of ERK activity for binding to HSP70 (Fig. 1h). Taken together, ERK was revealed as the specific kinase responsible for EGF signal-dependent phosphorylation of HSP70.

Serine at positions 385 and 400 of HSP70are phosphorylated by EGF stimuli

Next, the phosphorylation sites of HSP70 were determined. Strep-HSP70-expressing 293T cells were treated with or without EGF, and the precipitated Strep-HSP70 was subjected to LC-MS analysis for identifying the phosphorylated residues of HSP70 (Fig. 2a). Two other peptides containing the phosphorylated serine residues at positions 385 and 400 were identified by mass spectrometry (Fig. 2b). On the structure of HSP70, serine 385 and 400 are located in the linker and N-terminus of substrate binding domain (SBD), respectively (Fig. 2c). To validate whether the residues identified *via* mass spectrometry were the actual phosphorylation sites, I generated the alanine substitution mutants, S385A, S400A and S385A/S400A. 293T cells expressing each of these mutants were stimulated by treatment with EGF and the phosphorylation of HSP70 was examined by immunoblotting. S385A- or S400A-expressing cells showed mildly induced phosphorylation upon EGF treatment, however I could not detect the induced phosphorylation at all in case of double alanine

mutant, S385A/S400A, implying that serine 385 and 400 were the real EGF signal-dependent phosphorylation sites (Fig. 2d). Next, I further confirmed that these two other residues are phosphorylated by ERK. Ectopic expression of ERK phosphorylates HSP70 wild type (WT) upon treatment with EGF but not HSP70 double alanine mutant, S385A/S400A (Fig. 2e). Altogether serine residues at positions 385 and 400 of HSP70 are phosphorylated by ERK.

HSP70 phosphorylation enhances the protein folding

To elucidate the significance of phosphorylation in the cell proliferation, I firstly examined the canonical function, folding activity, of HSP70. From the re-folding assay using the purified HSP70 wild type (WT) and double phospho-mimic mutant, S385D/S400D,proteins, I observed that S385D/S400D mutant shows around 1.5 times higher folding activity compared to WT (Fig. 3a). Next the aggregated proteins due to improper folding were explored by monitoring the in-soluble fraction of cell lysates. Each of Strep-HSP70 WT, S385A/S400A and S385D/S400D was introduced into the cells and the amounts of soluble and in-soluble fractions from total cell lysates were monitored. When Strep-HSP70 was expressed, the level of soluble protein fraction was increased but in-soluble protein fraction was decreased (Fig. 3b, left). But S385A/S400A- and S385D/S400D-expressing cells showed significant increase in in-soluble and soluble protein fractions, respectively (Fig. 3b, middle and right, respectively). These results suggested that phosphorylation of HSP70 enhances its folding activity, resulting in productive folding of client proteins. The ubiquitination of whole proteins was also monitored in cellular condition which is ectopically expressed by each of HSP70 WT or mutant. The cells were treated with proteasome inhibitor and ubiquitination from total cell lysate was determined. Ectopic expression of HSP70 WT decreased the

amounts of ubiquitination (Fig. 3c, second lane). However, cells expressing HSP70 containing S385A/S400A and S385D/S400D exhibited higher and lower amounts of ubiquitination, respectively (Fig. 3c, third and fourth lane, respectively). These findings indicated the significance of HSP70 phosphorylation on its folding activity. I further explored the level of well-known client proteins, Akt and CDK4, under different condition of HSP70 phosphorylation. Expression of double phospho-mimic mutant, S385D/S400D, of HSP70 led to increase in the levels of its client proteins but not S385A/S400A as expected (Fig. 3d). Taken together, the results suggest that phosphorylation enhances the folding activity of HSP70, resulting in better quality control and proper folding of client proteins.

Conformational change of HSP70 *via* phosphorylation

To unveil how the phosphorylation enhances the folding activity of HSP70, I first investigated the binding affinity of HSP70 wild type (WT) or double phospho-mimic mutant protein, S385D/S400D, for NRLLLTG, well-known substrate peptide[22]. From the enzyme-linked immunosorbent assay (*ELISA*) the binding affinities of the two proteins to NRLLLTG were calculated, and double phospho-mimic HSP70 exhibited about 1.5 times higher affinity than WT (Fig. 4a). Similar result was also observed in *in vitro* pull-down assay using NRLLLTG peptide and HSP70 proteins (Fig. 4b).

HSP70 has distinctly different un-extended and extended conformations, and the flexible linker region of the extended form is more exposed than the un-extended from, resulting in stronger binding affinity of the extended form to the substrate[7]. Moreover, addition of ATP leads transformation of extended conformation to the un-extended[23]. Since the phosphorylated HSP70 shows stronger binding affinity to substrate and better folding

activity than WT, I hypothesized that the phosphorylated HSP70 shows the extended conformation harboring more exposed linker and the conformational change from the extended form to the un-extended is inhibited *via* phosphorylation, even after the addition of ATP (Fig. 4c). To prove this hypothesis, I conducted the limited digestion assay using proteinase K because the exposed linker region is easy to cut by proteinase[15]. As shown in Fig. 4d, as expected, HSP70 WT was protected from digestion of proteinase K by addition of ATP; however, ATP-dependent protection failed in case of the double phospho-mimic HSP70, suggesting that the phosphorylated HSP70 has the exposed linker region and conformation like ADP-bound form. However, there is a lack of understanding about exact conformation of the phosphorylated HSP70, and to further validate the issue, I constructed two other fragmented subunits, LgBiT and SmBiT, of nanoluciferase tagged at N- and C-terminal of HSP70, respectively; this system emits a luciferase signal if the distance between these two fragments is diminished (Fig. 4e). Luciferase signal from HSP70 WT declined upon exposure to EGF signal in a time-dependent manner, but not the double phospho-mimic HSP70, suggesting that EGF signal-mediated phosphorylation induces conformational change from the un-extended form to extended form (Fig. 4f). Thus, it was concluded that the phosphorylation on serine residues at 385 and 400 locations of HSP70 induces and enhances the formation of the extended conformation, resulting in stronger binding affinity of HSP70 to its substrate.

To understand how each phosphorylation residues contribute to the extended conformation of HSP70, I analyzed the structure of HSP70 by determining the interaction of the linker and SBD containing S385D and S400D, respectively (See Fig. 2c). Through the pull-down assay, it was revealed that linker containing S385D fails to bind the NBD and SBD

(Fig. 4g and h, respectively). On the contrary, SBD containing S400D also failed to bind with linker (Fig. 4i). These results indicated that each of corresponding domain containing S385D or S400D fails to bind with its adjacent interacting domain, implying that phosphorylation of HSP70 leads to its extended conformation.

Augmentation of cell proliferation *via* phosphorylation of HSP70

To investigate whether the enhanced folding activity of HSP70 *via* its phosphorylation leads the enhanced cell proliferation, I examined the viability of 293T cells ectopically expressing either HSP70 wild type (WT), S385A/S400A or S385D/S400D. First, I found that S385A/S400A and S385D/S400D show lower and higher cell viability than those expressing HSP70 WT, respectively (Fig. 5a). Second, I also performed anchorage-independent colony forming assay, which revealed similar result as cell viability assay, including significant enhancement of colony formation in cells expressing S385D/S400D (Fig. 5b). Third, using cytotoxicity assay, I found that the double phospho-mimic HSP70-expressing cells were protected from HSP70 inhibitor-mediated cell death. When the cells expressing HSP70 WT were treated withVER155008 (VER), which inhibits HSP70 activity by interacting with ATP-binding pocket in NBD, cell death was enhanced owing to the inhibition of HSP70 activity (Fig. 5c, grey). Similarly, S385A/S400A-expressing cells were more vulnerable to VER-mediated cell death than those expressing WT (Fig. 5c, blue); however, VER could not induce cell death in S385D/S400D-expressing cells (Fig. 5c, red), indicating that induction of the extended conformation of HSP70 *via* phosphorylation might protect the cells from VER-mediated cells death by augmented HSP70 folding activity. Moreover, the findings revealed

that phosphorylation-mediated regulation of HSP70 activity is more prominent than ATP-mediated regulation.

To further validate the pathological implication of HSP70 phosphorylation on cancer cells, I analyzed the basic phosphorylation of HSP70 in the absence of EGF signal in normal and cancerous lung cells harboring the mutation in EGFR or K-Ras, which is a well-studied activator of ERK[24]. Phosphorylated HSP70 was observed in tested cancer cells, but not in normal cells, indicating that cancer cells showing enhanced proliferation exhibit proper folding of the translated peptides due to phosphorylated HSP70 besides the other folding machinery (Fig. 5d, 1stlane on left). Interestingly, it was also observed that phosphorylation of HSP70 was positively correlated with ERK activity, suggesting that ERK, as a kinase, mediates phosphorylation of HSP70 (Fig. 5d, right). These results suggest that the activity of ERK is a critical determinant of HSP70 phosphorylation and the promoted protein synthesis is dependent on the activity of HSP70.

Taken together, I propose the schematic model for the regulation of the folding activity of HSP70 *via* phosphorylation (Fig. 6). In presence of EGF signal, activated ERK phosphorylates the serine residues at position 385 in the linker region and at position 400 in the SBD of HSP70. Phosphorylated HSP70 represents the extended conformation of HSP70, resulting in the enhanced HSP70 folding activity and cell proliferation. Through the process of dephosphorylation, the extended conformation of HSP70 could revert to the un-extended conformation.

Figure 1. EGF-dependent phosphorylation of HSP70 *via* ERK.

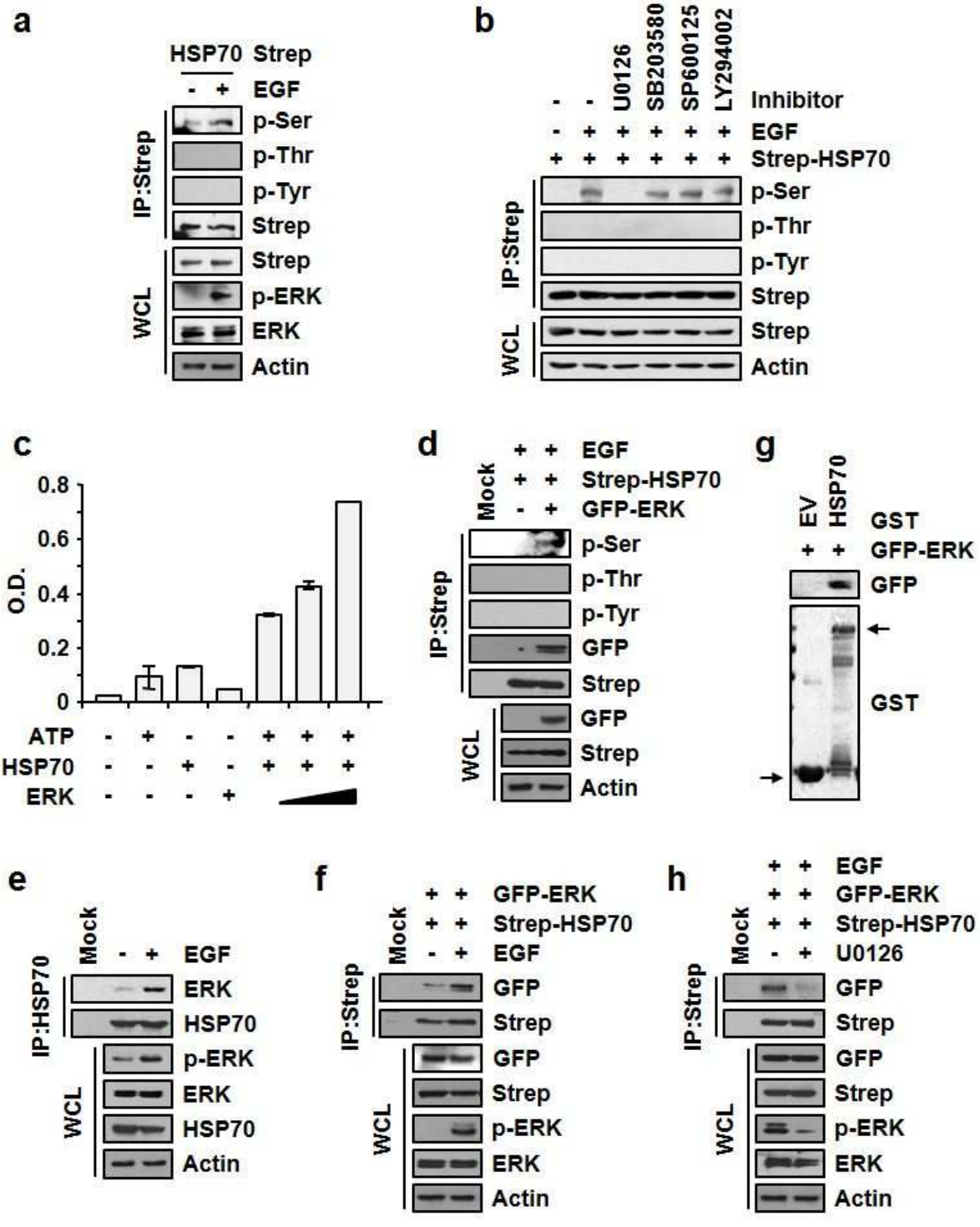

Figure 1. a, Determination of phosphorylated residues of HSP70 by EGF stimuli. 293T cells expressing Strep-HSP70 were treated with EGF and HSP70 was precipitated using

streptavidin-Sepharose beads. Precipitates were subjected to SDS-PAGE and immunoblotting using indicated antibodies. p-ERK and actin were used as positive controls for EGF signaling and loading control, respectively. **b,** Identification of kinase responsible for phosphorylation of HSP70. Strep-HSP70-expressing 293T cells were pre-incubated with indicated inhibitors and treated with EGF. Phosphorylation was detected as above. **c,** Determination of HSP70 phosphorylation *in vitro*. Indicated combinations of ATP, HSP70 and ERK were used for *in vitro* phosphorylation assay. The experiments were independently repeated three times with error bars denoting S.D. **d,** 293T cells containing Strep-HSP70 and GFP-ERK were treated with EGF and subjected to immuno-precipitation as above. **e,** EGF-dependent endogenous binding between HSP70 and ERK. H460 cells were treated with or without EGF and subjected to immunoprecipitation with antibody against HSP70. Co-precipitation of ERK with HSP70 was observed using antibody against ERK. **f,** 293T cells were transfected with Strep-HSP70 and GFP-ERK and treated with EGF. The cells were subjected to immunoprecipitation. **g,** *In vitro* binding between HSP70 and ERK. Purified GST-HSP70 were mixed with lysates expressing GFP-ERK and precipitated with glutathione-Sepharose beads. Co-precipitated ERK with HSP70 was detected by immunoblotting using anti-GFP antibody. GST proteins were observed by coomassie staining. **h,** 293T cells containing GFP-ERK and Strep-HSP70 were treated with EGF and U0126 as indicated. The cells were subjected to immunoprecipitation as above.

Figure 2. Identification of HSP70 phosphorylation residues.

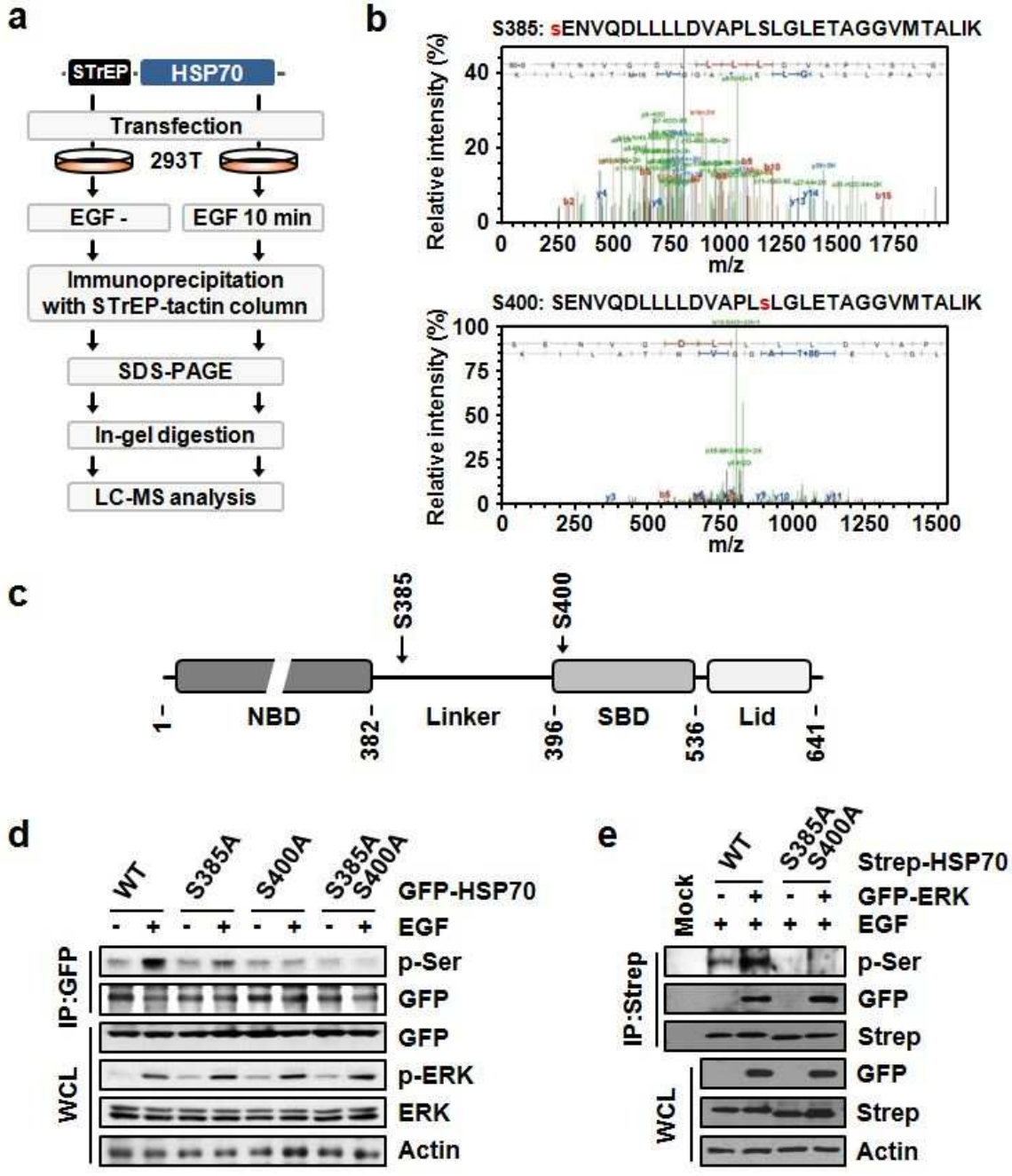

Figure 2. a-b, LC-MS analysis for identification of phosphorylated residues of HSP70 **a,** Strategy for identification of HSP70 phosphorylation sites *via* LC-MS analysis. **b,** Mass spectrum indicating phosphorylation of HSP70 serine residue at positions 385 (upper) and

400 (bottom). The identified peptide sequence including the phosphorylated residue was presented above its spectrum. Phosphorylated serine is colored as red. **c,** Cartoon showing HSP70 domain arrangement. NBD and SBD indicate nucleotide-binding domain and substrate-binding domain, respectively. Serine residues at positions 385 and 400 were located in linker and SBD regions, respectively. **d,** Indicated mutants-expressing 293T cells were either or not treated with EGF, and phosphorylation was determined by immunoblotting using specific antibodies. **e,** Strep-HSP70 and GFP-ERK were introduced into 293T cells as indicated. HSP70 phosphorylation and binding with ERK were detected by Western blotting.

Figure 3. Significance of HSP70 phosphorylation on protein folding.

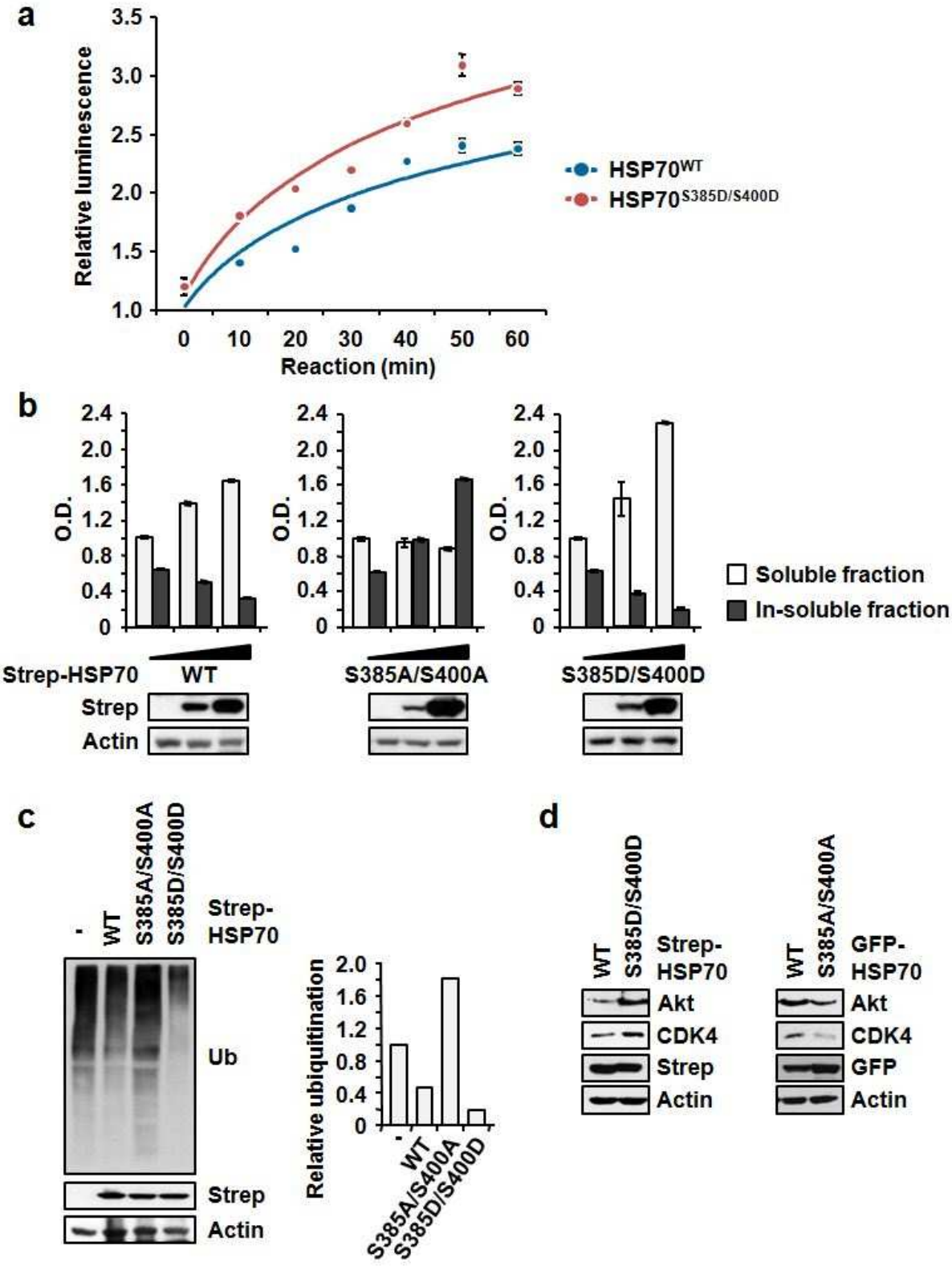

Figure 3. a, Re-folding activity of phosphorylated HSP70. Purified HSP70 wild type (WT) and double phospho-mimic proteins, S385D/S400D, were subjected to refolding assay. The experiments were independently repeated three times with error bars denoting S.D. **b,** Determination of soluble and in-soluble protein fractions following phosphorylation of HSP70. Strep-HSP70 wild type (WT), S385A/S400A and S385D/S400D mutants were expressed in 293T cells. Soluble and in-soluble protein fractions from whole cell lysates were separated and subjected to SDS-PAGE and immunoblotting using anti-Strep antibody. Actin was used as a loading control. **c,** Determination of ubiquitinated proteins *via* phosphorylation of HSP70. Same cells as above were treated with MG-132. The amounts of ubiquitinated proteins were determined by immunoblotting using specific antibody against ubiquitin (Ub). Quantitated degree of ubiquitination was shown as a bar graph in right. **d,** Indicated HSP70s were introduced into 293T cells and the endogenous levels of Akt and CDK4 were evaluated by Western blotting using specific antibodies.

Figure 4. Phosphorylation-mediated conformational change of HSP70.

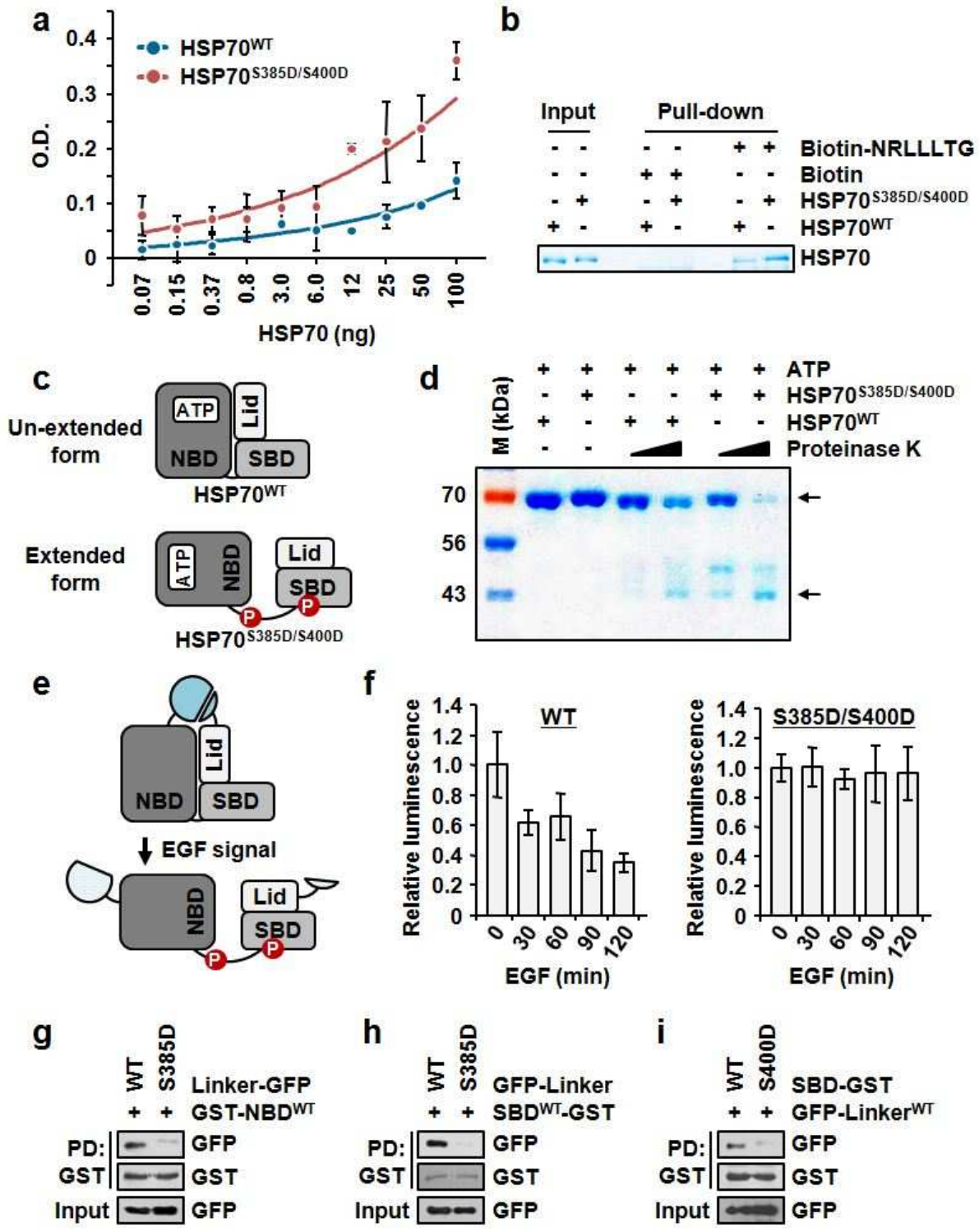

Figure 4. a, Enzyme-linked immunosorbent assay (*ELISA*) for monitoring interaction between HSP70 and NRLLLTG peptide. Binding affinity of NRLLLTG peptide to HSP70 wild type (WT) or double phospho-mimic, S385D/S400D, proteins were evaluated by ELISA. The experiments were independently repeated three times with error bars denoting S.D. **b,** *In vitro* pull-down assay showing the binding difference of NRLLLTG to HSP70 WT and S385D/S400D proteins. Biotin-NRLLLTG or biotin was mixed with two proteins and pulled-down by streptavidin-Sepharose beads. The precipitates separated by SDS-PAGE were subjected to coomassie staining. **c,** Cartoon showing two different conformations of HSP70. **d,** Limited digestion assay to confirm the conformation of HSP70. HSP70 WT or S385D/S400D was pre-incubated with ATP and mixed with varying concentrations of proteinase K. Digested proteins were separated and detected by SDS-PAGE and coomassie staining, respectively. M denotes the size marker. The number on the left of gel image denotes molecular weight (kDa). **e-f,** Determination of conformational change of HSP70 *via* nanoluciferase assay. **e,** Schematic diagram of nanoluciferase assay to check the EGF-dependent change in HSP70 conformation. LgBiT and SmBiT of nanoluciferase were tagged to N- and C-terminal of HSP70 WT and S385D/S400D. In presence of EGF signal, two distant fragments lead to the decline of luciferase signal. **f,** The cells expressing each type of HSP70 were treated with EGF for varying times and luciferase signal was determined. Luciferase signals relative to un-treated sample were shown as bar graph. The experiments were independently repeated three times with error bars denoting S.D. **g-i,** Lysates expressing GFP-tagged S385D mutant of HSP70-linker and the purified GST-HSP70-NBD **(g)** or -SBD **(h)** proteins were subjected to *in vitro* pull-down assay. Purified HSP70-SBD protein including S400D mutation was mixed with lysates expressing GFP-tagged HSP70-linker for *in vitro* pull-down assay **(i)**.

Figure 5. Significance of HSP70 phosphorylation in cell proliferation.

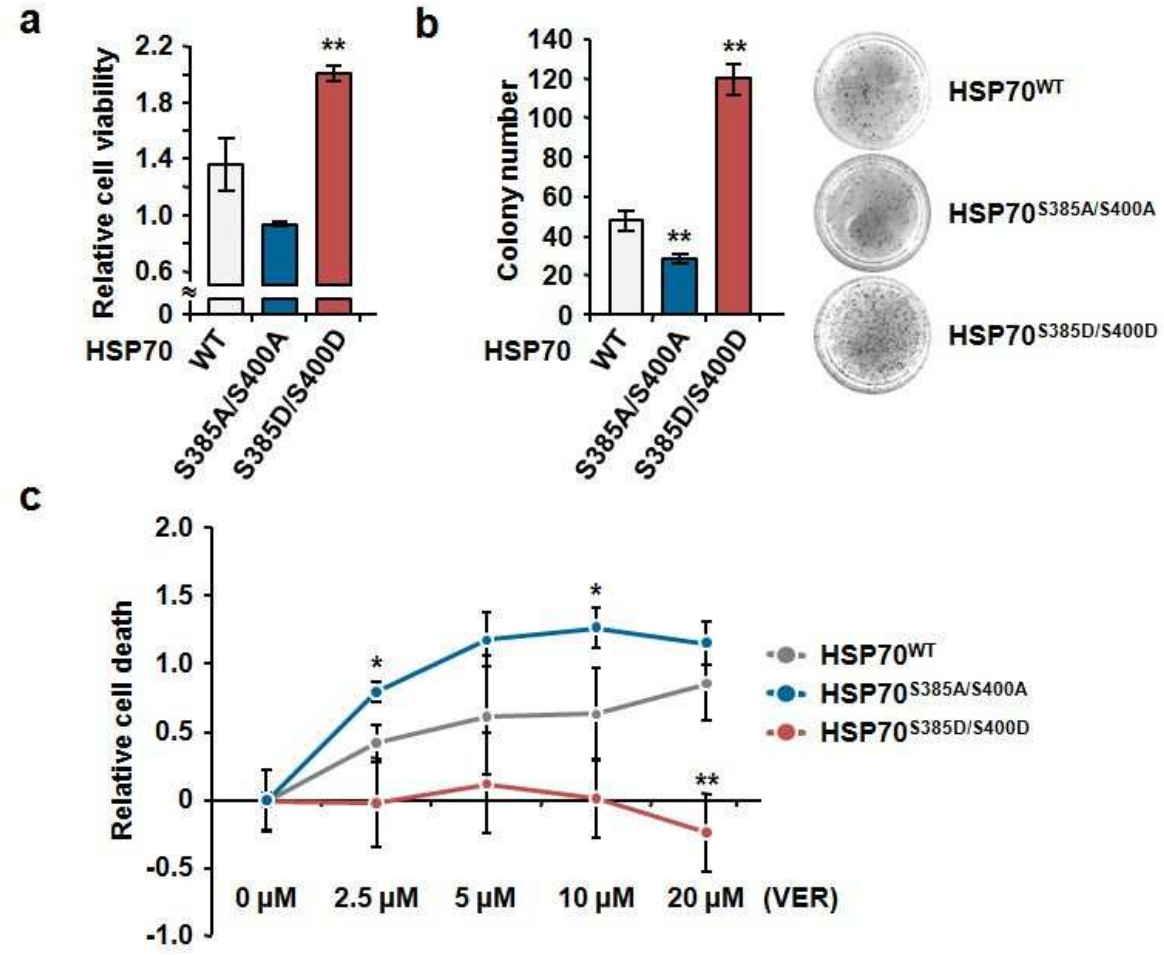

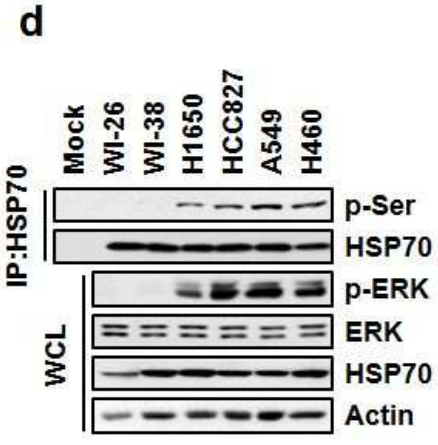

		Mutation		Phosphorylation	
	Cell lines	EGFR	K-Ras	ERK	HSP70
Normal	WI-26	-	-	-	-
	WI-38	-	-	-	-
Cancer	H1650	+	-	+	+
	HCC827	+	-	+	+
	A549	-	+	+	+
	H460	-	+	+	+

Figure 5. a-c, Determination of cellular function of phosphorylated HSP70. **a,** HSP70 wild type (WT), S385A/S400A and S385D/S400D mutants were introduced into 293T cells. The cells were subjected to MTT assay to examine cell viability. **b,** Same cells were subjected to anchorage-independent colony forming assay. The number of colonies was counted and shown as a bar graph. Image on the right denotes the settled colony. **c,** Same cells were treated with different concentration of VER155008 (VER) and subjected to cytotoxicity assay. All the experiments were independently repeated three times with error bars denoting S.D. (*P<0.05, **P<0.01) **d,** Cell line analysis showing the varying status of HSP70 phosphorylation. WI-26, WI-38, H1650, HCC827, A549 and H460 cells were subjected to immunoprecipitation to examine the phosphorylation of HSP70 (left). Mutations in EGFR and K-Ras and phosphorylation of ERK and HSP70 were summarized in the table (right).

Figure 6. Schematic representation for phosphorylation of HSP70 *via* ERK and its cellular function.

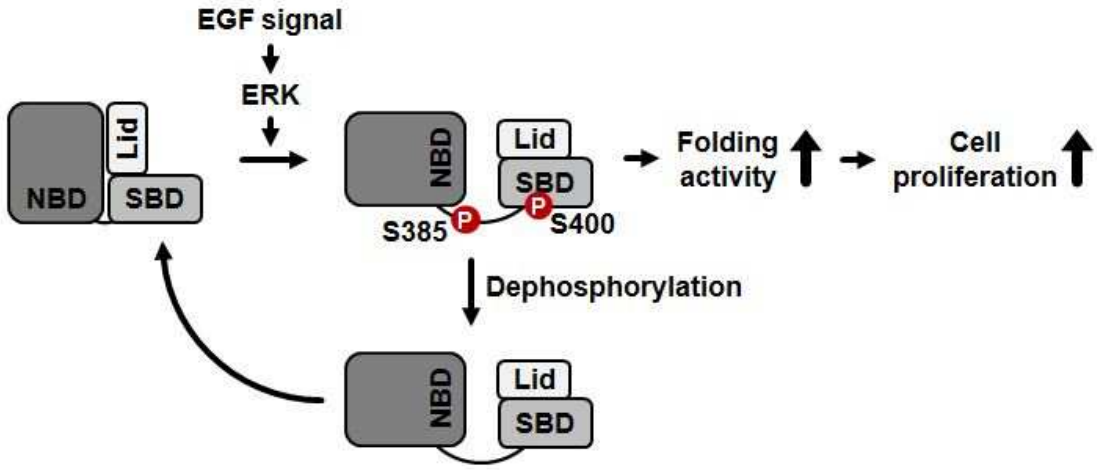

Schematic model for conformational change of HSP70 *via* phosphorylation of its serine residues at positions 385 and 400. In presence of EGF signal, serine residues at positions 385 and 400 of HSP70 were phosphorylated by ERK. Phosphorylation enhances the extended conformation of HSP70, resulting in its augmented folding activity.

Discussion

Cancer cells are characterized by rapid cell growth and division compared to normal cells and rapid growth and division requires accurate and rapid protein synthesis[25]. Among the many process of protein synthesis, accurate protein folding is very critical to maintain the exact structure of proteins, determining its function[3]. Heat shock proteins (HSPs) are a family of chaperones that takes charge of the proper folding of translated peptides[1]. Among HSPs, HSP70 is a well-studied and a promising target for cancer therapy[4]. However, the level of HSP70 does not correlate with the amounts of the productive folded proteins in cancer cells, and thus, protein folding efficiency has been studied[17]. This has raised a question whether HSP70 is a real cancer target and many studies tried to solve this problem. Here, I firstly report that the phosphorylation of linker region of HSP70 *via* ERK enhances the protein folding activity, resulting in rapid proliferation of cancer cells. It was determined that the serine 385 and 400 residues are phosphorylated by ERK upon EGF signaling and the phosphorylated HSP70 shows enhanced folding activity, enhancing the cellular protein folding. I also determined the mode of action for the increased folding activity *via* phosphorylation. Phosphorylation of serine residues at positions 385 and 400 in linker and N-terminus of SBD, respectively, leads to the induction of the extended conformation of HSP70, resulting in a strong binding affinity between substrate and HSP70.

HSP70 contains of two domains, NBD and SBD, divided by a flexible linker region[6]. Upon ATP hydrolysis, HSP70 exists in two distinct, un-extended and extended, conformations and the each conformation shows varied folding activity[7]. Recently the

dynamic conformational change *via* exposed flexible linker region has been studied[14]; however, there is no factor that affects the dynamics of linker region. Our discovery regarding the phosphorylation of serine 385 residue on linker region of HSP70 could be the answer for dynamics *via* linker region. Phosphorylated serine 385 residue on linker region failed to bind with NBD and SBD of HSP70. This result suggests that phosphorylation on linker of HSP70 enforces its exposure and enhances the dynamics to the extended conformation. In addition, I identified the serine 400 residue as another phosphorylation site. Serine 400 is structurally near SBDα, lid domain, in the N-terminus of SBD. Our results show that the phosphorylation on serine 400 of SBD leads to decrease of its binding with linker region. This result suggests the possibility that lid firmly covers the substrate-binding pocket of SBD, resulting in strong binding affinity of substrate to SBD because the lid is closed in the extended form of HSP70[23]. Thus, phosphorylation sites, serine 385 and 400, could be an efficient target to regulate the structural dynamics of HSP70.

Recently, a few research groups have reported the phosphorylation sites in NBD and SBD of HSP70 and revealed the significance of phosphorylation in pathological condition[26]. In cancer cells, hyperactive kinases phosphorylate HSP70, resulting in two hot spots for phosphorylation, one in NBD and another in SBD[27]. Increased HSP70 phosphorylation by hyperactive kinases promotes cancer progression *via* regulation of protein stabilization, cell cycle, and response to cancer drug[10,12,13]. However, there is no report about phosphorylation in the linker of HSP70, because the importance of linker for dynamics and function of HSP70 is not thoroughly studied. Here, I firstly reported the phosphorylation site, serine 385, in linker region and its significance in process of folding and cellular effect. Although I need to further elucidate which conformation is favorable to be phosphorylated by ERK, the

functional analysis of phosphorylation of serine 385 residue of HSP70 in this report is crucial for understanding the regulation of folding activity of HSP70 *via* phosphorylation in linker region.

ERK is a well-studied kinase activated by growth signal[24]. Activated ERK mainly regulates the transcription factors associated with protein translation and translational machinery molecules facilitating cell proliferation and survival[28]. In this study I unveiled that the activated ERK *via* EGF signal controls the conformation of HSP70 *via* phosphorylation, resulting in its augmented folding activity. Thus, the novel function of ERK, direct regulation of productive folding, is revealed from this study.

HSPs have been considered as an attractive therapeutic target to cure cancer since a long time; however, targeting HSPs accompanies a significant challenge from redundancy. In fact, the reason many trials targeting HSPs have failed was generation of toxicity to normal cells in addition to cancer[5]. In this regard, phosphorylated HSP70 could be a very attractive target for curing the cancer cells. Phosphorylation of HSP70 could be considered as a pathological, not physiological, phenomenon, and thus, therapeutic agents used to target the phosphorylated HSP70 could be specific to cancer cells, not normal cells. Resistance and addiction to the therapeutic agents targeting the phosphorylated HSP70 could not be found either because post translational modification, especially phosphorylation, is transient. Since phosphorylation of HSP70 is also tightly dependent on the activation of ERK and many studies have reported enhanced activation of ERK in cancercells[29], many patients could be benefitted by this approach. Thus, targeting the phosphorylated HSP70 for curing cancer could be a new alternative to solve the existing problem.

Methods

Cell culture and materials 293T and WI-26 cells were cultured in DMEM media supplemented with 10% FBS and 1% penicillin/streptomycin in 5% CO_2 at 37°C, respectively.WI-38, A549, H460, HCC827and H1650 were cultivated in RPMI with same as above. All the used cells and GFP-tagged ERK were gifted from biobank of Biocon. GFP-HSP70 (#15215) was purchased from addgene and sub-cloned into EcoRI/XhoI sites of pEXPR-IBA105. Each of HSP70 domains was cloned into EcoRI/XhoI sites ofpEGFP-C3, pEGFP-N1 and pGEX4T-1. Point mutagenesis of HSP70 was performed with Quik-ChangeII (Promega), following the manufacturer's instruction. EGF was purchased from Peprotech. MG-132 and antibody against p-Ser were purchased from Sigma. Antibodies for p-Thr, p-Tyr, p-ERK and ERK were purchased from Cell signaling Technology and others from Santa Cruz Biotechnology. StrepMAB-classic-HRP, for detecting Strep, was purchased from iba.

Identification of phosphorylation site Strep-HSP70-expressing 293T cells were incubated with or without EGF for 10 minutes and purified with strep-tactin column. The purified HSP70 was analyzed by SDS-PAGE and subjected to in-gel digestion with Trypsin/Lys-C (Promega). For identification of phospho peptides, the analysis of peptide mixture was performed using LTQ-OrbitrapVelos (Thermo Fisher Scientific) connected to Easy-nano LC II system (Thermo Fisher Scientific) incorporating an autosampler. Acquired data from data-dependent mode to simultaneously record full-scan mass and collision-induced dissociation (CID) spectra with multistage activation were analyzed. To identify the specific sites of

phosphorylation on phosphopeptides, CID spectra were searched for the peptides containing modification, p-Ser, p-Thr and p-Tyr, by a combination of database searches and by plotting neutral loss chromatograms to show characteristic loss of a phosphate group. Proteome Discoverer (version 1.3, ThermoScienific, Waltham, MA USA) and Scaffold program (version 4.8.4, Proteome Software Inc., Portland, OR) were used to validate MS/MS-based peptide and protein identifications and to process the quantitative analysis. Precursor mass tolerance and fragment mass tolerance were set to 25 ppm and 0.8 Da.

***In vitro* kinase assay** Phosphorylation of HSP70 by active ERK1 protein (Enzo life sciences) was monitored using universal kinase activity kit (R&D systems). 0.15 mM of purified HSP70 and 1 mM of ATP were mixed with 2 to 50 ng/ml of ERK1 in phosphatase buffer containing 250 mM HEPES, 1.5 M NaCl, 100mM $MgCl_2$ and 100 mM $CaCl_2$. Coupling phosphatase, CD39L2, was added for generation of inorganic phosphate from ADP resulted from kinase reaction. After incubation on room temperature for 10 minutes, malachite green reagent was added for termination of reaction. Amount of phosphorylated HSP70 was determined by measuring OD at 600 nm in microplate reader and the experiments were repeated three times independently.

Re-folding assay Glow-Substrate peptide was un-folded by heating at 40°C for 7 minutes and subjected to re-folding assay using HSP70/HSP40 Glow-Fold Protein Refolding kit (BoostonBiochem), following the manufacturer's instruction. For quantification of the re-folded amounts of peptide, luciferase signal was determined by luciferase reader (GloMax,

Promega) at various reaction times (10, 20, 30, 40, 50 and 60 minutes). The experiments were independently repeated three times.

Limited digestion assay For limited digestion assay using the purified HSP70 wild type and S385D/S400D mutants were incubated with proteinase K according to the previously reportedmethod[15,16]. 10 μg of HSP70 protein was pre-incubated with 200 μM ATP at room temperature and proteinase K was added in dose-dependent manner. Enzyme reaction was done in room temperature and stopped by adding the SDS sample buffer and boiling at 100 °C for 10 minutes before SDS-PAGE with coomassie staining.

Luciferase assay Each of HSP70 wild type orS385D/S400D mutants was cloned into pBiT1.1-N[TK/LgBiT], and SmBiT fragment of pBiT2.1-N[TK/SmBiT] was cloned at the C-terminus of HSP70 for generating the construct that LgBiT and SmBiT of nanoluciferase were tagged to N- and C-terminal of HSP70. 293T cells ectopically expressed with each plasmid were treated with EGF (50 μg/ml) for 30, 60, 90 and 120 minutes. After incubation for indicated time, the luciferase activity was determined by the nanoluciferase assay system, following the manufacturer's protocol (Promega). The experiments were independently repeated three times.

Enzyme-linked immunosorbent assay 150 ng of purified NRLLLTG peptide was diluted in 0.05 M sodium carbonate buffer (pH 9.6) and coated on a flat-bottom 96-well plate (Thermo). After overnight incubation, washing with PBST for 3 times and blocking with PBST

including 1% BSA solution were done. Each well was washed with PBST, and HSP70 wild type or S385D/S400D mutant protein was added in dose-dependent manner. After washing with PBST, primary antibody against HSP70 and its secondary antibody were incubated serially. 3,3',5,5'-tetramethylbenzidine (TMB) solution (Thermo) detected bound HSP70 using 1N $H_2SO_4$for developing and stopping the reaction. The absorbance was measured at 450 nm with 620 nm reference and all the experiments were repeated 3 times.

***In vitro* pull-down assay** Purified GST-tagged proteins were mixed with cell lysates containing GFP-tagged proteins in 50 mM Tris-HCl (pH 7.4) binding buffer containing 100 mM NaCl, 0.5% Triton X-100, 10% glycerol, 1 mM EDTA, and protease inhibitor (Calbiochem) at 4°C. After 12 hours, GST proteins were precipitated by glutathione Sepharose beads and washed with binding buffer three times, and co-precipitates with GST proteins were separated by SDS-PAGE. The amounts of GFP- and GST-tagged proteins were detected by immunoblotting using anti-GFP antibody and coomassie staining, respectively.

Immunoprecipitation The cells were lysed with 50 mM Tris-HCl (pH 7.4) lysis buffer containing 100 mM NaCl, 0.5% Triton X-100, 0.1% SDS, 10% glycerol, 1 mM EDTA, and protease inhibitor (Calbiochem). Whole cell lysates were mixed with interesting antibody pre-incubated with agarose G for 12 hours. After incubation, precipitates with agarose G were washed with cold lysis buffer excluding 0.1% SDS three times. Strep-tagged HSP70 were precipitated with strep-tactin column (IBA), following the manufacturer's instruction. Co-precipitates with bait proteins were subjected to SDS-PAGE and immunoblotting.

Soluble and in-soluble protein fractionation The 293T cells dose-dependently transfected with each of Strep-HSP70 wild type, S385A/S400A and S385D/S400D mutant were lysed with 50 mM Tris-HCl (pH 7.4) buffer containing 0.5% Triton X-100 and protease inhibitor (Calbiochem). After lysis for 30 minutes at 4 °C, whole cell lysates were separated into supernatant and pellet fraction by centrifugation at 13,200 rpm for 15 minutes at 4 °C. The pellet fraction was dissolved with the lysis buffer adding 1% SDS. The amounts of proteins in each fraction was measured by spectrophotometer using Bradford (Biorad) solution. The experiments were independently repeated three times.

Anchorage-independent colony forming assay Each of Strep-HSP70 wild type, S385A/S400A and S385D/S400D mutant was introduced into 293T cells. The cells were subjected to anchorage-independent colony formation assay using cell transformation assay kit (CELL BIOLABS, INC.), following the manufacturer's instruction. After cell culture for 1 week, soft agar was solubilized and the colonies were stained by MTT solution (Sigma) and counted. The experiments were independently repeated three times.

Cell viability assay 293T cells (1x 10^4) ectopically expressing each of Strep-HSP70 wild type, S385A/S400A and S385D/S400D mutant were cultured in single well of 96 well plate for 24 hours. The cells in the each well were treated with 10 μl of MTT solution (5 mg/ml, Sigma) and incubated for 1 hour at 37 °C. After discard the culture media, the precipitated formazan crystals were dissolved with 100 μl DMSO (Duchefa). Absorbance was measured

at 560 nm using a micro plate reader (Sunrise, TECAN). The experiments were independently repeated three times.

Cell toxicity assay The 293T cells expressing Strep-HSP70 wild, S385A/S400A or S385D/S400D were seeded in 96 well white plate and cultured for overnight. Several doses of VER155008 (2.5, 5, 10 and 20 μM) were treated for 6 hours and dead cells were evaluated with CytoTox-Glo kit (Promega). After adding the mixture of AAF-Glo substrate and buffer, cells were incubated in 37 °C for 10 minutes and luminescence signal from dead cells was measured by luciferase reader (GloMax, Promega). The experiments were independently repeated for three times.

Quantification and statistical analysis Statistical tests were performed with Prism (GraphPad). A value of $P<0.05$ was considered statistically significant. All error bars represent standard deviation (s.d.). For quantitative data, statistical parameters are reported in the figure legends.

References

1 Hartl, F. U., Bracher, A. & Hayer-Hartl, M. Molecular chaperones in protein folding and proteostasis. *Nature***475**, 324-332, doi:10.1038/nature10317 (2011).

2 Zemanovic, S. *et al.* Dynamic Phosphorylation of the C Terminus of Hsp70 Regulates the Mitochondrial Import of SOD2 and Redox Balance. *Cell Rep***25**, 2605-2616 e2607, doi:10.1016/j.celrep.2018.11.015 (2018).

3 Calderwood, S. K. & Gong, J. Heat Shock Proteins Promote Cancer: It's a Protection Racket. *Trends Biochem Sci***41**, 311-323, doi:10.1016/j.tibs.2016.01.003 (2016).

4 Wu, J. *et al.* Heat Shock Proteins and Cancer. *Trends Pharmacol Sci***38**, 226-256, doi:10.1016/j.tips.2016.11.009 (2017).

5 Kumar, S. *et al.* Targeting Hsp70: A possible therapy for cancer. *Cancer Lett***374**, 156-166, doi:10.1016/j.canlet.2016.01.056 (2016).

6 Sekhar, A., Rosenzweig, R., Bouvignies, G. & Kay, L. E. Hsp70 biases the folding pathways of client proteins. *Proc Natl Acad Sci U S A***113**, E2794-2801, doi:10.1073/pnas.1601846113 (2016).

7 Alderson, T. R., Kim, J. H. & Markley, J. L. Dynamical Structures of Hsp70 and Hsp70-Hsp40 Complexes. *Structure***24**, 1014-1030, doi:10.1016/j.str.2016.05.011 (2016).

8 English, C. A., Sherman, W., Meng, W. L. & Gierasch, L. M. The Hsp70 interdomain linker is a dynamic switch that enables allosteric communication between two structured domains. *J Biol Chem***292**, 14765-14774, doi:10.1074/jbc.M117.789313

(2017).

9 Humphrey, S. J., James, D. E. & Mann, M. Protein Phosphorylation: A Major Switch Mechanism for Metabolic Regulation. *Trends Endocrinol Metab***26**, 676-687, doi:10.1016/j.tem.2015.09.013 (2015).

10 Morgner, N. *et al.* Hsp70 forms antiparallel dimers stabilized by post-translational modifications to position clients for transfer to Hsp90. *Cell Rep***11**, 759-769, doi:10.1016/j.celrep.2015.03.063 (2015).

11 Muller, P. *et al.* C-terminal phosphorylation of Hsp70 and Hsp90 regulates alternate binding to co-chaperones CHIP and HOP to determine cellular protein folding/degradation balances. *Oncogene***32**, 3101-3110, doi:10.1038/onc.2012.314 (2013).

12 Truman, A. W. *et al.* CDK-dependent Hsp70 Phosphorylation controls G1 cyclin abundance and cell-cycle progression. *Cell***151**, 1308-1318, doi:10.1016/j.cell.2012.10.051 (2012).

13 Liu, T. *et al.* Identification and characterization of a 66-68-kDa protein as a methotrexate-binding protein in murine leukemia L1210 cells. *Cell Stress Chaperones***18**, 223-234, doi:10.1007/s12192-012-0376-9 (2013).

14 Mayer, M. P. & Gierasch, L. M. Recent advances in the structural and mechanistic aspects of Hsp70 molecular chaperones. *J Biol Chem***294**, 2085-2097, doi:10.1074/jbc.REV118.002810 (2019).

15 Mukherjee, M. *et al.* Mitotic phosphorylation regulates Hsp72 spindle localization by uncoupling ATP binding from substrate release. *Sci Signal***11**, doi:10.1126/scisignal.aao2464 (2018).

16 Preissler, S. *et al.* AMPylation targets the rate-limiting step of BiP's ATPase cycle for

its functional inactivation. *Elife***6**, doi:10.7554/eLife.29428 (2017).

17 Moran Luengo, T., Mayer, M. P. & Rudiger, S. G. D. The Hsp70-Hsp90 Chaperone Cascade in Protein Folding. *Trends Cell Biol***29**, 164-177, doi:10.1016/j.tcb.2018.10.004 (2019).

18 Moran Luengo, T., Kityk, R., Mayer, M. P. & Rudiger, S. G. D. Hsp90 Breaks the Deadlock of the Hsp70 Chaperone System. *Mol Cell***70**, 545-552 e549, doi:10.1016/j.molcel.2018.03.028 (2018).

19 Cloutier, P. & Coulombe, B. Regulation of molecular chaperones through post-translational modifications: Decrypting the chaperone code. *Bba-Gene Regul Mech***1829**, 443-454, doi:10.1016/j.bbagrm.2013.02.010 (2013).

20 Wee, P. & Wang, Z. Epidermal Growth Factor Receptor Cell Proliferation Signaling Pathways. *Cancers (Basel)***9**, doi:10.3390/cancers9050052 (2017).

21 Scaltriti, M. & Baselga, J. The epidermal growth factor receptor pathway: a model for targeted therapy. *Clin Cancer Res***12**, 5268-5272, doi:10.1158/1078-0432.CCR-05-1554 (2006).

22 Clerico, E. M., Tilitsky, J. M., Meng, W. L. & Gierasch, L. M. How Hsp70 Molecular Machines Interact with Their Substrates to Mediate Diverse Physiological Functions. *Journal of Molecular Biology***427**, 1575-1588, doi:10.1016/j.jmb.2015.02.004 (2015).

23 Sekhar, A., Rosenzweig, R., Bouvignies, G. & Kay, L. E. Mapping the conformation of a client protein through the Hsp70 functional cycle. *P Natl Acad Sci USA***112**, 10395-10400, doi:10.1073/pnas.1508504112 (2015).

24 Kolch, W. Coordinating ERK/MAPK signalling through scaffolds and inhibitors. *Nat Rev Mol Cell Bio***6**, 827-837, doi:DOI 10.1038/nrm1743 (2005).

25 Sherman, M. Y. & Gabai, V. L. Hsp70 in cancer: back to the future. *Oncogene***34**,

4153-4161, doi:10.1038/onc.2014.349 (2015).

26 Nitika & Truman, A. W. Cracking the Chaperone Code: Cellular Roles for Hsp70 Phosphorylation. *Trends Biochem Sci***42**, 932-935, doi:10.1016/j.tibs.2017.10.002 (2017).

27 Beltrao, P. *et al.* Systematic functional prioritization of protein posttranslational modifications. *Cell***150**, 413-425, doi:10.1016/j.cell.2012.05.036 (2012).

28 Roskoski, R. ERK1/2 MAP kinases: Structure, function, and regulation. *Pharmacological Research***66**, 105-143, doi:10.1016/j.phrs.2012.04.005 (2012).

29 McCubrey, J. A. *et al.* Roles of the Raf/MEK/ERK pathway in cell growth, malignant transformation and drug resistance. *Biochim Biophys Acta***1773**, 1263-1284, doi:10.1016/j.bbamcr.2006.10.001 (2007).

국문초록

Heat shock protein 70의 결합에 의한 AIMP2-DX2 안정화 기전과 결합 억제제를 이용한 항암 효능 연구

정상세포에 비해 비정상적으로 증식하는 암세포는 세포의 성장과 사멸을 조절하기 위해 oncoprotein의 증가를 요한다. 이 때문에 oncoprotein의 안정성을 도모하는 Heat Shock Protein (HSP)은 암을 억제하기 위한 주요한 표적이 된다. 그러므로 HSP을 직접적 또는 간접적으로 조절하는 방법은 암 치료에 이용될 수 있다.

암유발인자인 Aminoacyl-tRNA synthetase interacting multifunctional protein2-deleted exon2(AIMP2-DX2)는 여러 가지 암세포에서 증가되어 있음에도 불구하고 그의 세포 내 단백질조절기전이 알려져 있지 않다. 이 연구는 HSP70이 AIMP2-DX2의 레벨을 조절하는 중요인자임을 보고한다. Mass spectrometry를 기반으로 한 interactome 분석을 통해 HSP70이 AIMP2-DX2의 interactor임을 확인하였고, X-ray crystallography와 NMR으로 두 단백질의 결합구조를 분석하였다. HSP70의 substrate-binding domain은 AIMP2-DX2의 N-terminal flexible 부분과 GST-domain 부분을 인지하고 결합하여, Siah1에 의한 ubiquitination을 억제함으로서 AIMP2-DX2 단백질을 안정화시킨다. AIMP2-DX2로 인해 유도되는 세포형질전환과 암의 진행은 HSP70에 의해 촉진되었다. 또한 다양한 폐암 세포들과 폐암환자조직분석은 두 단백질의 정적상관관계를 보여준다. 더 나아가 AIMP2-DX2:HSP70 결합을 저해하는 화합물은 세포와 동물모델에서 암 증식 억제효과를 보였다. 그러므로 이 연구

는 암 진행을 촉진하는 AIMP2-DX2:HSP70 결합을 증명하며, 그의 억제가 암 치료제로 이용될 수 있는 가능성을 제시한다.

빠르게 증식하는 암세포는 생존을 위해서 HSP70에 의한 단백질 folding 의 효율적 작동을 필요로 한다. 이로 인해, HSP70은 암 진행을 저해할 수 있는 주요표적으로 연구된다. 하지만, 아직까지 HSP70의 활성을 조절할 수 있는 인자나 그에 대한 기전연구가 미비하다. 본 연구는 HSP70의 인산화가 folding activity 에 미치는 영향을 규명한다. HSP70 linker 의 385 그리고 substrate-binding domain 의 400번 serine residue 가 EGF 신호에 의해 인산화된다는 것이 mass spectrometry 와 mutant study 를 통해 확인되었다. EGF 신호 아래에서 직접적으로 HSP70을 인산화시키는 kinase 는 ERK 임을 확인하였다. 두 serine 잔기의 인산화는 HSP70의 구조변화를 야기하고, 결과적으로 펼쳐진 구조를 갖게 된다. 변화된 구조는 HSP70과 client 단백질의 결합을 증진시켜 HSP70에 의한 folding 을 증가시키고, 이로 인한 세포의 증식을 가속화시킨다. EGF 신호의 중요인자인 EGFR 과 KRAS 의 변이를 갖는 다양한 세포에서 높은 활성을 갖는 ERK 에 의한 HSP70인산화가 증가되어 있음이 확인되었다. 본 연구는 ERK 에 의한 HSP70 인산화가 HSP70의 canonical function 을 조절하고 세포증식의 변화에 영향을 미친다는 것을 보여준다.

위 두 가지 연구결과를 통하여 HSP70을 조절할 수 있는 서로 다른 두 가지 방법을 보여준다. HSP70과 specific substrate 의 결합을 억제하는 방법과 HSP70의 활성에 영향을 미치는 인산화를 조절하는 방법을 제시한다. 두 가지 접근은 모두 암세포에서 특이적으로 발현이 높거나 활성화되어 있는 표적을

조절하는 방법이기 때문에, 암을 억제하는 전략으로 이용되기에 충분한 가치를 지닌다.

주제어: HSP70, AIMP2-DX2, 단백질-단백질 결합, stabilization, ubiquitination, folding, 암의 증식, 인산화, ERK

학번: 2014-30557